FINAL TECHNICAL REPORT

Power Take-off System for Marine Renewable Devices

Ocean Renewable Power Company, Inc.

DE-EE0006398

Principal Investigator: Jarlath McEntee

February 28, 2018

Ocean Renewable Power Company, LLC
254 Commercial Street, Suite 119B
Portland, ME 04101
Phone (207) 772-7707
www.orpc.co

Acknowledgment: "This material is based upon work supported by the Department of Energy's Office of Energy Efficiency and Renewable Energy (EERE) under the Marine & Hydrokinetic Program under Award Number(s) DE-EE0006398."

Disclaimer: "This report was prepared as an account of work sponsored by an agency of the United States Government. Neither the United States Government nor any agency thereof, nor any of their employees, makes any warranty, express or implied, or assumes any legal liability or responsibility for the accuracy, completeness, or usefulness of any information, apparatus, product, or process disclosed, or represents that its use would not infringe privately owned rights. Reference herein to any specific commercial product, process, or service by trade name, trademark, manufacturer, or otherwise does not necessarily constitute or imply its endorsement, recommendation, or favoring by the United States Government or any agency thereof. The views and opinions of authors expressed herein do not necessarily state or reflect those of the United States Government or any agency thereof."

CONTENTS

1 EXECUTIVE SUMMARY 7
1.1 How research adds to the understanding of area investigated 7
1.2 Technical effectiveness and economic feasibility of methods investigates 7
1.3 How the Project benefits the public 8
2 COMPARISON OF ACCOMPLISHMENTS WITH GOALS AND OBJECTIVES 9
2.1 Project Description 9
2.2 SPA Metrics 10
2.3 Project Milestones 11
3 SUMMARY OF PROJECT ACTIVITIES 11
3.1 Project Management – Task 1.0 Project Planning 11
3.1.1 Original Hypotheses 11
3.1.2 Approaches Used 12
3.1.3 Problems Encountered and Departure from Planned Methodology 12
3.1.4 Assessment of Their Impact on the Project Results 13
3.2 Driveline Development – Task 2.0 Driveline Design, and Task 4.0 Driveline Build and Validation 13
3.2.1 Driveline Design – Task 2.0 Driveline Design, and Subtask 4.1 Flume Test 14
3.2.1.1 Load Assessment and Requirements – Subtask 2.1 Load Assessment 14
3.2.1.1.1 Original Hypotheses 14
3.2.1.1.2 Approaches Used 15
3.2.1.1.2.1 Streamtube Modeling – Milestone 2.1.1 16
3.2.1.1.2.2 Vortex Modeling – Milestone 2.1.2 20
3.2.1.1.2.3 2D RANS – Milestone 2.1.3 22
3.2.1.1.2.4 2D DES – Milestones 2.1.4 and 2.1.5 27
3.2.1.1.2.5 3D RANS – Milestone 2.1.6 36
3.2.1.1.2.6 Foil Loads at Various Sites 43
3.2.1.1.2.7 Structural Analysis – Milestone 2.1.7 45
3.2.1.1.2.8 Bearing Load Assessment from 2D Analyses – Milestone 2.1.8 50
3.2.1.1.2.9 Bearing Specification – Milestone 2.1.9 51
3.2.1.1.3 Problems Encountered and Departure from Planned Methodology 52
3.2.1.1.4 Assessment of Their Impact on the Project Results 52
3.2.1.2 Bearing Design 52

3.2.1.2.1 Original Hypothesis 52
3.2.1.2.1.1 Subtask 2.2 Bearing Design and Preliminary Testing 52
3.2.1.2.1.2 Subtask 4.1 Flume Testing 52
3.2.1.2.2 Approaches Used 53
3.2.1.2.2.1 Flume Testing 55
3.2.1.2.3 Problems Encountered and Departure from Planned Methodology 58
3.2.1.2.4 Assessment of Their Impact on the Project Results 58
3.2.2 Driveline Build and Validation – Subtask 4.2, Driveline System Testing 61
3.2.2.1 Original Hypotheses 61
3.2.2.2 Approaches Used 61
3.2.2.2.1 Bearing and Driveline Test Components Design 61
3.2.2.2.1.1 Bearing Design Refinement 62
3.2.2.2.1.2 Driveline Configuration 62
3.2.2.2.1.3 Radial only / End Bearing supports 62
3.2.2.2.2 Driveline Test 64
3.2.2.2.2.1 Test Setup 65
3.2.2.2.2.2 Unexplained Behaviors 75
3.2.2.2.2.3 Test Results Summary 77
3.2.2.2.3 Generator Bearing Test 79
3.2.2.2.4 Component Metrics and Project Milestones 79
3.2.2.3 Problems Encountered and Departure from Planned Methodology 80
3.2.2.4 Assessment of Their Impact on the Project Results 80
3.3 Generator Development – Task 3.0 Generator Design, Build and Test 81
3.3.1 Subtask 3.1 Initial Trade Studies, Simulations and Analysis 81
3.3.1.1 Original Hypothesis 81
3.3.1.2 Approaches Used 81
3.3.1.3 Problems Encountered and Departure from Planned Methodology 85
3.3.1.4 Assessment of Their Impact on the Project Results 85
3.3.2 Subtask 3.2 Design Phase 86
3.3.2.1 Original Hypothesis 86
3.3.2.2 Approaches Used 86
3.3.2.3 Problems Encountered and Departure from Planned Methodology 88
3.3.2.3.1.1 Detailed Application Design of the RRM Generator 90
Generator wet bearing design 92
3.3.2.4 Assessment of Their Impact on the Project Results 93

3.3.3 Subtask 3.3 Manufacture and Subassembly Test 93
3.3.3.1 Original Hypothesis 93
3.3.3.2 Approaches Used 93
3.3.3.2.1 Generator Build 93
3.3.3.2.2 Wet bearing development 94
3.3.3.3 Problems Encountered and Departure from Planned Methodology 96
3.3.3.4 Assessment of Their Impact on the Project Results 96
3.3.4 Subtask 3.4 Test, Demonstration, and Final Report 96
3.3.4.1 Original Hypothesis 96
3.3.4.2 Approaches used 97
3.3.4.2.1 Factory Acceptance Test Report 97
3.3.4.2.1.1 Measurement of Motor Parameters 97
3.3.4.2.1.2 Open Circuit Voltage Test 98
3.3.4.2.1.3 Insulation Resistance Test 100
3.3.4.2.1.4 Single Operating Points 101
3.3.4.2.1.5 Efficiency Estimation 102
3.3.4.2.1.6 Temperature Rise Test 104
3.3.4.2.2 Generator wet bearings 105
3.3.4.2.3 Encapsulation qualification 107
3.3.4.3 Problems Encountered and Departure from Planned Methodology 107
3.3.4.4 Assessment of Their Impact on the Project Results 107
3.4 System Refinement and Integration – Task 5.0 System Integration Plan 107
3.4.1 Original Hypotheses 107
3.4.2 Approaches Used 108
3.4.2.1 Basic Loads – Forces Overview. 108
3.4.2.2 Turbine Configurations 109
3.4.2.3 System Design Philosophy 110
3.4.2.4 Middle Bearing Housing: Combination Axial / Radial Bearing 111
3.4.2.5 End Bearing Housing: Radial Bearing 112
3.4.2.6 Generator Bearing Mechanical Design 112
3.4.3 Problems Encountered and Departure from Planned Methodology 112
3.4.3.1 End Stanchion Bearing Design 112
3.4.3.2 Mid Stanchion Bearing Design 113
3.4.3.3 Turbine Shaft Design 114
3.4.3.4 Generator Bearing Design 114

3.4.3.5 Driveline: Final Design 114
3.4.4 Assessment of Their Impact on the Project Results 114
3.5 Project Metrics 114
3.5.1 Original Hypotheses 115
3.5.1.1 Subtask 2.3 System Performance Advancement (SPA) Goals – Driveline and Generator Design Improvements 115
3.5.1.2 Subtask 3.4 Generator Test, Demonstration, and Final Report 115
3.5.1.3 Subtask 4.2, Driveline System Testing 115
3.5.1.4 Task 6.0 Impact Analysis 116
3.5.2 Approaches Used 116
3.5.2.1 Subtask 2.3 System Performance Advancement (SPA) Goals – Driveline and Generator Design Improvements 116
3.5.2.2 Subtask 3.4 Generator Test, Demonstration and Final Report – Component Metrics. 117
3.5.2.3 Subtask 4.2 Driveline System Test – Component Metrics 118
3.5.2.3.1 Supporting Analyses 120
3.5.2.3.1.1 Friction Reduction 120
3.5.2.3.1.2 Rated Power and Rated Efficiency 120
3.5.2.3.1.3 Mass Reduction 122
3.5.2.3.1.4 Bearing Wear 122
3.5.2.4 Task 6.0 Impact Analysis 122
3.5.2.5 LCOE Calculation for the System Integration Design 125
3.5.2.5.1 Availability 126
3.5.2.5.2 LCOE 126
3.5.3 Problems Encountered and Departure from Planned Methodology 127
3.5.4 Assessment of Their Impact on the Project Results 127
4 PRODUCTS 128
4.1 Publications 128
4.2 Inventions/Patent Applications, licensing agreements 128
5 REFERENCES 128

1 EXECUTIVE SUMMARY

1.1 How research adds to the understanding of area investigated

The Power Take-off (PTO) System for Marine Renewable Devices (Project) envisioned the design, manufacture and testing of a generator that would ultimately be suitable for fully flooded seawater operation. This would require a generator design and bearing system capable of operating in the presence of seawater without corrosion. The original generator concept design focused on a switched reluctance electromagnetic design for the generator with the understanding that the switched reluctance design would be more robust and tolerant of a seawater medium. A trade study was conducted to prove that hypothesis, but the results of the study indicated that there was no benefit to adopting a switched reluctance design over a more conventional synchronous permanent magnet design. In addition, the novelty of the switched reluctance design added more technical risk to the Project than was warranted.

ORPC's cost of energy analyses pointed to reliability as being the most critical factor for achieving Project systems performance advancement (SPA) metrics. Consequently, the choice of a permanent magnet (PM) machine design over a potentially less reliable switched reluctance design was necessary to achieve the Project results. As a result, ORPC determined that a PM design was a more appropriate design to achieve the Project goals and ORPC selected a highly qualified PM generator firm for the design, manufacture and factory testing of the generator. The factory acceptance test (FAT) of the generator took place on March 20-22, 2017 and all tests were successfully passed.

Developing a design for a driveline as part of the PTO system required a full understanding of the loads and operating conditions expected. Detailed analyses for developing turbine loads and subsequent definition of bearing specifications were performed using various analytical methods. Two candidate bearing designs were proposed as part of the Project.

After initial design work had been completed, ORPC designed a representative full-scale driveline to validate the detailed design of the advanced driveline components. Full-scale components were manufactured, instrumented and tested, simulating actual system parameters. This full-scale bearing test was conducted at the University of Maine Advanced Structures and Composites Laboratory.
The purpose of this test was to characterize the frictional losses associated with bearings and test the suitability and functionality of some commercially available shaft couplings and expansion bushings in cross-flow turbine drivelines.

In parallel with component testing and dynamometer testing of the PTO system, ORPC performed design work to demonstrate how the advanced PTO system will be integrated with all ORPC turbine generator units (TGUs). The work would focus primarily on the TidGen® TGU and assess how the advanced PTO would be integrated into TidGen® 001 or other units, then field-deployed and tested in an open water environment under actual operational conditions.

1.2 Technical effectiveness and economic feasibility of methods investigates

The Project's SPA goals included improvements in availability, power-to-weight ratio (PWR) and reduction in levelized cost of energy (LCOE).

Table 1. Summary of project achievement of system performance advancement goals.

SPA Metric	Goal	Actual
System Availability	Increase in the system availability from 79% to 94%	*Meets requirement.* Improvements in generator and bearing reliability result in conservative estimates of 93.7%.
PWR	Increase in PWR of 23%	*Exceeds requirement.* The PWR was assessed as system available power at Admiralty Inlet (kW/metric ton). The PWR for the improved system is 0.65 kW/ton, an improvement of 28% over the baseline value of 0.50.
LCOE	Reduction in LCOE of 25%	*Exceeds requirement.* Final projections are $2.49/kWh, an improvement of 81.7% over the baseline $13.58/kWh (calculated for the DOE reference site of Admiralty-Inlet Lower). AEP for a single system increased from 136.6MWh to 182.3MWh, for an improvement of 32.7%. The number of systems required in an array producing 136,000MWh annually decreased from 998 to 746.

1.3 How the Project benefits the public

In addition to the benefits provided to the MHK industry in general, and ORPC in particular, the Project provided benefits to the general public, including the following:

- Increased general awareness of the potential for generation of electricity from ocean energy resources
- Demonstrated continuing advancements in the commercialization of MHK technologies, making them more likely to contribute to the electricity generation supply in America in the coming years
- Continued awareness of the local economic benefits from the MHK industry through job creation and local spending
- Confirmation of a path to improvements in availability, power-to-weight ratio (PWR) and reduction in levelized cost of energy (LCOE).

All Project tasks were completed, and the Project objectives were accomplished. All project milestones and deliverables were met. The designs, methodologies, practices, testing, data, analysis and lessons learned from the Project are a step forward in the development of the U.S. MHK industry and provide a sound basis for ultimate commercialization of ORPC's power systems. Based on the what was learned and demonstrated during the Project, ORPC has determined that the ORPC power systems have the potential of accelerating the commercialization of tidal and ocean current MHK power systems.

2 COMPARISON OF ACCOMPLISHMENTS WITH GOALS AND OBJECTIVES

2.1 Project Description

The Project envisioned the design, build and test of a generator which would ultimately be suitable for fully flooded seawater operation. This would require a generator design capable of operating in the presence of seawater without corrosion, and a bearing system capable of such operating conditions. The original generator concept design focused on a switched reluctance electromagnetic design for the generator with the understanding that the switched reluctance design would be more robust and tolerant of a seawater medium. A trade study was conducted to prove that hypothesis, but the results of the study indicated that there was little benefit to adopting a switched reluctance design over a more conventional synchronous permanent magnet design, and that the novelty of the switched reluctance design added more technical risk to the Project than was warranted.

The original contractor for the generator design and delivery was RCT Systems, Linthicum, MD, which had significant experience in the design of switched reluctance electromagnetic machines. ORPC had performed an extensive survey of generator manufacturers for the Project, and originally selected RCT Systems based on its existing switched reluctance machine (SRM) generator technology.
ORPC's cost of energy analyses pointed to reliability as being the most critical factor for achieving Project SPA metrics. Consequently, the choice of a permanent magnet machine design over a potentially less reliable switched reluctance design was necessary to achieve the Project results. As a result of this analysis, ORPC determined that a permanent magnet (PM) design was a more appropriate design to achieve the Project goals.

Because of these considerations, ORPC contracted with RRM to complete the detailed application design, and to build and test a permanent magnet generator as well as a subsea-worthy converter electronics unit. RRM completed a design package for a CDR. The final generator design was adapted to ORPC's application, with mechanical interfaces, sensors, hybrid oil system requirements (compensators, seals) and electrical braking comprising design details finalized.

The factory acceptance test (FAT) of the generator from RRM took place on March 20-22, 2017. The intention of this test was to show functionality of the generator as per the documented design by IEC test standards which were outlined in the FAT report. All tests were successfully passed during the test period.

To develop a design for a driveline as part of the power take off system requires a full understanding of the loads and operating conditions expected. Detailed analyses for developing turbine loads and subsequent definition of bearing specifications were performed using various analytical methods.
Two candidate bearing designs were proposed as part of the Project. These were an innovative polymer roller element bearing design, and a low friction diamond sliding bearing concept.[1] To obtain information related to how these bearing concepts would perform, ORPC conducted flume testing for different bearing implementations.

[1] C.H. Cooley, M.M. Khonsari, & B. Lingwall, (2012). The Development of Open Water-lubricated Polycrystalline Diamond (PCD) Thrust Bearings for Use in Marine Hydrokinetic (MHK) Energy Machines, https://www.osti.gov/servlets/purl/1056274/

After initial design work had been completed, ORPC designed a representative full-scale driveline to validate the detailed design of the advanced driveline components. Full-scale components were manufactured and instrumented and tested, simulating actual system parameters. This full-scale bearing test was conducted at the University of Maine Advanced Structures and Composites Laboratory.
The purpose of this test was to characterize the frictional losses associated with bearings and test the suitability and functionality of some commercially available shaft couplings and expansion bushings in cross-flow turbine drivelines.

In parallel with component testing and dynamometer testing of the PTO system, ORPC performed design work to demonstrate how the advanced PTO system will be integrated with all ORPC TGUs. The work would focus primarily on the TidGen® TGU and assess how the advanced PTO would be integrated into TidGen® or other units, then field-deployed and tested in an open water environment under operational conditions.

2.2 SPA Metrics

The Project's SPA goals included improvements in availability, power-to-weight ratio (PWR), and reduction in LCOE. Section 3.5.2.1 for Subtask 2.3, outlined methodologies for estimating annual energy production (AEP) and LCOE, based on the Project results. Table 2 provides a summary of the final project achievement of SPA goals.

Table 2. Summary of project achievement of SPA goals.

SPA Metric	Goal	Actual
System Availability	Increase in the system availability from 79% to 94%	*Meets requirement.* Improvements in generator and bearing reliability result in conservative estimates of 93.7%.
PWR	Increase in PWR of 23%	*Exceeds requirement.* The PWR was assessed as system available power at Admiralty Inlet (kW/metric ton). The PWR for the improved system is 0.65 kW/ton, an improvement of 28% over the baseline value of 0.50.
LCOE	Reduction in LCOE of 25%	*Exceeds requirement.* Final projections are $2.49/kWh, an improvement of 81.7% over the baseline $13.58/kWh (calculated for the DOE reference site of Admiralty-Inlet Lower). AEP for a single system increased from 136.6MWh to 182.3MWh, for an improvement of 32.7%. The number of systems required in an array producing 136,000MWh annually decreased from 998 to 746.

2.3 Project Milestones

All project milestones and deliverables were met (Table 3).

Table 3. Project milestones, goals and actual deliverables

Milestone	Goal	Actual
4.2.3 PTO Friction Reduction	Driveline frictional losses will have been demonstrated to be less than 5% of rated power as compared to a baseline of 15% of rated power.	*Exceeds requirement.*
4.2.4 PTO Rated Power	Complete PTO will demonstrate achievement of rated power.	*Exceeds requirement.*
4.2.5 PTO Rated Efficiency	Complete PTO will demonstrate achievement of rated efficiency.	*Exceeds requirement.*
4.2.6 PTO Mass Reduction	Complete PTO will demonstrate achievement in mass per unit power of 20% as compared to baseline.	*Meets requirement.* Available power calculations with the RRM generator and new bearings show a mass per unit reduction from baseline of 22.1%.
4.2.7 PTO Bearing Wear	Complete PTO will demonstrate achievement of 5+ year maintenance intervals for all bearings through measured bearing wear and supporting engineering analyses.	*Meets requirement.* New bearings had no measured wear after driveline testing, or from testing of scale model bearings by the supplier. Failure mode is thermal fracture rather than wear; with a driveline design that avoids edge loading of the bearings and promotes water flow through bearings during operation, the bearings show potential to last for entire system service life of 20 years. Validation in open water is required for predictions greater than 5-year component life.

3 SUMMARY OF PROJECT ACTIVITIES

3.1 Project Management – Task 1.0 Project Planning

3.1.1 Original Hypotheses

Project Planning was performed per Task 1.0 Project Plan.

Under Subtask 1.1, a Project Management Plan (PMP) was to be developed by Project participants, finalizing the Project objectives, deliverables, schedules, Gantt charts, technical risk mitigations, risk management procedures, funding and costing profiles, work breakdown structures, organization, and structure. Maintenance of the Gantt chart was to be performed by ORPC. ORPC was to hold monthly meetings with Project partners by teleconference and quarterly meeting in person at a location of mutual convenience.

Under Subtask 1.2, ORPC and partners were to finalize the Intellectual Property Management Plan (IPM). The IPM was to serve as the coordinating document between Project partners and address issues related to control and dissemination of confidential information, intellectual property and data, and handling of commercialization arrangements, as well as to provide means and methods for resolving intellectual property disputes between partners.

3.1.2 Approaches Used

A PMP was developed by the Project partners, which included Project objectives, deliverables, schedules, Gantt charts, technical risk mitigations, risk management procedures, funding and costing profiles, work breakdown structures, organization, and structure. ORPC maintained the Project Gantt chart. ORPC held monthly meetings with Project partners by teleconference and quarterly meeting in person at a location of mutual convenience.

ORPC and partners finalized the IPM plan, which served as the coordinating document between Project partners and addressed issues related to control and dissemination of confidential information, intellectual property and data, and handling of commercialization arrangements, as well as provided means and methods for resolving intellectual property disputes between partners.

3.1.3 Problems Encountered and Departure from Planned Methodology

The Project envisioned the design, build and test of a generator which would ultimately be suitable for fully flooded seawater operation. This would require a generator design capable of operating in the presence of seawater without corrosion, and a bearing system capable of such operating conditions. The original generator concept design focused on a switched reluctance electromagnetic design for the generator with the understanding that the switched reluctance design would be more robust and tolerant of a seawater medium. A trade study was conducted to prove that hypothesis, but the results of the study indicated that there was little benefit to adopting a switched reluctance design over a more conventional synchronous permanent magnet design, and that the novelty of the switched reluctance design added more technical risk to the Project than was warranted.

The original contractor for the generator design and delivery was RCT Systems, Linthicum, MD, who had significant experience in the design of switched reluctance electromagnetic machines. ORPC had performed an extensive survey of generator manufacturers for the Project, and originally selected RCT Systems based on its existing switched reluctance machine (SRM) generator technology.
ORPC's cost of energy analyses pointed to reliability as being the most critical factor for achieving Project SPA metrics. Consequently, the choice of a permanent magnet machine design over a potentially less reliable switched reluctance design was necessary to achieve the Project results. As a result of this analysis, ORPC determined that a permanent magnet (PM) design was a more appropriate design to achieve the Project goals.

ORPC directed RCT Systems to continue with a detailed design of a permanent magnet generator, while in parallel ORPC worked with another, more proven generator manufacturer of subsea PM machines to mitigate technical and project risk. The manufacturer, SmartMotor AS, since acquired by Rolls-Royce Marine (RRM), performed a preliminary design to adapt their existing encapsulated permanent magnet systems for ORPC's application. The two designs were compared to each other as an additional trade study prior to procurement. A direct comparison of the PM designs indicated that the RRM design would be less costly, less risky, and would provide a clearer path towards a water filled machine.

With nineteen years of experience with development, build and test of permanent magnet machines, RRM had a track record of multi-year, reliable subsea operation. RRM possessed a wealth of design and subsea operations experience in permanent magnet machines and power convertors. Their products were easily scalable to meet the RPM/torque specifications for ORPC's tidal applications. Advantages include proven, reliable field deployments such as subsea oil-filled machines that have been in operation for more than ten years and at service depths of 4500m, as well as commercialized encapsulation technology in tunnel thrusters developed by SmartMotor prior to being acquired by RRM in 2013. Their design for ORPC's application scaled an existing product already under qualification for RRM and was part of a detailed system validation program that leveraged a high-quality manufacturing facility as well as a new prototype and test center capable of testing frequency converters up to 1.7 MVA and generators up to 1 MVA in a back to back arrangement. With an extensive set of performance and reliability data and the provision of conditional monitoring capability, RRM provided a high confidence of being able to achieve the design goals for the Project.

Because of these considerations, ORPC contracted with RRM to complete the detailed application design, and to build and test a permanent magnet generator as well as a subsea-worthy converter electronics unit. RRM completed a design package for a CDR.

In addition to a change in generator manufacturer, ORPC decided that instead of RRM performing driveline testing, this would instead be performed by ORPC. This decision was driven by budgetary and project schedule considerations.

IPM plans and other project documentation was revised to include RRM in the project build.

3.1.4 Assessment of Their Impact on the Project Results

The plans added a level of control and transparency to the Project which improved Project management and control. The Project was completed and within budget for all team members.

The IP management plan clarified means and methods of publication for team members. Multiple papers and presentations were made related to the Project. Intellectual property concerns related to the publication of these results were not an issue.

The trade study approach provided a structured means for assessing and pivoting Project towards best opportunities to achieve Project objectives.

3.2 Driveline Development – Task 2.0 Driveline Design, and Task 4.0 Driveline Build and Validation

To develop a design for a driveline as part of the power take off system requires a full understanding of the loads and operating conditions expected. Detailed analyses for developing turbine loads and subsequent definition of bearing specifications were performed using various analytical methods.

Two candidate bearing designs were proposed as part of the Project. These were an innovative polymer roller element bearing design, and a low friction diamond sliding bearing concept[2]. To obtain information related to how these bearing concepts would perform, ORPC conducted flume testing for

[2] Cooley, 2012

different bearing implementations. The testing of polymer roller element bearings replicated flume testing of polycrystalline diamond bearings (PCD) undertaken as part of a prior effort funded by the Department of Energy – "Abrasion Testing of Critical Components of Hydrokinetic Devices."[3] Several plastic roller bearings were manufactured for evaluating the performance of these plastics in comparison to the PCD bearing solution. In addition to flume testing, corrosion testing of the PCD bearings was conducted to confirm that they would have acceptable long-term behaviors.

After initial design work had been completed, ORPC designed a representative full-scale driveline to validate the detailed design of the advanced driveline components. Full-scale components were manufactured and instrumented and tested, simulating actual system parameters. This full-scale bearing test was conducted at the University of Maine Advanced Structures and Composites Laboratory. These separate tasks are discussed together here since the design of the bearing system necessarily involved design work, validation of the design by testing, and redesign based on test results obtained.

3.2.1 Driveline Design – Task 2.0 Driveline Design, and Subtask 4.1 Flume Test

3.2.1.1 *Load Assessment and Requirements – Subtask 2.1 Load Assessment*

3.2.1.1.1 Original Hypotheses

ORPC was to determine the structural loading upon a reference TidGen® installation from computational models to assess loads upon individual bearing, shaft, and coupling components. Torque and speed parameters to inform generator system design were to be extracted from these models (to include streamtube, vortex codes, and 2D and 3D CFD models), with multiple turbulence models, including detached eddy simulations (DES). A reference design speed of 4.5 m/s was to be used as the upper speed range to fit with expected highest flow applications of the demonstration system. Inflow turbulence was to be included in the vorticity codes to assess the effect of turbulence on the system loads. Structural analysis of the drive-line would include calculation of stresses and deflections under load and analysis of unsteady loads and vibration.

Loads reporting would present results for the following analytical cases:

- Streamtube model of the TidGen® turbine at the defined reference speed predicting coefficient of power (Cp) versus tip speed ratio (TSR), driveline torques, and turbine drag loads
- Vortex code model of the TidGen® turbine at the defined reference speed predicting Cp versus TSR and driveline torques
- 2D RANS analysis of the TidGen® turbine at the defined reference speed predicting Cp versus TSR, transient driveline torques, turbine drag loads, flow diversion in the turbine flow direction
- 2D DES analysis of the TidGen® turbine at the defined reference speed predicting Cp versus TSR, transient driveline torques, turbine drag loads under the conditions of zero inflow turbulence
- 2D DES analysis of the TidGen® turbine at the defined reference speed predicting Cp versus TSR, transient driveline torques, turbine drag loads under the conditions of an assumed inflow turbulence intensity representative of tidal sites
- 3D RANS analysis of the TidGen® turbine at the defined reference speed predicting Cp versus TSR, transient driveline torques, turbine drag loads, turbine axial loads, and flow diversion in the turbine long axis
- Structural analysis of the stresses and deflections of the driveline under load and analysis of unsteady loads and vibration under the worst-case loadings from the above analyses

[3] Worthington, M., Ravens, T., & Ali, M. (2013). Abrasion Testing of Critical Components of Hydrokinetic Devices, Final Technical Report, US Department of Energy, DE-EE0003631

- Assessment of the loads (axial, lateral, and bending) experienced by each bearing in the driveline under the worst-case loadings from the above analyses

The load report was to detail modeling techniques and assumptions, codes, means, and methods for the above analyses. These load analyses were to define the loads acting on the bearing and hence the bearing design criteria.

3.2.1.1.2 Approaches Used

ORPC's advanced design cross-flow turbine has multiple twisted foils attached by spokes to the shaft about which the turbine rotates. As a turbine foil rotates it presents a varying angle to the oncoming flow – the angle of attack (Figure 1). This angle of attack is measured between the relative flow and mean chord line of the foil. At angles of attack less than the stall angle, the foil generates a lift force perpendicular to the relative flow direction and a drag force parallel to the relative flow direction. The relative positions of these forces generate a component of force tangential to the turbine, creating a net positive torque on the turbines. This causes them to rotate and transmit torque to the generator.

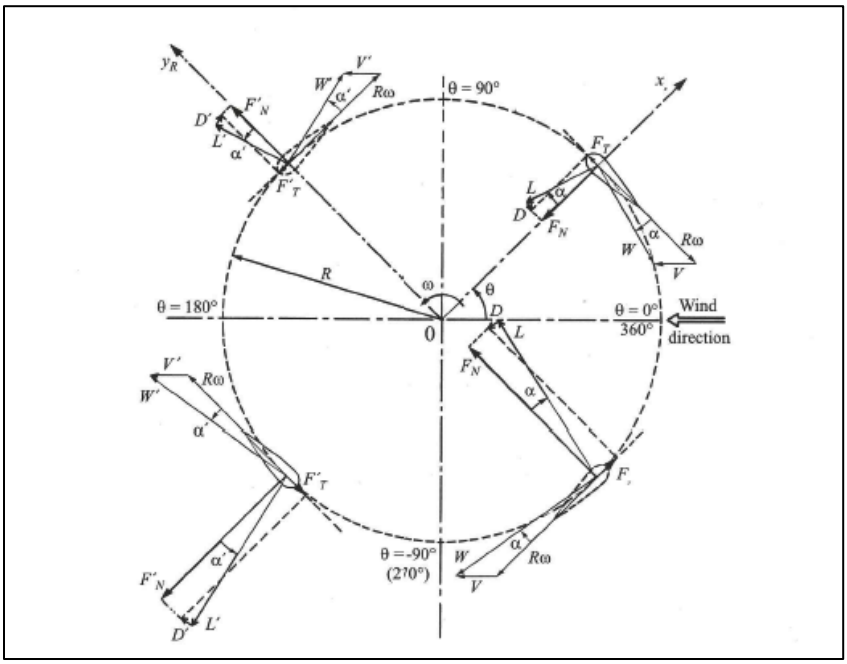

Figure 1. Cross-flow turbine geometry showing angles of attack, lift, and drag forces for different rotational positions of a hydrofoil.[4]

Specific input parameters for this model are the TidGen® 1.0 turbine geometry, a lookup table for lift and drag coefficients for the TidGen® 1.0 foil profile, and physical properties of seawater (Table 4).

Table 4. Properties for the TidGen® 1.0 turbine

Turbine Radius (m)	1.4 m
Number of foils	4
Turbine Solidity (Nc/πD)	0.172
Foil chord	0.351 m

Turbine Length (m)	5.6 m
Number of turbines	4
Turbine area (m^2)	14.8 m^2
Total turbine area (m^2)	59.1 m^2
Free stream water speed (m/s)	3.0 m/s
Seawater density	1025 kg/m^3
Seawater viscosity	0.001 Ns/m^2
Lift and drag curves	NACA0018[4]

The turbine foils in the TidGen® 1.0 configuration twist in spiral fashion 90 degrees about the circumference of the turbine. The turbine generator units (TGUs) are distributed so that the foil orientation alternates to resemble a herringbone configuration. This arrangement leads axial forces generated by adjacent turbines to balance each other. Additionally, each foil may be contoured, or barreled, so that when assembled the TGU is no longer perfectly rectangular.

The goal of the analysis work was to develop a conservative estimate of the hydrodynamic loads that the turbines and bearings will experience during operation. A discussion of each analysis is presented, and a summary of the loads predicted by each analysis is provided.

3.2.1.1.2.1 Streamtube Modeling – Milestone 2.1.1

A primary modeling tool to predict turbine performance and loadings is the multiple streamtube momentum model.[5] Using this model, the turbine frontal area is divided into streamtubes. The aerodynamic and axial drag forces on the foil elements are calculated for each streamtube. The axial drag force is also calculated using the momentum-based actuator disk theory.[6] The effective stream velocity at the turbine foil is iterated until calculations of drag force from the streamtube momentum model and actuator disc theory methods produce equal results. The amount by which the free-stream velocity is modified is the axial induction factor (*a*).

$$V_{axial} = (1-a)\cdot V_{free_stream}$$

The vector addition of the modified axial velocity and foil velocity give the relative velocity for calculation of the aerodynamic forces.

[4] Lift and drag tables for a full range of angle of attack over a wide range of Reynolds numbers are available for only a very few profiles. Using data for NACA0018 profiles has been found to be sufficiently accurate given other deficiencies in the streamtube modeling methodology.

[5] J.H. Strickland, (1975). The Darrieus Turbine: A Performance Prediction Model Using Multiple streamtubes, SAND75-0431, Sandia Labs, Energy Report.

[6] H. Glauert, (1999). The Elements of Aerofoil and Airscrew Theory, Cambridge Science Classics.

Glauert's theory works for induction factor values less than a = 0.5, but additional correlations are required above a = 0.5. These are provided by M.L. Buhl.[7]

Streamtube models are accurate for prediction of cross turbine power and efficiency performance. Performance of the turbine is presented below in terms of Cp as a function of turbine TSR where TSR is defined as:

$$Tip\ Speed\ Ratio = \frac{Foil\ Speed}{Free\ Flow\ Speed}$$

Embedded in the streamtube model are assumptions of upstream and downstream symmetry, which results in equal foil loads for the upstream and downstream turbine sections, which is clearly unrealistic. However, the ability of the streamtube model to predict global turbine loads is well known.

The two operating points presented represent opposite ends of the operating range. In the freewheel condition when no power is produced, the turbine operates at its highest TSR. This condition is achieved by providing a zero-torque command. At the baseline operating condition, a torque is demanded. This baseline operating condition was selected as it provided a good balance of power output while also allowing extended on-grid operation without disconnects. Higher power performance is achievable but at the risk of uncontrolled grid disconnects (Figure 2).

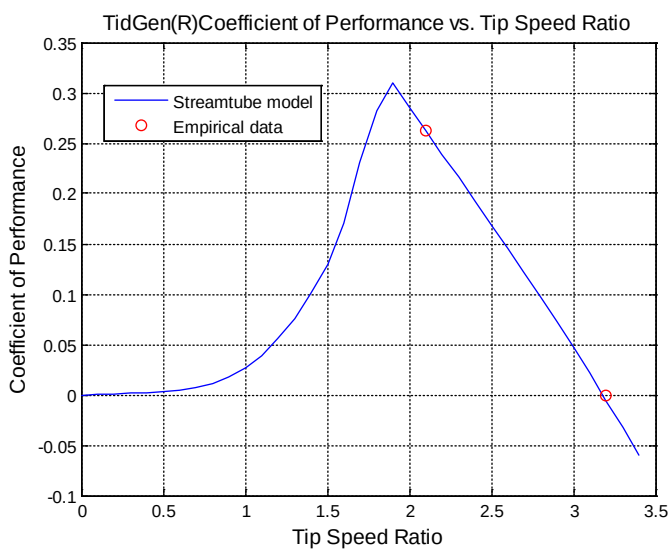

Figure 2. Coefficient of performance as a function of TSR as predicted by ORPC's streamtube model and compared with empirical data, with an assumed bearing model drag parameter (μ) of 0.53.

Normalized tangential foil loads are presented for the maximum power condition and freewheel condition as a function of foil angular position (Figure 3). The plot clearly illustrates the upstream/downstream load symmetry predicted by the multiple streamtube models, as the torque in the downstream section is equal to the torque produced by the upstream section. This is inaccurate as

[7] M.L. Buhl, (2005). A New Empirical Relationship Between Thrust Coefficient and Induction Factor for the Turbulent Windmill State, National Renewable Energy Laboratory, Technical Report NREL/TP-500-36834.

downstream torque performance will be significantly affected by local flow conditions in the turbine. At the freewheel condition, torque production is low.

Normalized normal foil loads are presented for the maximum power condition and freewheel condition as a function of foil angular position (Figure 3). The direction of normal load applied changes from the upstream to the downstream side of the turbine, as the local foil coordinate system changes orientation relative to the Cartesian coordinate system. Normal loads are an order of magnitude greater than tangential loads and are a maximum in the freewheel condition. Again, several assumptions implicit in the streamtube modeling technique will adversely affect the accuracy of foil load predictions. In addition, the presence of high induction factors for many of the streamtubes in the freewheel condition and lack of a fully verified induction factor correlation make these results doubtful.[8]

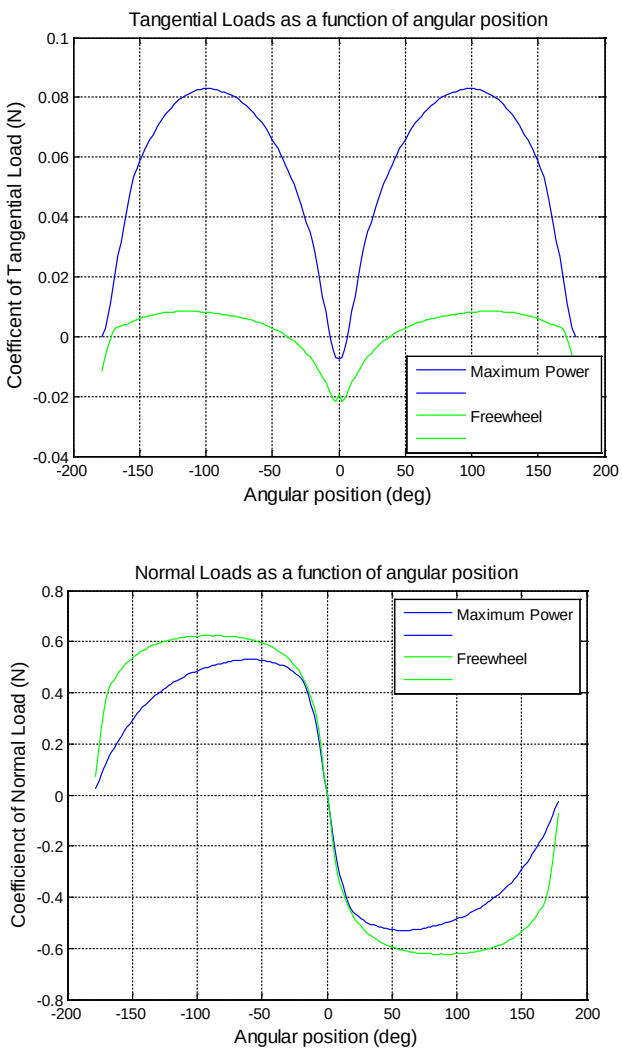

Figure 3. Non-dimensional force coefficient from streamtube model as a function of angular foil position for the maximum power and the maximum speed cases. The upper curve shows the tangential loads,

[8] Chapman et al, The Buhl High-Induction Correction for Blade Element Momentum Theory Applied to Tidal Stream Turbines, Renewable Energy, Volume 60, December 2013, Pages 472–480

with higher tangential forces evident for the maximum power case. The lower curve shows normal loads, indicating that maximum loads occurs at freewheel.

These force coefficients may be translated into X and Y coefficients representing the forces acting in the flow direction and normal to the flow direction. This can be done for the individual foil and for the entire turbine. Here we present data for non-dimensional X and Y force coefficients for a single foil. The streamtube model cannot predict axial loads (Fz), (Figure 4).

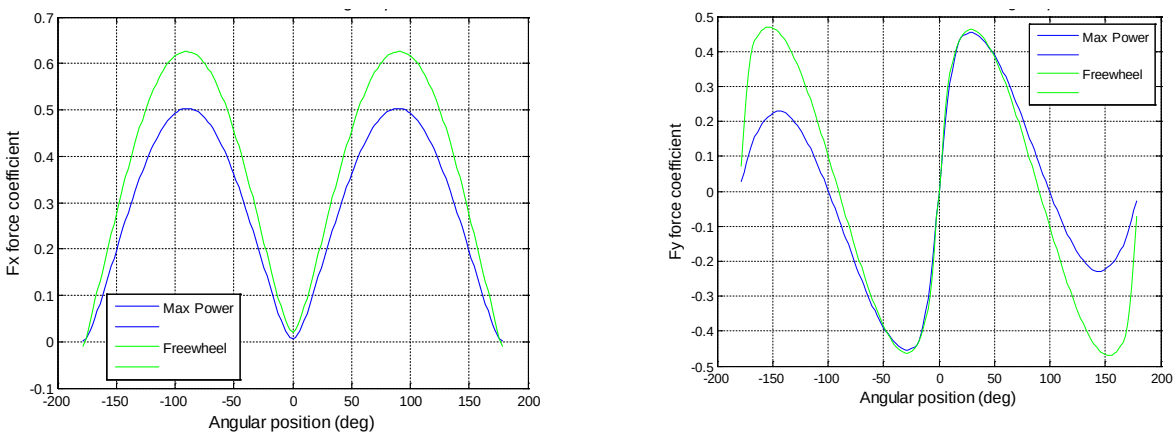

Figure 4. Non-dimensional force coefficient, Fx and Fy, for the maximum power and the maximum rotational speed case as a function of foil angular position, for a single foil. The x direction force is aligned with the flow, and y perpendicular to the flow.

Reducing solidity of the turbine will improve efficiency of the device. We investigated the effect of changing from a four-foil to a three-foil turbine using the same chord foil (Figure 5).

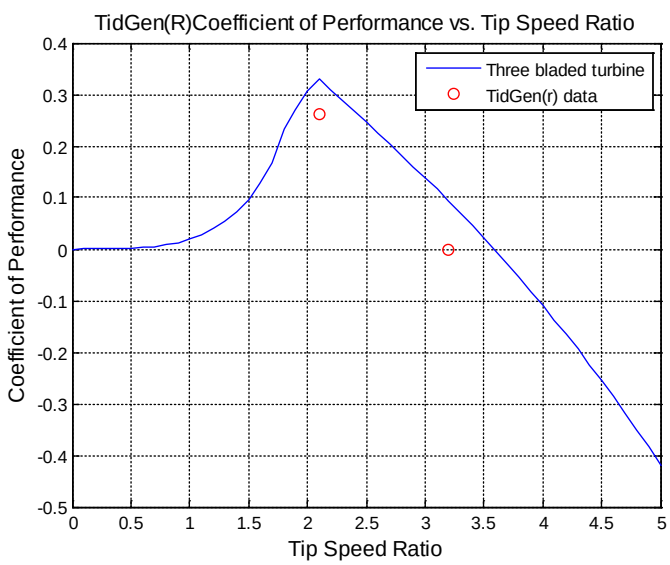

Figure 5. Coefficient of performance versus TSR for a TidGen® with three foils instead of four. The measured data for the four-foil TidGen® turbine is shown. Reducing the solidity of the turbine increases the maximum efficiency achievable and increases the freewheel speed but does not necessarily shift the optimum tip speed ratio for maximum efficiency.

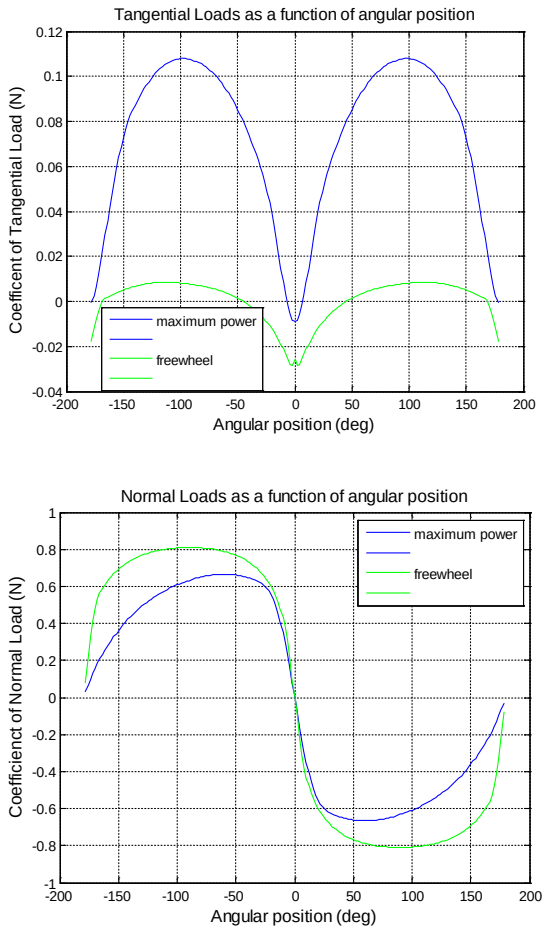

Figure 6. Tangential and normal force coefficient for a three foil TidGen® turbine. Normal loads are greatest for the freewheel condition and tangential loads are higher for the operating condition.

Loads on the turbine may be developed from these data for different flow speeds. These results are presented below when comparing the results of differing analysis techniques.

3.2.1.1.2.2 Vortex Modeling – Milestone 2.1.2

Sandia National Laboratory (SNL) developed CACTUS, a vorticity code for analysis of cross-flow turbines.[9] SNL worked with ORPC to develop a model of the TidGen® turbine in CACTUS. As the CATCUS code proved unwieldy to use this particular CACTUS model was provided by SNL.[10]

A sweep of TSRs was performed with CACTAS for helical and straight foil turbines. Results indicated a maximum CP of 0.47 (Figure 7).

[9] J.C. Murray, & M. Barrone, (2011). The Development of CACTUS, a Wind and Marine Turbine Performance Simulation Code, 49th AIAA Aerospace Sciences Meeting including the New Horizons Forum and Aerospace Exposition 4 - 7 January 2011, Orlando, Florida

[10] Technical Support of Marine & Hydrokinetic Technology Industry Solicitation, Task 3: Model-to-Model Comparison

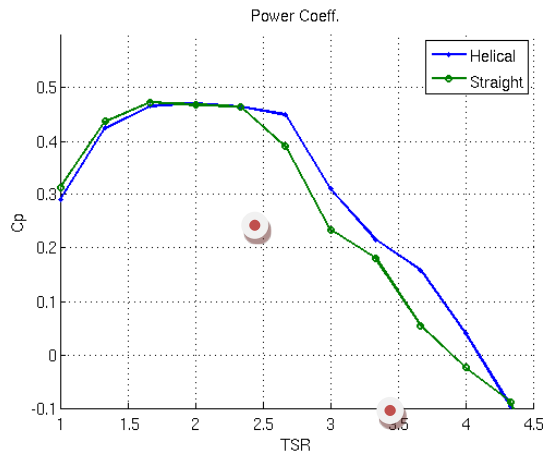

Figure 7. CACTUS model results for coefficient of performance as a function of TSR. Empirical TidGen® 1.0 data is also shown. Two runs for CACTUS are compared with a straight foil TidGen® arrangement and the as built TidGen® with a 120° helical twist to the foil. CACTUS predicts little difference between the two geometries but does predict a higher performance than the empirical data.

Clearly the performance predicted by CACTUS overestimate the efficiency of the turbine, primarily due to the exclusion of bearing friction in the model.

For a TSR of 1.75, force coefficients for a single turbine are generated from CACTUS. Horizontal flow forces dominate as expected. Results are presented below comparing Fx and Fy between CACTUS and the streamtube model at a TSR of 1.75 (Figure 8 and Figure 9).

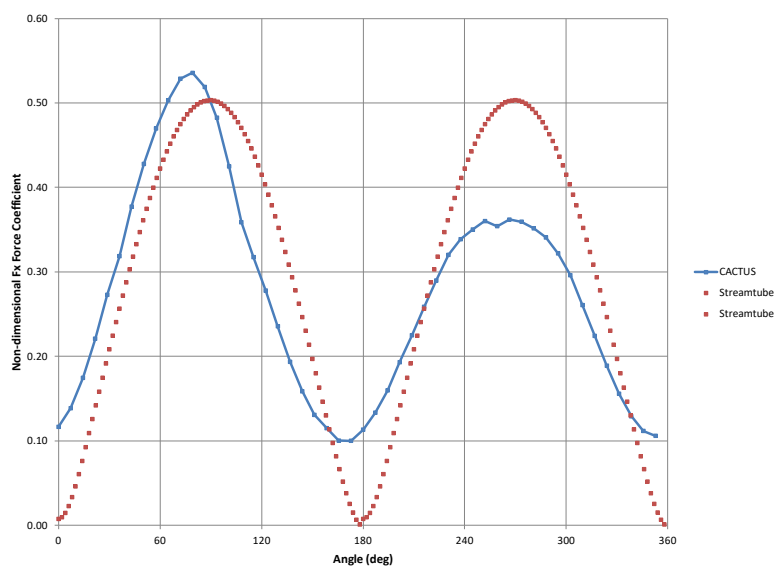

Figure 8. Fx force coefficients for TSR = 1.75, TidGen® turbine as a function of rotational position for a single foil, comparing CACTUS with streamtube model results. Streamtube model results have upstream/downstream symmetry, while CACTUS models results show higher loadings upstream.

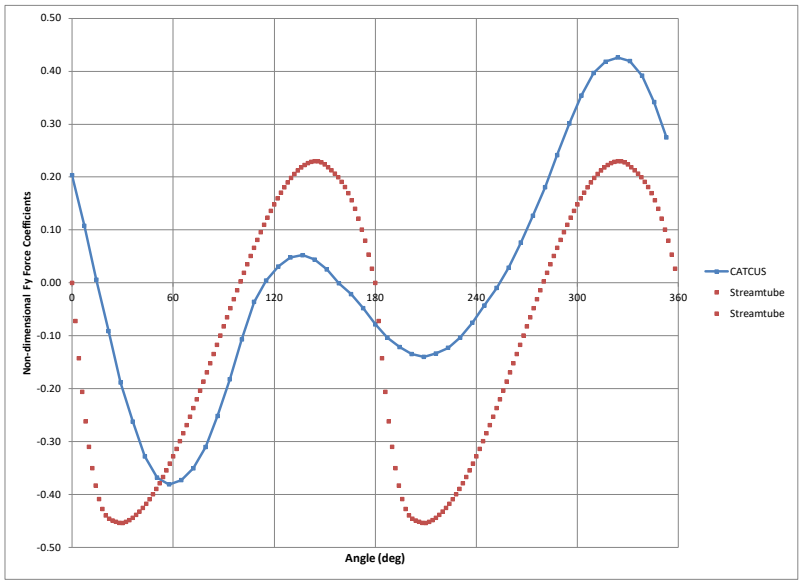

Figure 9. Fy force coefficients for TSR = 1.75, TidGen® turbine as a function of rotational position for a single foil, comparing CACTUS with streamtube model results. Streamtube model results have upstream/downstream symmetry, while CACTUS models results show higher loadings upstream.

The vortex method shows differences between upstream and downstream foil loads, but loads are similar in magnitude and shape to those predicted by the simpler and easier to use streamtube model.

3.2.1.1.2.3 2D RANS – Milestone 2.1.3

A CFD model for the TidGen® turbine rotor was developed and run for multiple tip speed cases. The grid was generated by Pointwise and extruded to 1 cell deep to provide a quasi-3D grid suitable for the FLUENT v14.5 2D unsteady analysis solver. Rotor cases were run to obtain steady periodic forces, starting from most recent run or previous unsteady moving mesh run when available, or from uniform flow initial conditions. Physical properties of seawater were used. The model was run with a uniform inflow speed of 1.75 m/s and rotor RPM is varied to provide the desired TSR (Figure 10).

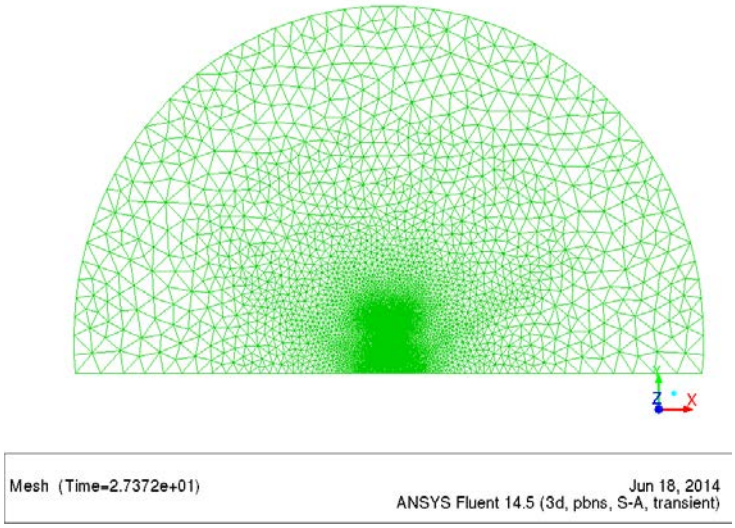

Figure 10. Outer mesh for the stationary flow domain. The sea floor is represented at the horizontal X boundary. The turbine is located at the center of the domain.

The seafloor is modeled as a no-slip wall. The semicircular boundary is modeled with a fixed x-flow velocity and zero y-flow component. A turbulence viscosity ratio (ratio of turbulent viscosity to molecular dynamic viscosity) of 10 was selected for this modeling work, a relatively low inflow turbulence level which had been used extensively in previous 2D simulations of TidGen® (Figure 11 and Figure 12).

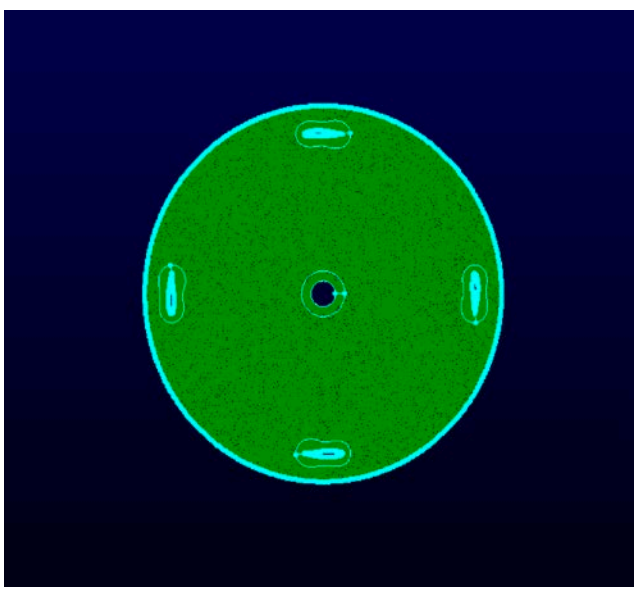

Figure 11. Rotor rotating mesh, embedded within the stationary mesh. Hollow space in the center represents the rotating shaft. A fine level of mesh is used to transition from the outside flow field to the rotor domain

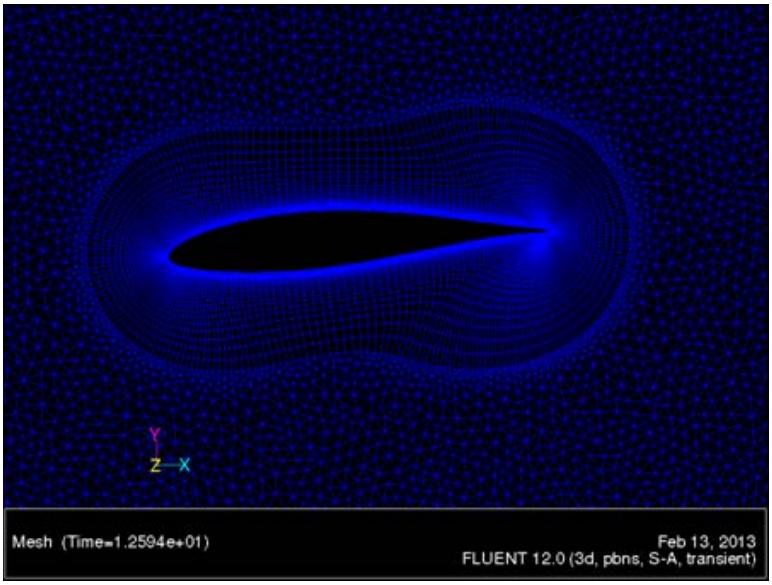

Figure 12. Mesh in the vicinity of the foils. The mesh is refined close to the foil surface and at the trailing edge.

A series of TSRs were modeled in FLUENT. Figure 13 presents the results for coefficient of performance as a function of TSR for these 2D CFD models.

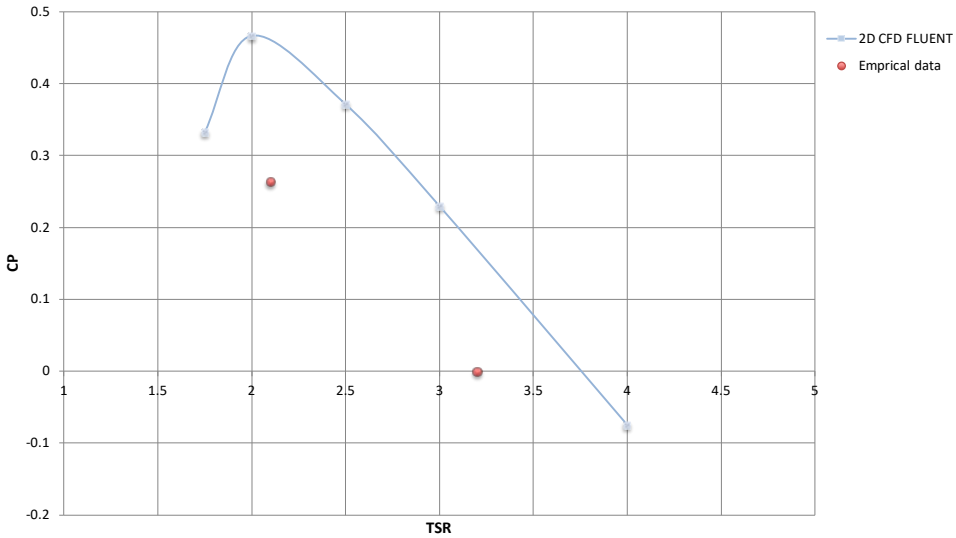

Figure 13. Coefficient of performance as a function of TSR as predicted by a 2D CFD FLUENT model of the TidGen® turbine. Turbulent viscosity ratio is set equal to 10. Empirical data from TidGen® is also presented, showing that 2D CFD overpredicts efficiency.

The 2D CFD results clearly over predict the power performance of the turbine. This is consistent with other work performed by ORPC, which shows that significant 3D effects are present in cross-flow turbines and that 2D CFD work will consistently over predict performance (Figure 14 and Figure 15).[11]

[11] Numerical Modeling Study to Investigate RivGen® Strut Drag on Power Performance, Sandia National Laboratory.

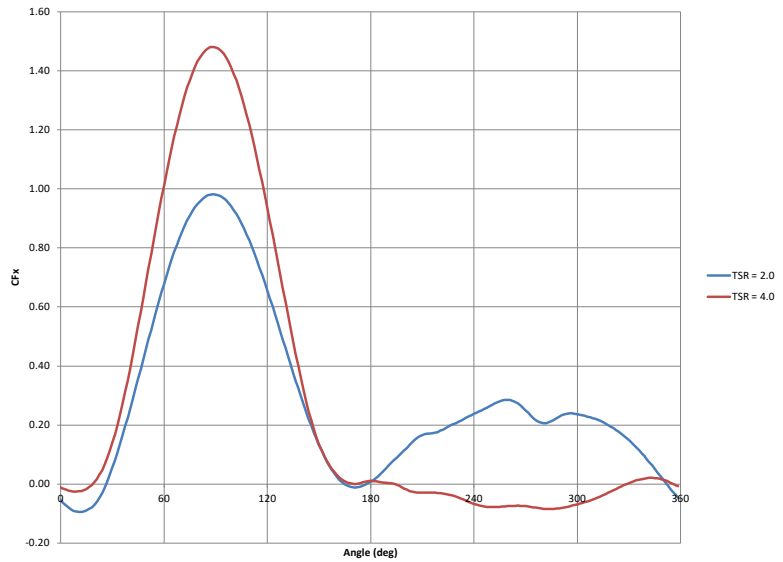

Figure 14. 2D CFD results for non-dimensional X force (drag) coefficients (flow direction) for TidGen® turbine foils. At TSR = 2.0, and at TSR = 4.0. The blue curve show drag forces for the max power operating condition. The red curve shows drag forces for the freewheel condition.

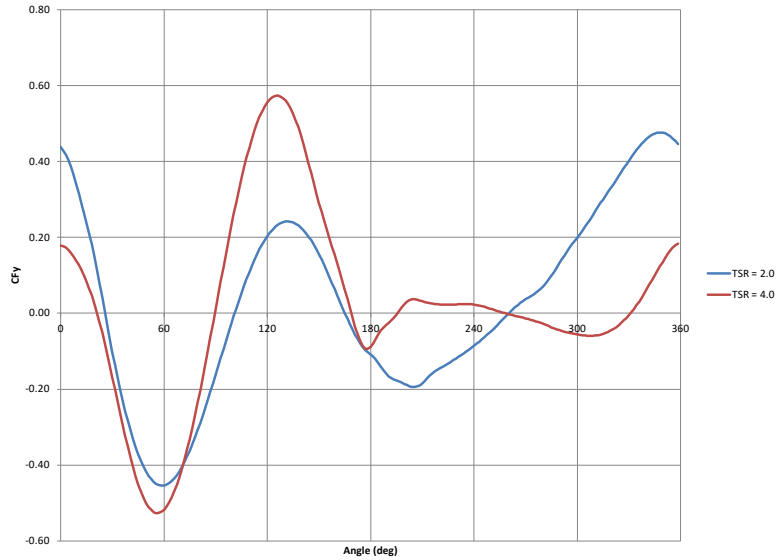

Figure 15. Non-dimensionnel Y force coefficients for TidGen® turbine foils. At TSR = 2.0 and at TSR = 4.0. The blue curve show lift forces for the max power operating condition. The red curve shows lift forces for the freewheel condition.

These plots confirm that drag loads on the turbine are maximum at the freewheel condition.

Comparison with Streamtube and CACTUS Models

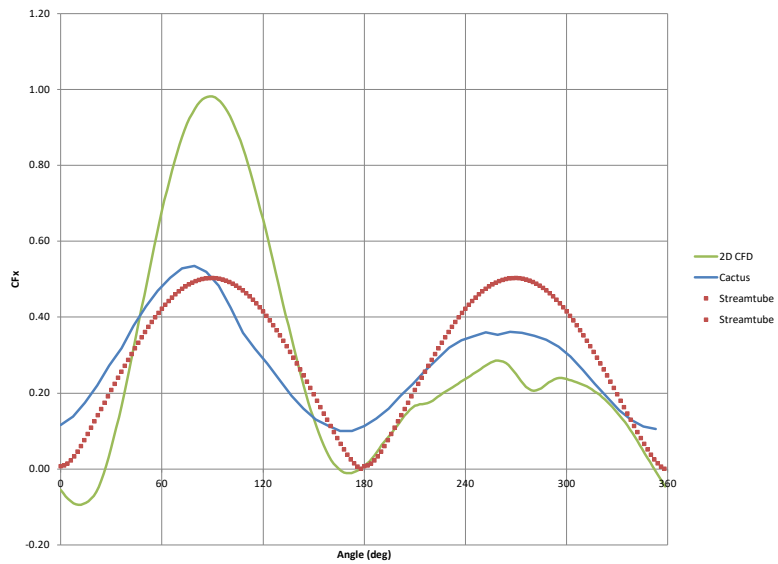

Figure 16. Non-dimensional X force coefficients for TidGen® turbine foils for a TSR of 2.0. Results are compared for 2D CFD, CACTUS and streamtube models. At this maximum power condition represented by the 2D CFD results (green) show higher forces on the upstream side of the turbine than either the streamtube or vortex method models.

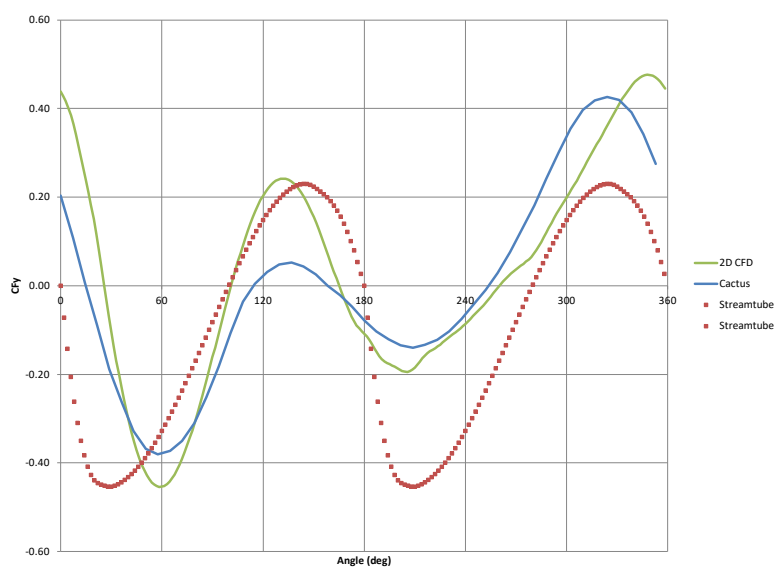

Figure 17. Non-dimensional Y force coefficients for TidGen® turbine foils for a TSR of 2.0. Results are compared for 2D CFD, CACTUS and streamtube models. At this maximum power condition represented by the 2D CFD results (green) show similar forces on the upstream side of the turbine as compared with the streamtube, and similar loads to the cactus model for upstream and downstream.

Results for the foil Fx values from the 2D CFD model are larger than from the streamtube and CACTUS models for the maximum power condition, showing a strong bias towards upstream loading. The

average values are similar. The Fy values for this operating condition are consistent between models. This bias towards upstream loads is consistent with our understanding of cross-flow turbine operation, where flow speed in the wake is reduced. This provides some confidence in these results as compared with streamtube and vortex methods foil load predictions.

3.2.1.1.2.4 2D DES – Milestones 2.1.4 and 2.1.5

A scale-resolving CFD model for the TidGen® turbine rotor utilizing the detached eddy simulation (DES) method was developed and run for a selected TSR.

Conventional RANS (or unsteady URANS) CFD simulation models the effects of turbulence using a simplified approach (the Boussinesq approximation) that uses an “effective” or “eddy” viscosity to represent all scales (both large and small) of turbulent mixing effects in a flow. There are a wide range of RANS turbulence models that can be applied to flow simulations, which were developed for a wide range of flow problems. These RANS models are relatively simple and computationally efficient but often fail to correctly model the effects of flow separation which involve the larger scales of turbulent motions.

The intent of large eddy simulation (LES) and DES is to simulate the larger scales of turbulent flow (the larger eddies) while modeling the smaller scales (smaller than the mesh size) with a RANS turbulence model. This approach generally gives improved accuracy for separated flows which are not universally well modeled with a purely RANS formulation. Figure 18 shows the differences for URANS, LES, and DES models of a separated flow. The URANS model “smears out” the effects of mixing in the separated flow region while LES and DES largely replicate realistically the larger scale flow effects in the wake.

LES and DES are typically applied to specific regions of the flow and require a very refined, nearly isotropic mesh in the areas of interest to capture larger scale turbulent motion. Because they model larger scales of the turbulent flow DES (and LES) are inherently 3D and are inherently unsteady. The mesh refinement required in LES or DES regions, plus the smaller timesteps required by the finer mesh, vastly increases the computational cost of these scale-resolving methods.

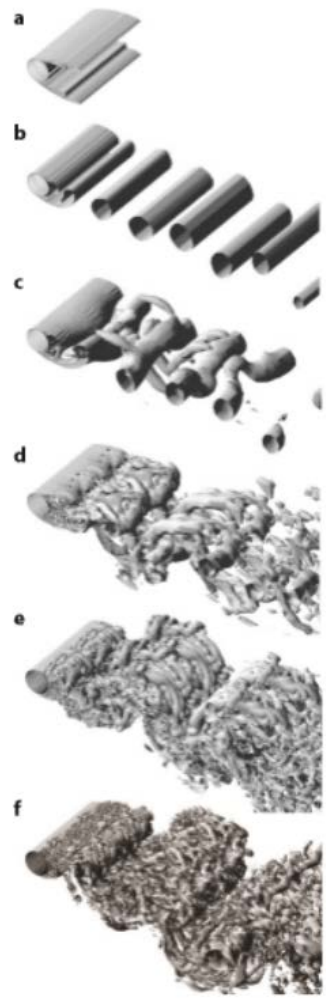

Vorticity isosurfaces by a circular cylinder: $Re_D = 5 \times 10^4$, laminar separation. Experimental drag coefficient $C_d = 1.15–1.25$. (*a*) Shear-stress transport (SST) turbulence model steady Reynolds-averaged Navier-Stokes (RANS), $C_d = 0.78$; (*b*) SST 2D unsteady RANS, $C_d = 1.73$; (*c*) SST 3D unsteady RANS, $C_d = 1.24$; (*d*) Spalart-Allmaras (SA) detached-eddy simulation (DES), coarse grid, $C_d = 1.16$; (*e*) SA DES, fine grid, $C_d = 1.26$; (*f*) SST DES, fine grid, $C_d = 1.28$. Figure courtesy of A. Travin.

Figure 18. Figure illustrating the differences in flow field resolution from RANS models for different turbulence models (a thru d) and DES for a coarse and finer grid. Figure courtesy of A. Travin.

A 3D version of the 2D mesh for TidGen®, including the seafloor was created for DES simulation. The TidGen® rotor flow domain was meshed with fine chordwise mesh resolution on the foils and a slightly larger size but refined mesh throughout the region of the rotor where interaction was expected between the foils and wakes. The dominant scale length in the flow was assumed to be the foil chord and this scale length was resolved with 20 cells throughout the region of the rotor and immediately downstream. This level of resolution was applied isotropically in all grid directions within the DES region. The DES mesh was 2 foil chords (2x 0.35 m) wide in the spanwise direction, divided into intervals comparable to the nominal spacing in the x, y plane (cross plane) which is approximately 1/20 of a chord. The foils mesh for DES was the same as used for the 2D CFD TidGen® cases. The rotor and immediate downstream region were enclosed in an elongated oval mesh to concentrate mesh near the device to better capture details in the flow. The total size of the mesh is roughly 8 million cells. This is about 20-40 times more cells than used in the various 2D CFD models studied.

The seafloor is modeled as a no-slip wall. The inlet boundary (left side of the mesh in the figure) is modeled with velocity inlet conditions (specified velocity and turbulence) at 30 rotor diameters

upstream of the rotor. The outlet (right side of the figure) is modeled with constant static pressure boundary condition 30 rotor diameters downstream of the rotor.

The inflow conditions assumed a turbulence viscosity ratio (TVR) of 10, a relatively low inflow turbulence level, which had been used extensively in previous 2D simulations of TidGen®. The power and rotor forces were found to vary weakly with inflow turbulence levels, and TVR from 10 to 100 gave results that were well matched to previous CFD work in 2D (Figure 20 and Figure 21).

The DES solution used a specialized delayed detached eddy simulation (DDES) variant of the Spalart-Allmaras turbulence model and runs at finer time steps than previous URANS models (the DES model used 600 steps per rev, or 0.1 deg per time step).

The DES case was initialized from an unsteady RANS solution with a TSR of 2.0 case which was run to periodic force convergence (6 complete rotor revolutions). This took over 2 days of clock time, running on 96 and later 112 cores.

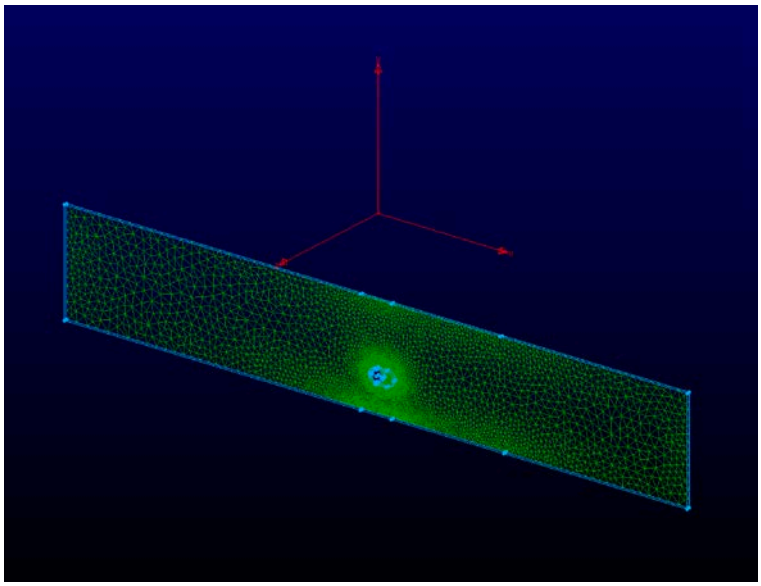

Figure 19. Outer mesh for the stationary flow domain for a 2D DES simulation. The sea floor is represented at the horizontal X lower boundary. The turbine is located at the finer mesh in the center of the domain.

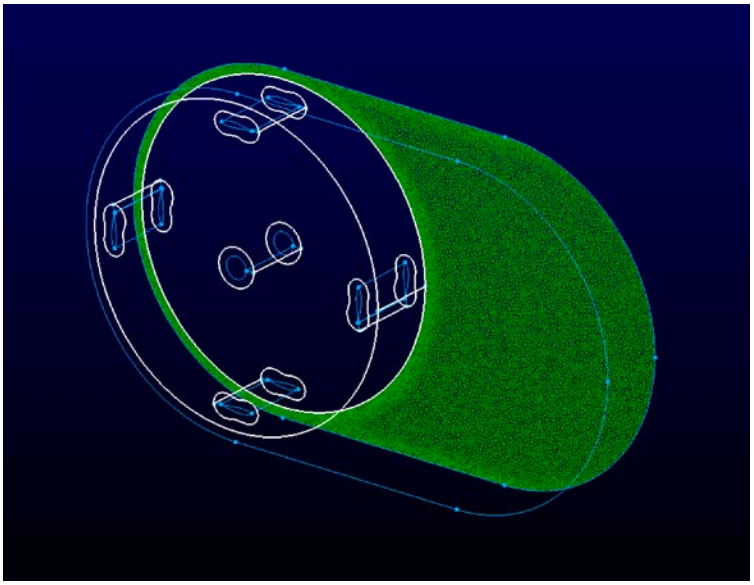

Figure 20. Refined mesh zone for 2D DES surrounding the rotor region, embedded within the stationary mesh. The central cylinder (mesh not shown) is a rotating zone that includes embedded meshes surrounding the four foils and central shaft.

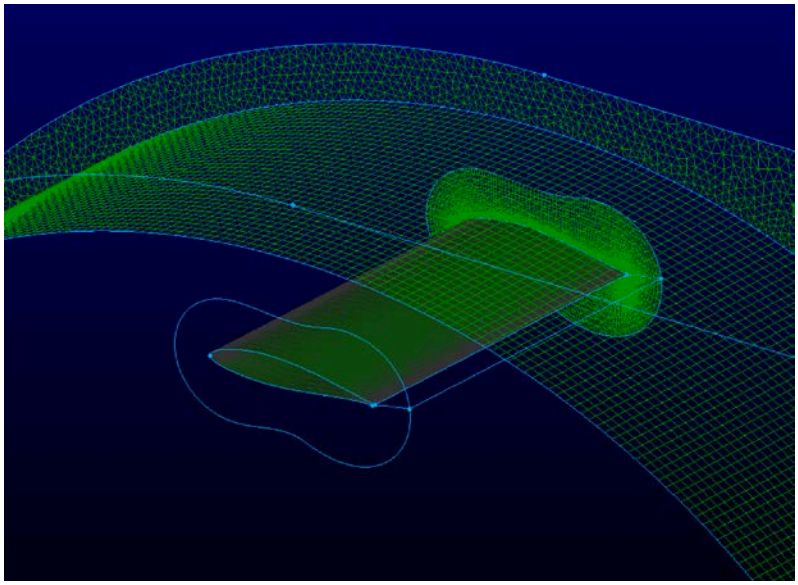

Figure 21. 2D DES Mesh around the foil, showing spanwise mesh resolution and mesh on faces of surrounding flow zone.

A series of TSRs were modeled in FLUENT. Figure 23 presents the results for coefficient of performance as a function of TSR for these 2D DES CFD models. The force data from the URANS initialization run closely duplicates the previous 2D CFD results within less than 1 percent. This indicates that the flow model is consistent with previous CFD models and results (Figure 19).

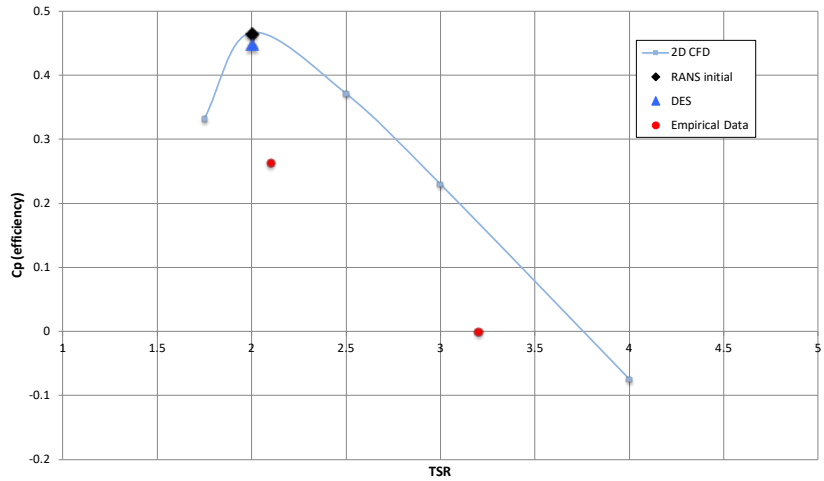

Figure 22. Coefficient of performance as a function of TSR as predicted by a DES CFD FLUENT model of the TidGen® turbine. results for the 2D DES are shown for one point only as the analysis is numerical intensive. The results are very similar to those obtained from 2D RANS. Empirical data for TidGen® is also shown.

Table 7. Tabular results for CP as a function of TSR for TidGen® turbine from 2D CFD and from DES models.

Tip speed ratio	*2D CFD Coefficient of Performance*	*DES CFD Coefficient of Performance*
2.0	0.466	0.448

All 2D CFD results clearly over predict the power performance of the turbine, which is consistent with other work which shows that significant 3D effects are present in cross-flow turbines. The DES model does not show any significant difference in results as compared to RANS CFD at this TSR (Figure 23).

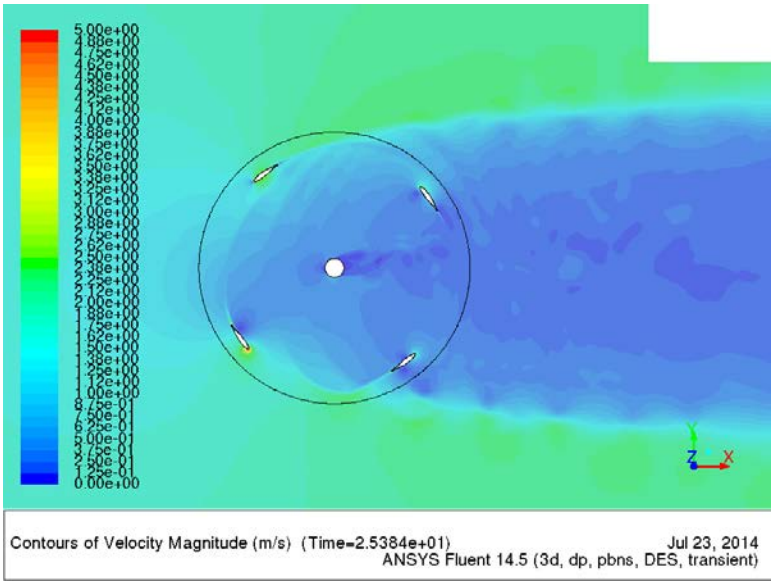

Figure 23. Contours of velocity magnitude around the turbine, showing the wake zone (DES model). The free stream flow field is 1.75m/s. Flow speeds increase above and below the turbine and decrease in the wake.

The wake zone is clearly illustrated in Figure 24, where lower velocities are visible in the downstream wake. Vortex cores are visible at locations along the upper and lower wake boundaries.

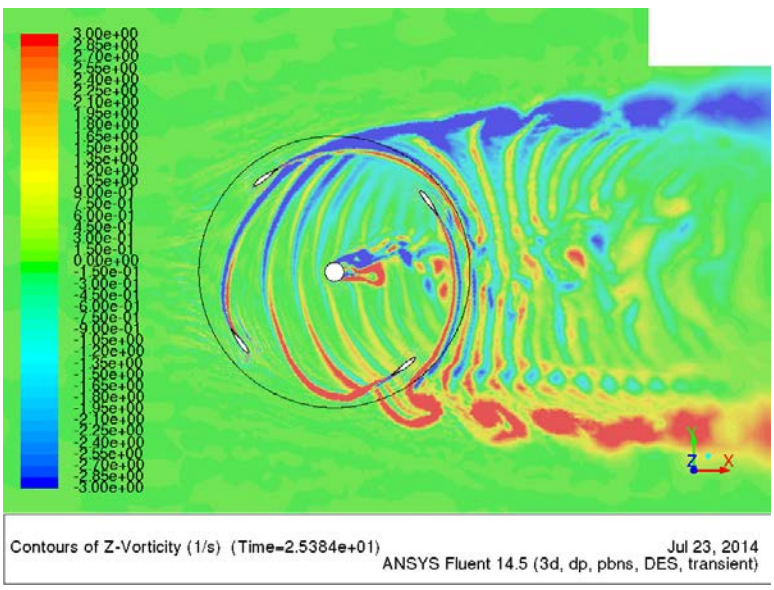

Figure 24. Vorticity contours for the TidGen® turbine at a TSR of 2.0. (DES model). Vorticity rotational sense is opposite above and below the turbine.

The vortex structures showing the wakes from the rotor are clearly illustrated in Figure 24. The rotational direction of vortices on the upper wake boundary is opposite that on the lower wake boundary line. The flow inside the wake zone has greatly reduced velocity and has residual vortex structures shed from the upstream foils and shaft.

It appears that there are two “streets” of shed vortices that remain as more or less 2D vortices, and they do not appear to break down significantly for this constant rotor cross section model. There are more random structures of vorticity appearing in the wake of the shaft, but the upper and lower main vortex groups appear to stay coherent rather than break up significantly in this DES model. The forces, as a result, look very much the same (with small variations to the back-side loading) to the previous 2D CFD result (Figure 25).

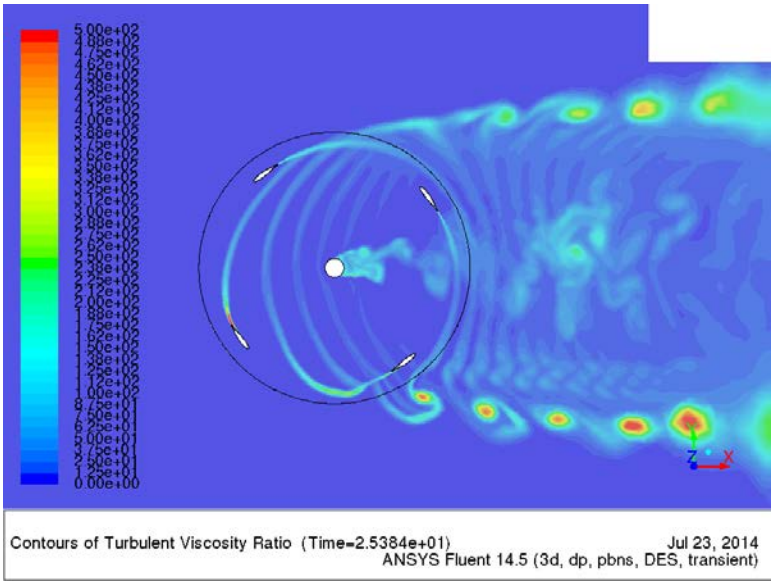

Figure 25. Turbulent viscosity ratio for the TidGen® turbine at a TSR of 2.0 (DES model). In areas with high turbulent viscosity ratio are areas where the RANS model is active. In areas with low turbulent viscosity ratio the DES model is active.

Plots of the turbulent viscosity ratio can be used to evaluate the utility of the DES modeling technique. In areas with zero to low turbulent viscosity ratio the DES model is active. In areas with a measurable turbulent viscosity ratio the RANS model is active. Figure 26 indicates that the turbulence in the wake structure is actually being modeled largely using a RANS approximation, rather than by DES. However, these areas where the RANS code is active are not in locations with high foil loads and the utility of capturing these fully in more highly resolved DES CFD does not warrant the extra computational effort required.

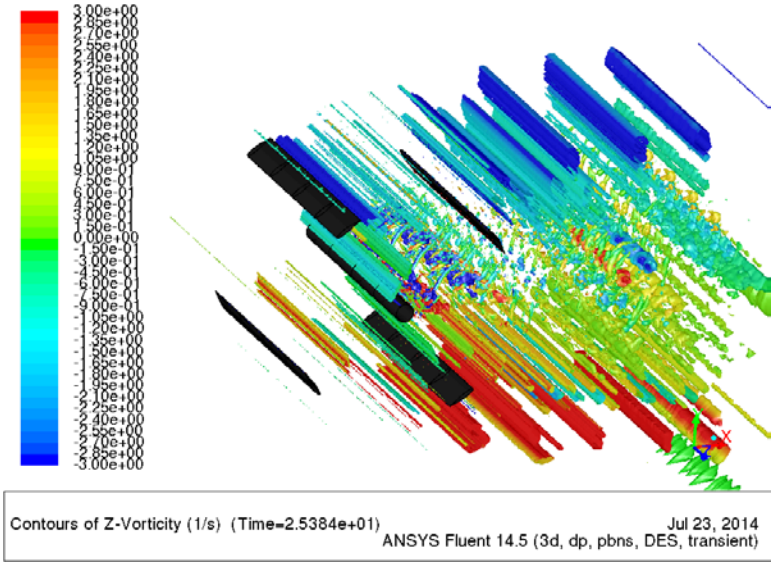

Figure 26. Isosurfaces of constant Q-criteria (velocity gradient and strain) colored by Z vorticity, as predicted by the DES model. Q-critera isosurfaces are used to locate vortex structures in LES and DES simulations.

For the maximum power point the TSR is close to 2.0. We present the torque, and force data on the foils for this operating condition obtained from the DES model. The results are presented as non-dimensional torque and force coefficients and compared to 2D CFD results (Figure 27).

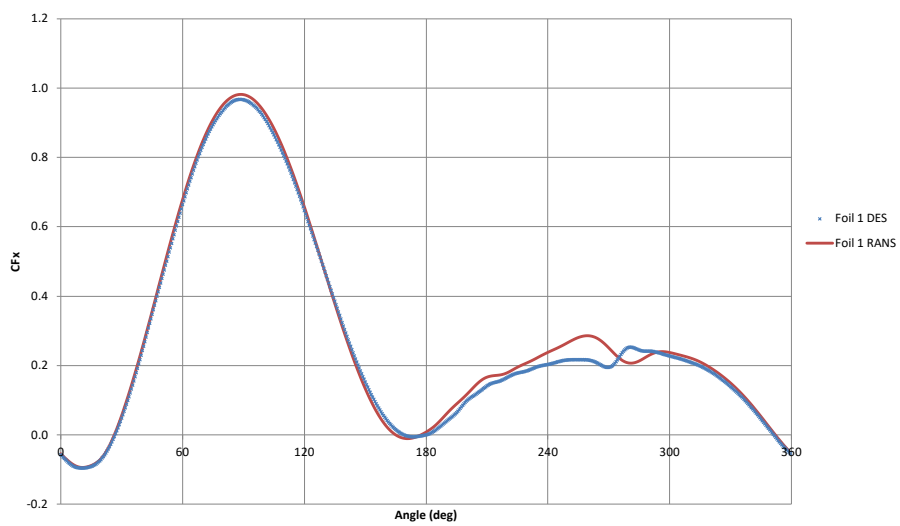

Figure 27. Non-dimensional X force coefficients (flow direction) for TidGen® turbine foils at TSR = 2.0, comparing DES load predictions on a single foil and a single turbine with RANS load predictions showing that the 2D DES results are practically identical to those obtained from 2D RANS.

Predictions of X force components on the foil are compared in Figure 27 for both RANS and DES models. The difference between the RANS and DES results are not significant, with DES results being of slightly lower magnitude.

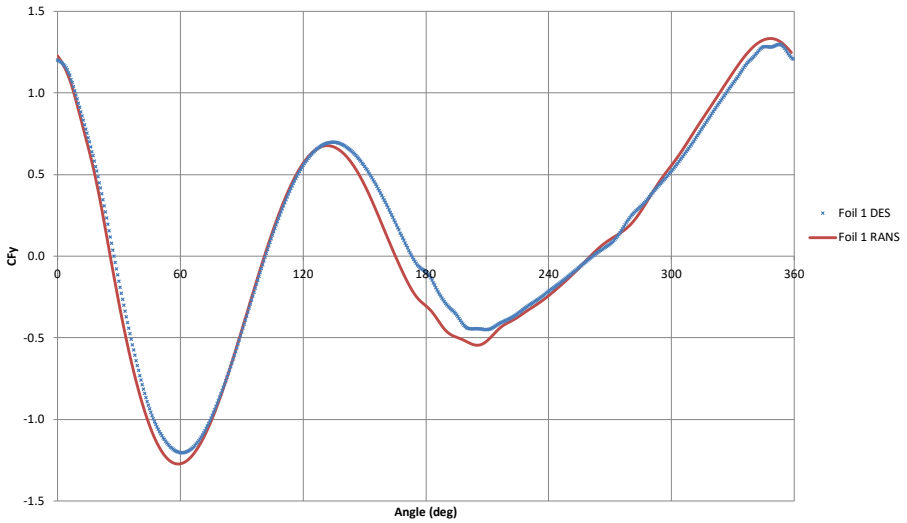

Figure 28. Non-dimensional Y force coefficients for TidGen® turbine foils at TSR = 2.0, comparing DES load predictions on a single foil and a single turbine with RANS load predictions showing that the 2D DES results are practically identical to those obtained from 2D RANS.

Predictions of Y force components on the foil are compared in Figure 28 for both RANS and DES models. The difference between the RANS and DES results are not significant, with DES results being of slightly lower magnitude.

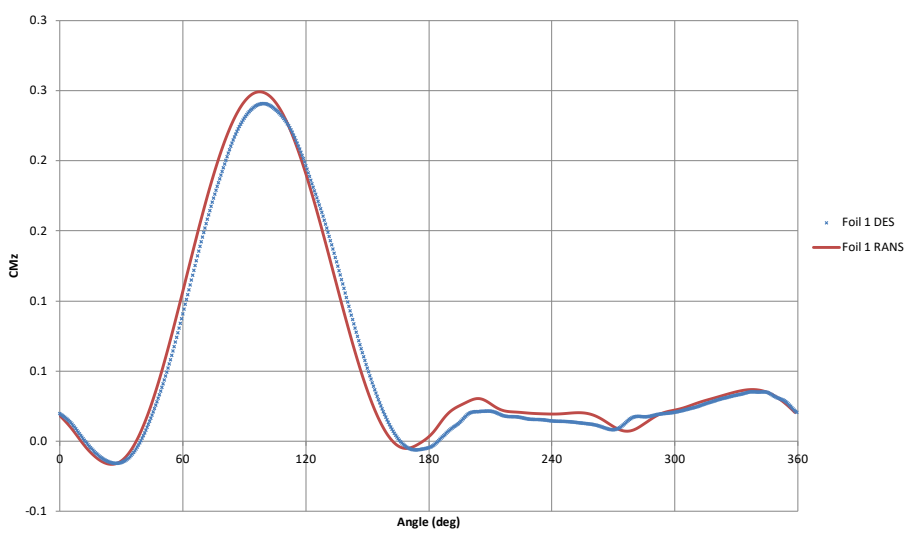

Figure 29. Non-dimensional torque coefficients for TidGen® turbine foils at TSR = 2.0, comparing DES load predictions on a single foil and a single turbine with RANS load predictions showing that the 2D DES results are practically identical to those obtained from 2D RANS.

Predictions of torque components on the foil are compared in Figure 28 for both RANS and DES models. The difference between the RANS and DES results are not significant, although the DES model does show lower torque values, which is reflected in the lower CP estimate obtained from the DES model (Figure 30).

Originally, it was intended that the 2D DES be conducted for multiple turbulence regimes, but given the results obtained it was decided the computational resources were better targeted at 3D CFD.

3.2.1.1.2.5 3D RANS – Milestone 2.1.6

Where results from 2D analyses provide radial loading requirements for bearings in the driveline, significant uncertainty in predicted axial thrust loads required 3D CFD simulation both in the absence and presence of off-axis flows to the turbine. A horizontal component to the inflow changes the lift and drag loads on the helical foils and increases the drag on foil supports, which adds to the axial bearing load.

ORPC has found in the past that commercial 3D RANS CFD packages are capable of determining the performance and associated loading of a turbine with greater accuracy than any other simulation tool. There are difficulties, however, associated with the use of 3D CFD, namely, the large computational resources and time required to complete a simulation. A mesh must have sufficient cell density around the foils, particularly the trailing edges, to properly resolve the flow. ORPC has found that this can require as many as 35 million cells for the rotor alone. The flow field of this mesh is solved 240 times per revolution, and several revolutions are required for simulation to converge to a periodic solution. This process must be repeated for each TSR examined, and the whole simulation effort can take weeks for a sufficiently complicated problem. ORPC has found 2D RANS CFD simulations to have sufficient information to be a useful design tool with adequately quick turn-around times. With meshes of approximately a quarter million cells, 2D problems can be solved in a matter of hours and are able to give qualitative estimations of turbine performance. Two-dimensional results informed the eventual set of 3D CFD simulations to be performed.

However, 2D CFD systematically overestimates the performance of the turbine. Two-dimensional results are for an infinite span turbine with straight foils. They fail to take account for the effects of 3D geometries.

The finite extent of the foils and the interference of the foil supports produce substantial reductions of lift at each foil support and foil end. This loss of lift is one of the primary reasons for the difference in 2D and 3D turbine performance. The loss of lift is modeled by assuming elliptical foil load distributions with the lift dropping to zero at the foil supports. Previous 3D CFD results indicate that this is a reasonable approximation.

In addition to the substantial reduction of lift produced by the foil supports, there is drag associated with foil supports. Power loss from foil support drag increases considerably at higher TSRs and is one of the factors that accounts for 2D predictions showing peak power at higher angular velocities than recorded in field tests.

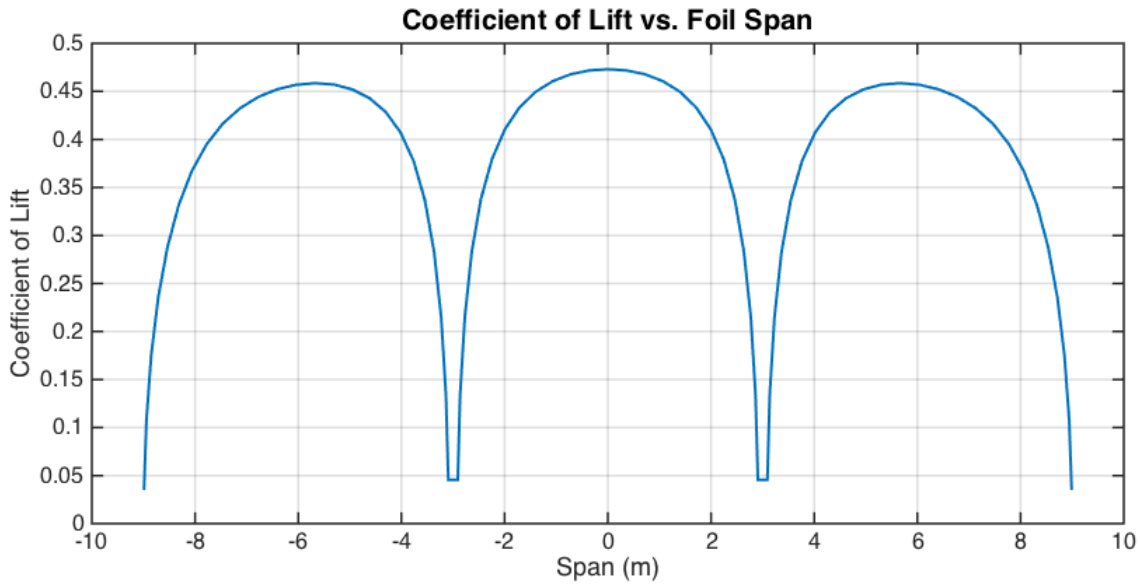

Figure 30. The coefficient of lift of a wing with gaps as predicted by AVL.[12] The AVL results are illustrative of the effect that foil supports have on the turbine's lift as, like gaps, the foil supports interrupt lift on the foil.

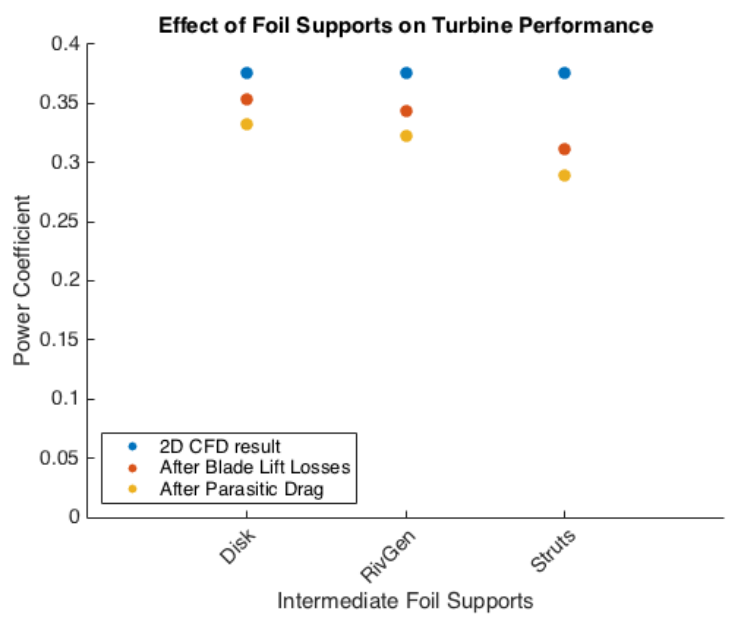

Figure 31. A 3D CFD study of foil supports shows that parasitic drag (the power lost between the red and yellow dots) is relatively constant while power due to lift loss (the power lost between the blue and red dots) depends significantly on foil support geometry. The solid disk foil support had the smallest effect on foil lift, and consequently the lowest overall power loss.

[12] AVL is a vortex-lattice model for airplane wings developed by Mark Drela and Hal Youngren, http://web.mit.edu/drela/Public/web/avl/

A three-foil turbine was chosen as a conservative bearing design basis due to its higher impulse loads on the bearings and drive train (Figure 32).

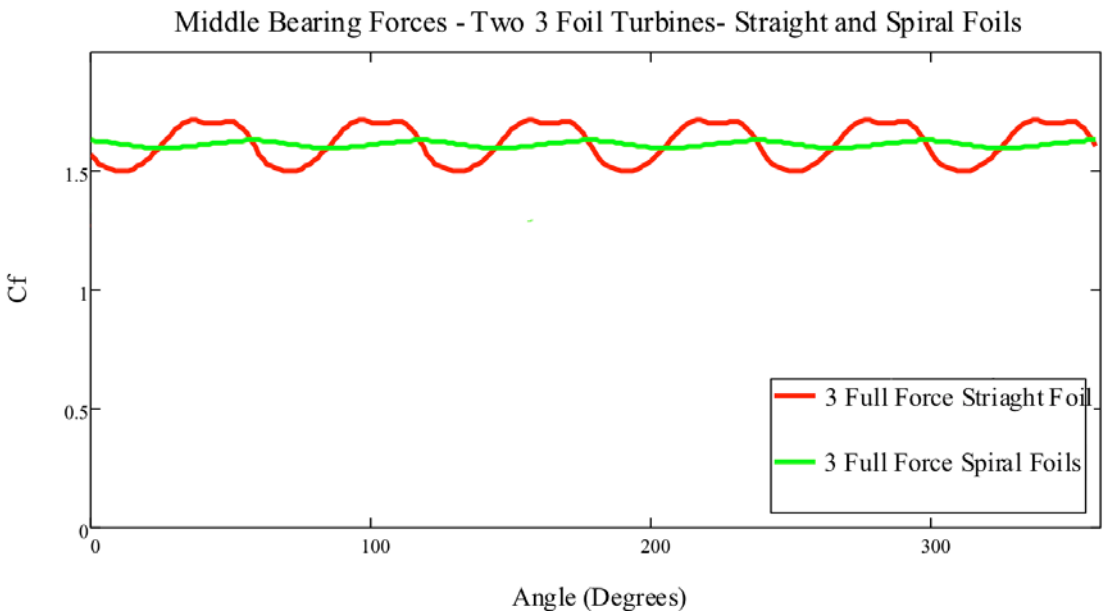

Figure 32. The maximum load on a middle bearing shown for both straight and spiraled foils. Spiraling the foils 120 degrees (green) results in a considerable reduction is oscillation and magnitude in the bearing forces as compared to a straight foil turbine (red)

Fairings may improve power production by increasing the effective capture area of the turbine and by redirecting the flow so that a foil can produce more torque over a larger percentage of a rotation. ORPC has had success with preliminary fairing designs on its RivGen® turbine where the addition of a small fairing increased power production by 25 percent.

3D CFD Configuration and Simulation

After an examination of the above parameters, ORPC settled upon a turbine configuration for the 3D CFD simulations required to finalize the bearing requirements. ORPC's chosen configuration produces the highest reasonable bearing loads within the current turbine design space. The chosen 3D configuration has three foils spiraled 120 degrees, supported by discs, and set within ORPC's double fairing design.

While the next-generation TidGen® turbine will consist of four rotors, simulating four rotors with sufficient mesh density to properly resolve forces at the trailing edges is requires more computer resources than are practical or available to ORPC. To obtain sufficient mesh resolution for a single rotor requires approximately 35 million cells per rotor. A four-rotor mesh including fairings and generator could easily exceed 150 million cells. ORPC chose to model a single rotor with fairings, which can reasonably approximate the behavior of each rotor in a next generation design.

The turbine mesh has 15 individual elements on which forces were tracked. These include two fairings, four foil supports, one shaft, and 9 foil elements. Each foil, swept 120 degrees, was divided into thirds enabling the forces to be examined on each foil and on each of the three sections (port, midships, and starboard) of the turbine.

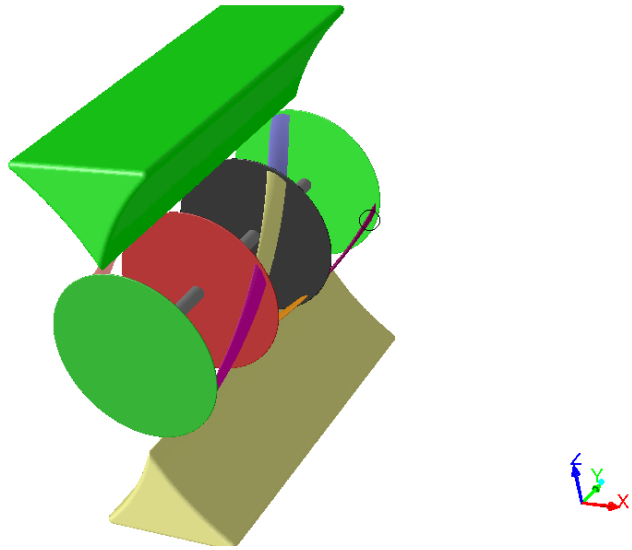

Figure 33. Geometry of the 3D turbine used to estimate driveline loads. The turbine includes two fairings, four foil supports, a shaft, and three foils each spiraled 120 degrees.

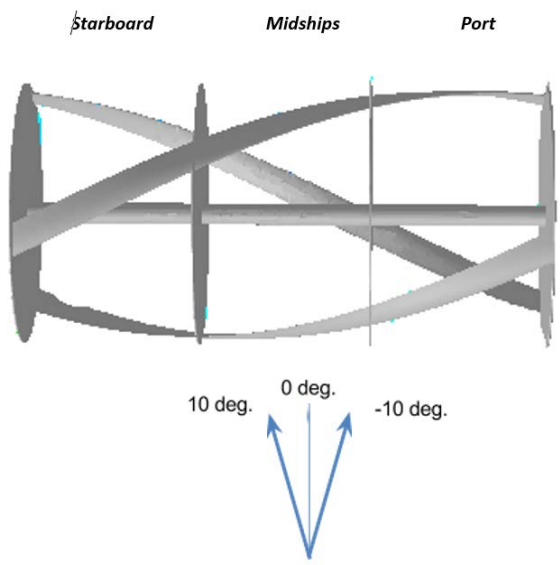

Figure 34. Turbine showing the three inflow angles examined using 3D CFD

The complex nature of tidal flows virtually guarantees that a cross-flow turbine may not always be directly perpendicular to the flow. Foil supports such as disks show the lowest drag and performance degradation of the foil support geometries investigated by ORPC; however, the axial forces of these disks in flows that are not perfectly aligned with the turbine were a source of concern. ORPC examined behavior of the turbine in flows that were at ±10-degree angles to the turbine in addition to the usual straight inflow (Table 8).

Table 8: 3D CFD runs completed.

COMPLETED 3D CFD RUNS			
TSR	**-10 deg. Inflow Angle**	**0 deg. Inflow Angle**	**10 deg. Inflow Angle**
2.0		X	X
2.5	X	X	X
3.5			X

A TSR of 2.5 was chosen as the primary operation point. All three inflow angles were investigated at TSR of 2.5. Higher loads were expected for short durations at higher TSRs, so an effort was made to find the approximate zero-power point, or free-wheel TSR of the turbine, which occurs approximately at a TSR of 3.5.

For the bearing and driveline design, a maximum flow speed of 4.5 m/s was chosen.

The 3D CFD work also shows little variation in radial forces from -10 degrees to 10 degrees. The highest radial forces occur at an inflow angle of 10 degrees, with a straight inflow providing the next highest loads. The variation, however, is relatively small, with no more than a 5 percent change in maximum radial force over the various inflow angles. The greatest deviation from the rotor's mean radial force is 7 percent.

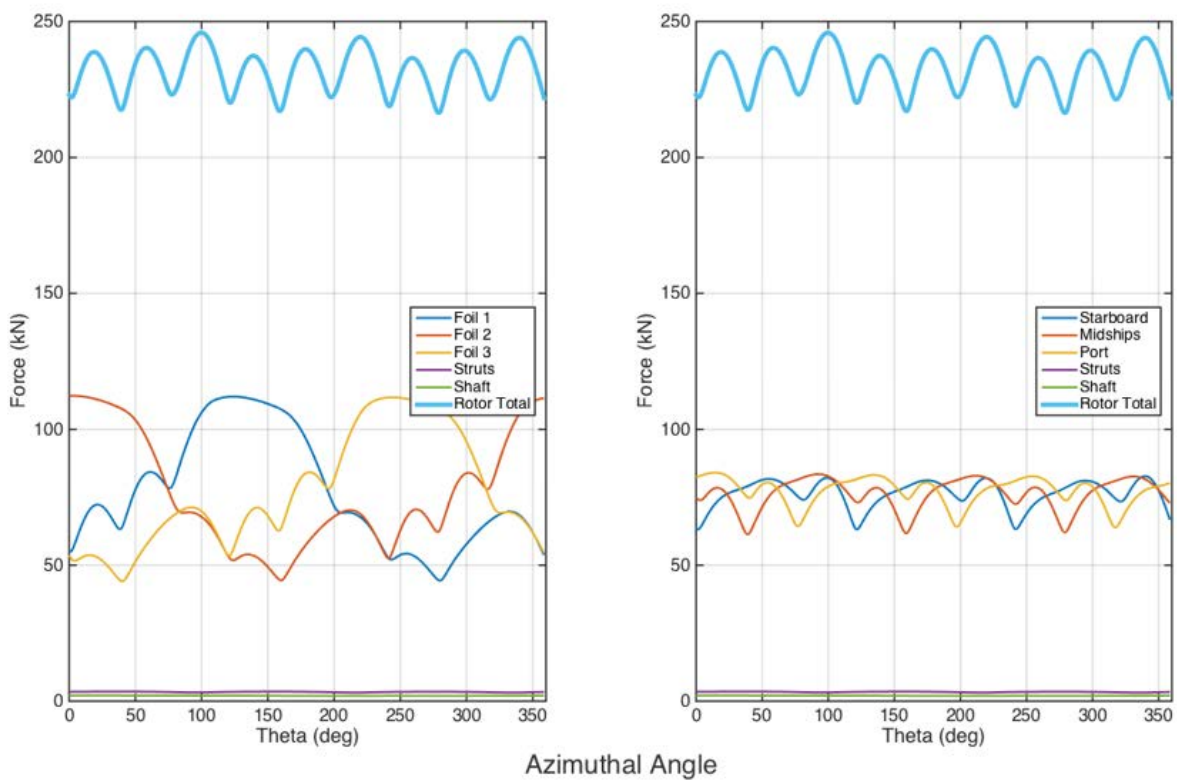

Figure 35. Breakdown of the radial forces on the rotor at a zero-degree inflow angle. The forces are separated by foil (left) and by rotor section (right). The relatively constant forces when broken down by section indicate that the turbine will create low bearing force variation. These results are representative of the radial forces at 10 and -10-degree inflow angles.

Figure 35 shows the axial loads for all three inflow angles, and reveals that the axial loading for a turbine with a 10 degree inflow angle is considerably lower than for one with a 0 or -10 degree inflow angle, for a flow speed of 4.5m/s

Understanding and quantifying axial loads was an important goal of the 3D CFD work (Table 9). We note the following:

1. The axial forces can vary wildly with inflow angle.
2. The axial loading on the turbine is not symmetric with respect to inflow angle.
3. Disk supports do not present a particularly large source of axial drag on the system. The largest portion of the axial loads generally comes from foil spiraling.

Table 9. Summary of axial forces on the disk foil supports. The forces at 0 and -10-degree inflow angles were notably lower than at a 10-degree inflow angle. Flow speed = 4.5m/s

FOIL SUPPORT AXIAL FORCES			
	Average	**Maximum**	**Minimum**
-10 deg.	3,226 *N*	*3,380 N*	3,043 *N*
0 deg.	3,356 *N*	3,532 *N*	3,135 *N*
10 deg.	21,777 *N*	25,797 *N*	17,650 *N*

At a 10-degree inflow angle, the forces on the foil support were also more variable.

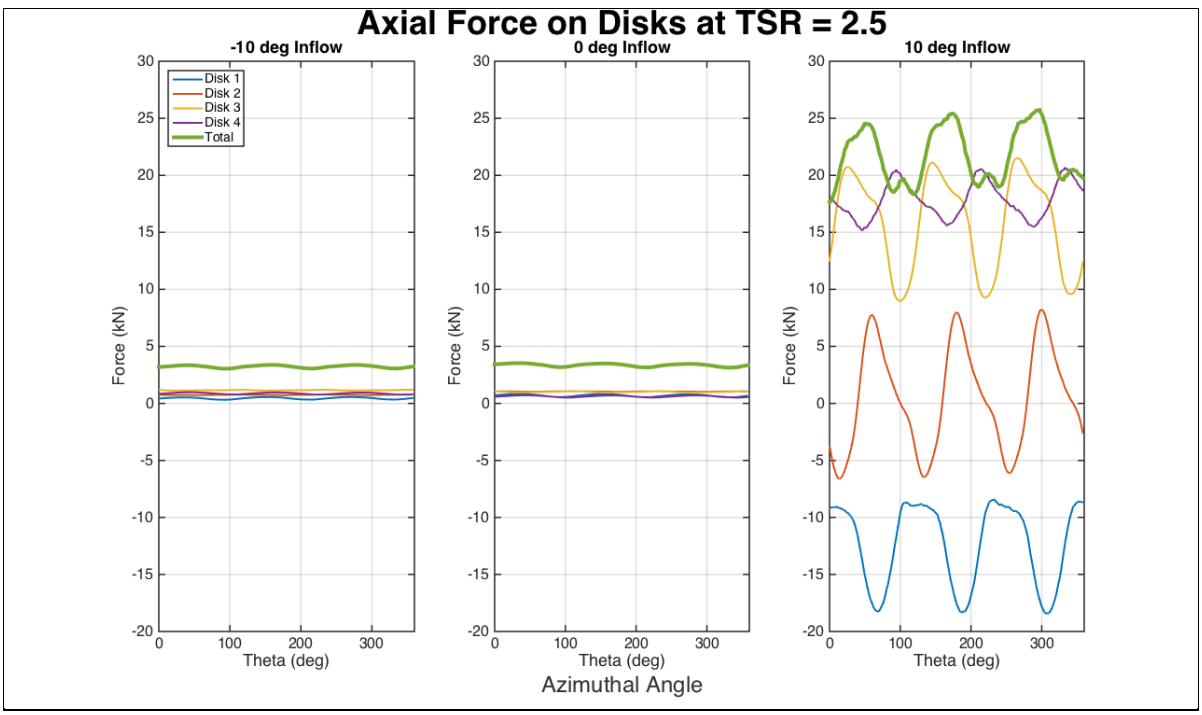

Figure 36. Axial forces on the disk foil supports. The 10-degree inflow case showed considerably more volatility than either of the other flow cases. Flow speed = 4.5m/s

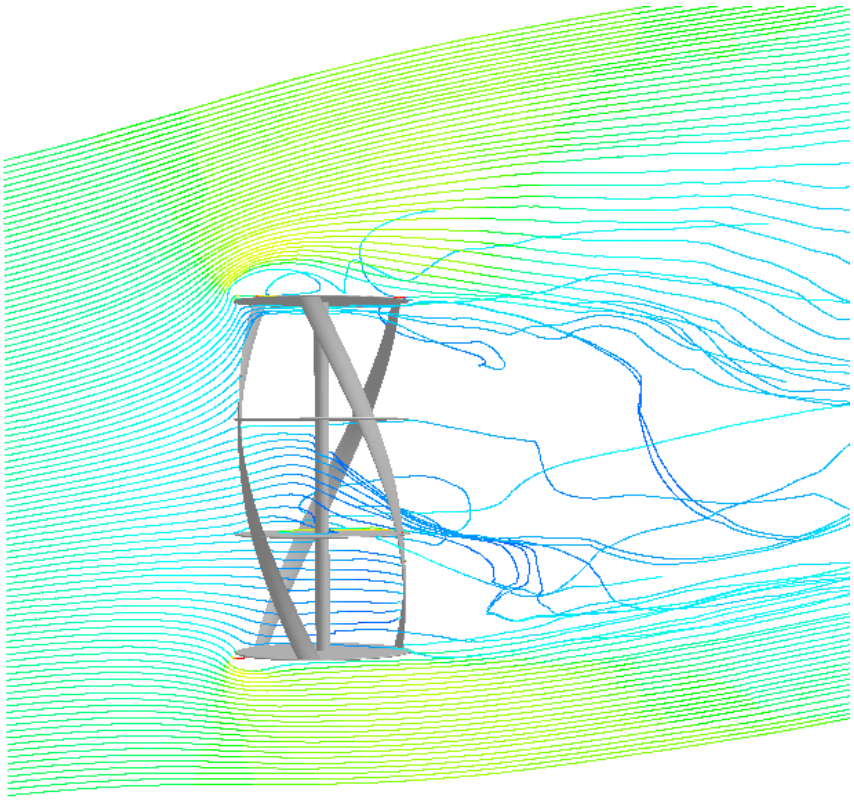

Figure 37. Stream line diagram of the flow through the turbine for a 10-degree inflow angle.

This sensitivity to inflow angle was also evident in the 3D results for a TSR of 2.0. A similar trend was suggested in low axial forces shown in the single run completed at a TSR of 3.5.

Higher Tip-Speed Ratios

Comparing the free-wheel TSR of 3.5 to the operating TSR of 2.5 indicated a modest increase in radial and axial loads. On average, radial forces increased by 15 percent and axial forces by 30 percent (Figure 38).

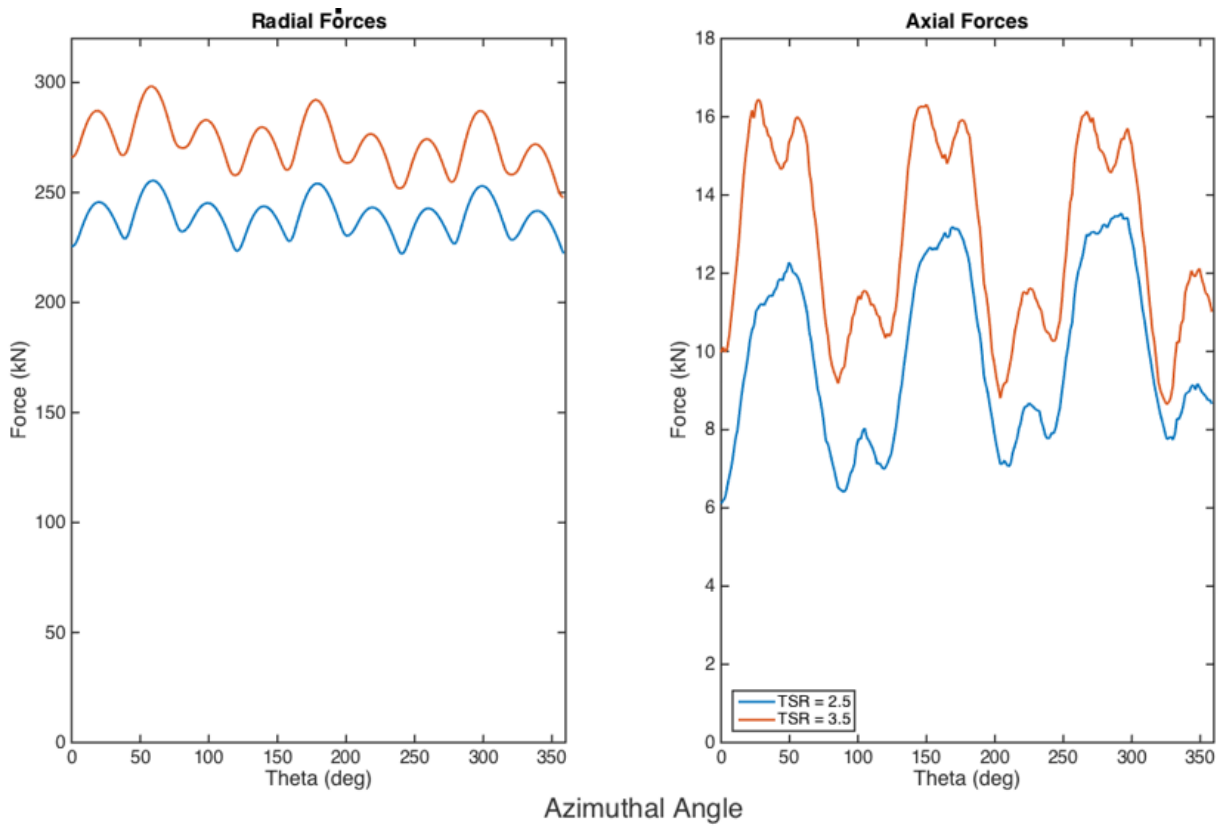

Figure 38. Comparison of the radial and axial forces at TSRs of 2.5 and 3.5, the operating and free-wheeling conditions of the turbine. Radial and axial forces are higher for the freewheel case

3.2.1.1.2.6 Foil Loads at Various Sites

Each analytical approach has different natural structures. We must find a way to present the results from each analysis in a fashion that allows for direct comparison and express these results in a manner that can be utilized at different installation sites. Non-dimensionalization works well for these purposes, but for the design of a bearing, actual load values are required. Here we extract the results from each analysis and present them for a flow speed of 4.5m/s

To determine loads for a given site we must select a representative water speed for the site and scale the non-dimensional load coefficients by the appropriate factors.

$$F_{tangential} = \frac{1}{2}\rho V^2 A C_t$$

$$F_{normal} = \frac{1}{2}\rho V^2 A C_n$$

$$F_x = \frac{1}{2}\rho V^2 A C_x$$

$$F_y = \frac{1}{2}\rho V^2 A C_y$$

Where V is the water speed, density is represented by ρ, A is the turbine frontal area, and the Ct and Cn are tangential and normal force coefficients, and Cx and Cy are drag and lift force coefficients.
For the streamtube analysis we are provided with non-dimensional force coefficients for the normal, radial, flow direction, and vertical directions. Turbine loads are presented below for a four-foil TidGen® turbine and also for a three-foil turbine (Table 10 and Table 11).

Table 10. Streamtube Model Total Turbine Loads for a four-foil TidGen® TGU

	2.0m/s	*2.5m/s*	*3.0m/s*	*3.5m/s*	*4.0m/s*	*4.5m/s*
Max Tangential Load (N)	9,898	15,465	22,270	30,311	39,590	50,107
Max Normal Load (N)	74,333	116,146	167,250	227,646	297,334	376,313
Max X Load (N)	74,644	116,631	167,949	228,597	298,576	377,885
Max Y Load (N)	56,043	87,567	126,096	171,630	224,170	283,716

Table 11: Streamtube Model Total Turbine Loads for a three-foil TidGen® TGU

	2.0m/s	*2.5m/s*	*3.0m/s*	*3.5m/s*	*4.0m/s*	*4.5m/s*
Max Tangential Load (N)	12,882	20,129	28,985	39,452	51,530	65,217
Max Normal Load (N)	96,540	150,844	217,216	295,655	386,161	488,736

The loads predicted by CACTUS were similar to the operating load condition obtained from streamtube models. The maximum normal load at 4.5 m/s from the streamtube model was 377kN for the freewheel condition, 304kN for the max power condition, and the CACTUS code predicts a maximum X load of 323kN for the max power condition (Table 12 and Table 13).

Table 12. CACTUS Vortex Model Loads for a four-foil TidGen® TGU

	2.0m/s	*2.5m/s*	*3.0m/s*	*3.5m/s*	*4.0m/s*	*4.5m/s*
Max X Load (N)	63,940	99,907	143,866	195,817	255,762	323,698
Max Y Load (N)	50,860	79,469	114,435	155,758	203,439	257,478
Max Z Load (N)	-7,266	-11,353	-16,348	-22,252	-29,064	-36,784

Table 13. 2D CFD Loads for a four-foil TidGen® TGU

	2.0m/s	*2.5m/s*	*3.0m/s*	*3.5m/s*	*4.0m/s*	*4.5m/s*
Max X Load (N)	37,134	58,022	83,551	113,722	148,535	187,990
Max Y Load (N)	2,717	4,245	6,113	8,321	10,868	13,755

Average loads predicted from 2D CFD are lower than the equivalent operating load condition obtained from streamtube or vorticity models. Upstream predicted loads from the 2D CFD are higher as expected, and the overall turbine load is consequently increased.

Force coefficients for the DES analysis do not differ significantly from the RANS results. This can be interpreted in two ways. We could state that there are no significant force differences to be found by using the DES method as compared to RANS, or we could infer that this particular implementation of the DES method for this model was not sufficient to uncover fundamental differences in results. Figure 26 shows the turbulent viscosity ratio for this model and indicates that in the wake zone the DES model is inactive as there are measurable values of turbulent viscosity ratio present (which indicates that the

RANS model is active in these zones). This would imply that a smaller length scale (perhaps the scale of the foil viscous layer, roughly a factor of 10 smaller than the chord) is required to resolve wake vortex structures in the DES model. If we examine the force and torque profiles for CFx and CMz we see that wake areas where the RANS model is active coincide with areas of low force and torque. The CFy values are higher in these areas. Even in the areas where the DES model is active we do not find significant differences between the force coefficients. Having made these remarks we do note that there is a qualitative difference between these results and results obtained in prior DES work for the TidGen® turbine. Prior work indicated a higher level of oscillation in the foil loadings. This prior work was done using a refined 2D DES model with a much finer grid and time step resolution which resolved smaller vortex structures. The additional computational time required to perform a full 3D DES analysis at this more refined scale is significant.

We conclude that the additional computational effort required for the DES modeling technique does not provide significant additional information on the load coefficients.

The radial loads generated by the 3D CFD simulations are consistent with those estimated using other methods. However, it should be noted that the 3D loads are higher than those predicted by the 2D CFD models, which is primarily due to the inclusion of a fairing in the 3D models. The results are summarized in Table 14.

Table 14. 3D CFD Loads for a three-foil TidGen® TGU

ROTOR RADIAL FORCES			
	Average	**Maximum**	**Minimum**
-10 deg.	229.19 *kN*	243.83 *kN*	213.29 *kN*
0 deg.	235.38 *kN*	249.05 *kN*	219.64 *kN*
10 deg.	238.83 *kN*	255.44 *kN*	222.11 *kN*

3.2.1.1.2.7 Structural Analysis – Milestone 2.1.7

To develop a specification for bearing loads, it is also important to understand the structure within which the bearing resides and how the shafts are to be implemented. Stiffness of the bearing support effects the load on the bearings.

Bearings are located between TGUs, noted as middle bearings, and on the ends of the shafts, noted as end bearings (Figure 39 and Figure 40).

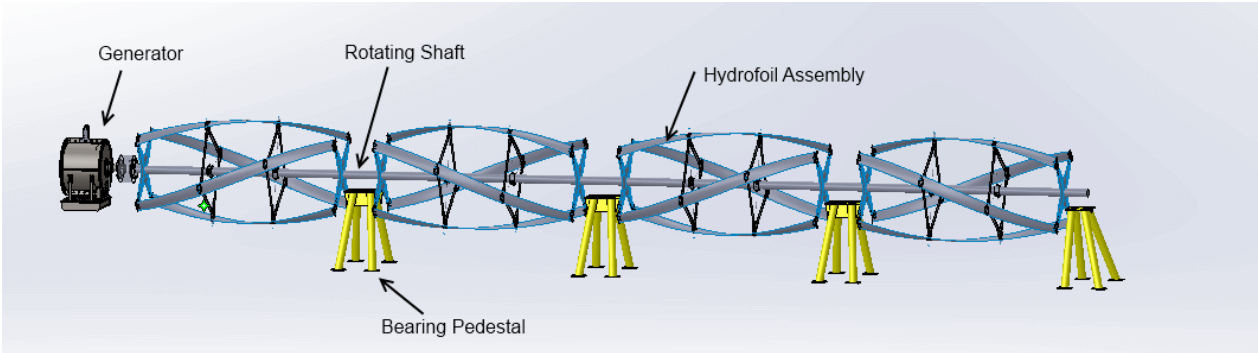

Figure 39. Driveline/bearing overview showing the arrangement for the proposed TidGen® TGU. A single generator located at the end of the driveline is connected by a coupling to the first of four turbines in line.

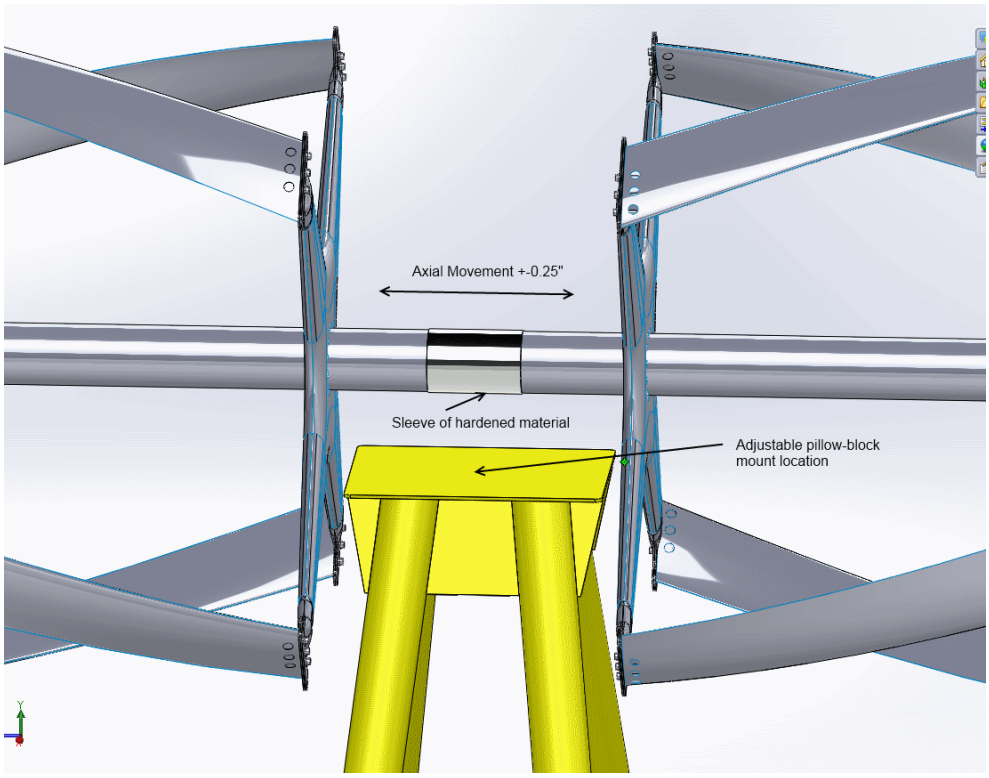

Figure 40. Bearing install detail. The bearing will sit on top of the pedestal and capture the shaft between the turbines. This section of the turbine will comprise a different section from the main shaft.

The bottom support frame cannot be made stiff enough or maintained stationary enough over the life of an installation to ensure perfect alignment of the bearings. It is also not likely that the turbine shaft will be perfectly straight once field assembled. Thus, the objective is to arrive at an optimum trade-off in which the shaft is stiff and strong enough to carry the loads safely, yet not so stiff that reasonable bearing displacements or shaft bend produced unreasonable bearing loads or stresses. In addition, the material should have a high strain to failure to allow stress concentrations to be safely spread and reduced. Since the rotating turbine shaft is essentially a fully reversing load fatigue testing machine, the shaft should also operate below the fatigue limit to allow for “unlimited” fatigue life.

Bearing sets and flexible couplings are required between the generator shaft and turbine driveshaft and at each turbine-to-turbine interconnection. Bearings sets are housed in a custom flexible plate housing to allow for drivetrain flexure and limit bearing edge loading. The flexible couplings are required in addition to the flexible bearing housings to limit bending moments being transferred from each drivetrain section.

Each flexible plate bearing housing requires two internal bearing assemblies in order to orient the flexible housing to accommodate driveshaft flexure and misalignments. Each turbine will have a dedicated flexible housing on either side, with one housing containing radial-axial bearing assemblies and the other housing only radial bearings so that each turbine is constrained axially on only one side.

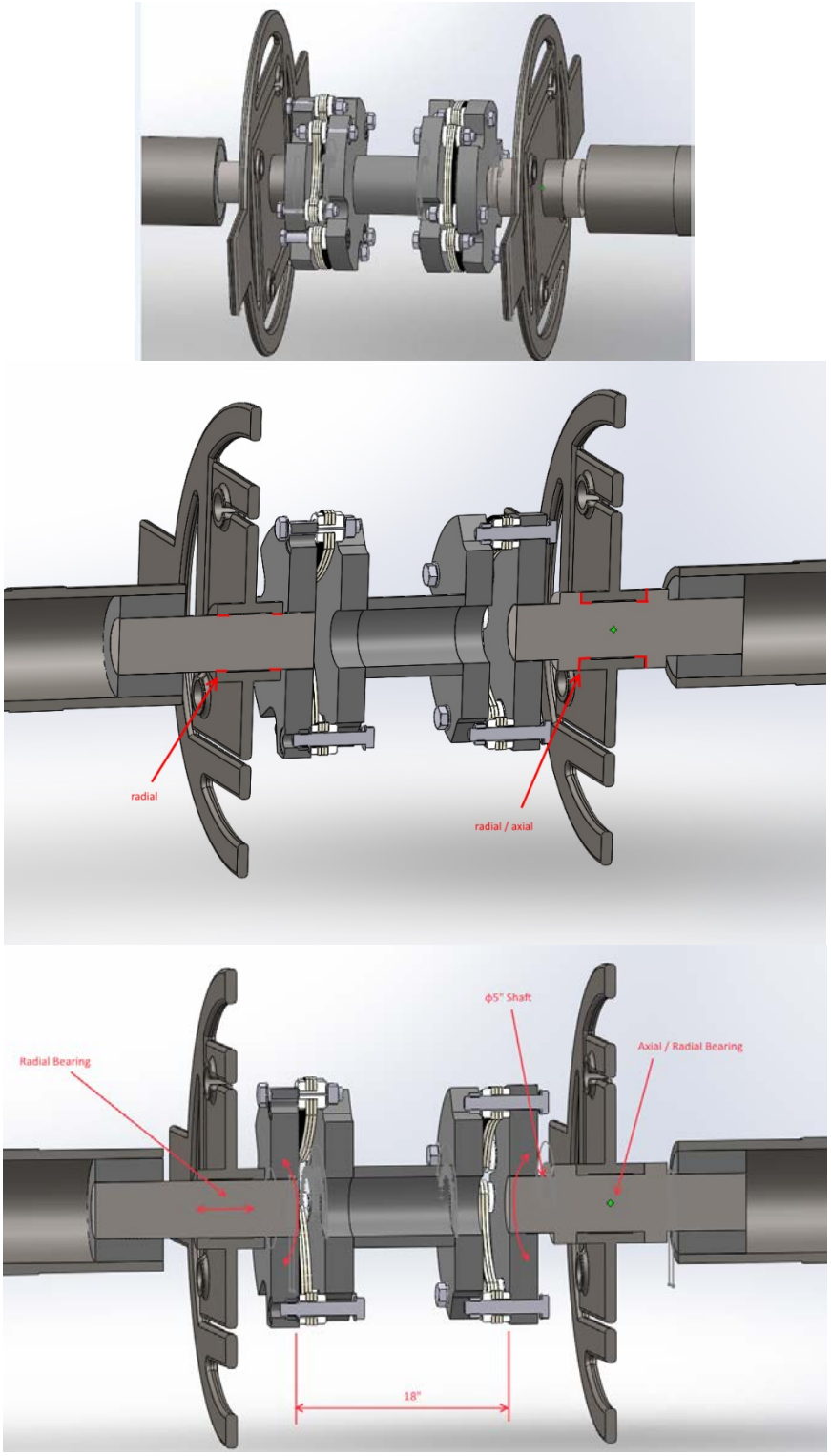

Figure 41. Turbine to turbine interconnection showing two flexible plate housings with internal radial and radial-axial bearings sets that are separated by a flexible coupling assembly. The lower image shows dimensions for the bearing shaft

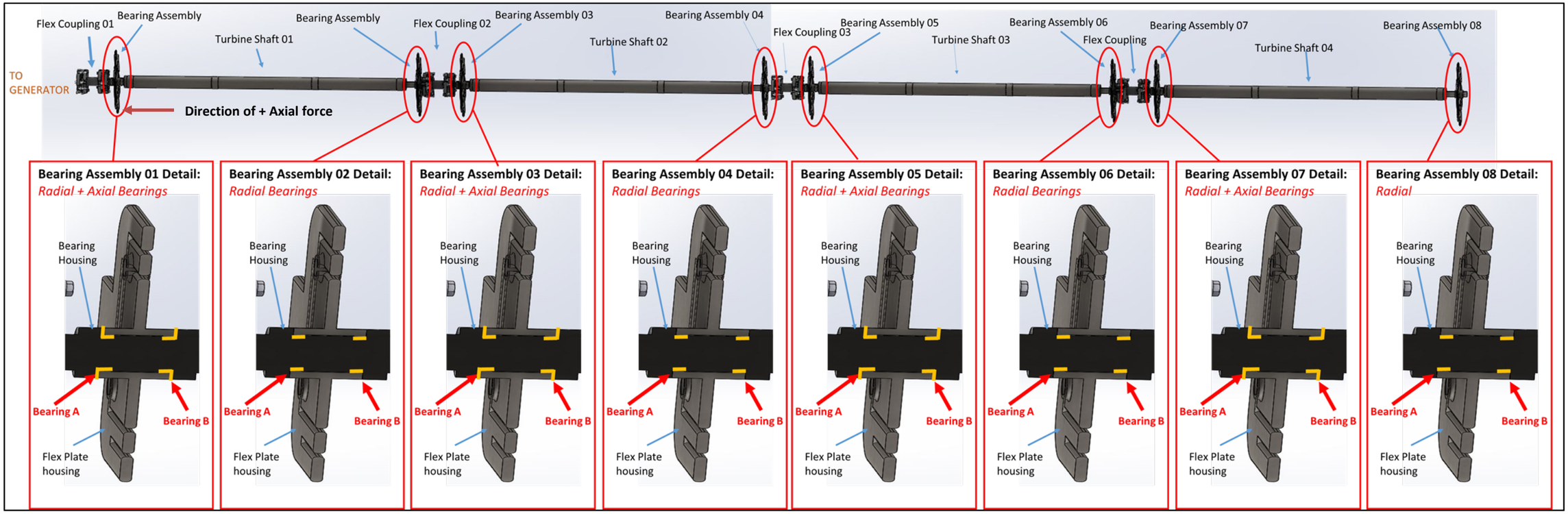

Figure 42. Layout of driveline subassembly calling out bearing assemblies and component bearings. The driveline consists of 8 bearing assemblies, and each bearing assembly consists of a flexible plate bearing housing that contains two component bearings, which are either a pure radial bearing or a composite axial thrust/radial bearing. The design is such that only one type of radial bearing and one type of axial/radial composite bearing are required by the bearing supplier. In summary, the driveline contains 16 total component bearings: 8X radial bearing, and 8X axial/radial composite bearing.

Bearings will be located on a 5 in. shaft, a "stub" shaft that will use fixed couplings to interconnect with a larger driveshaft section of approximately 10 in. to 12 in. individually supporting the turbines. The bearings will be installed on the stub shaft using a tapered sleeve. Figure 43 provide a schematic of the bearing installation detail.

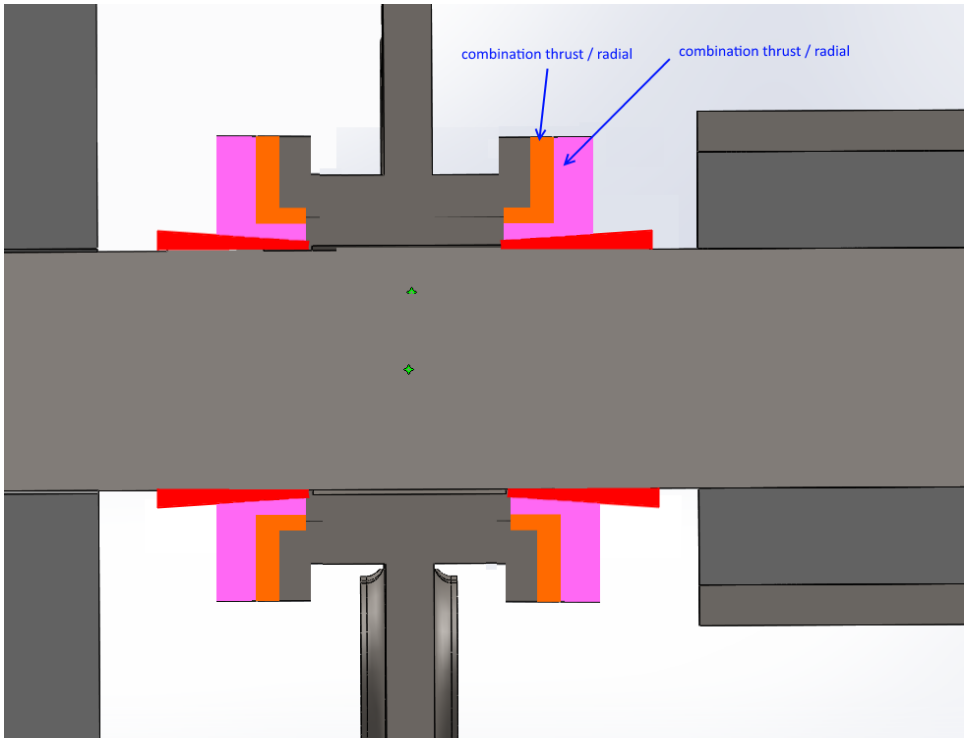

Figure 43. Tapered sleeves will locate each component bearing on a stub shaft between each turbine driveshaft section. Component bearings will either be a pure radial bearing or a composite axial thrust and radial bearing.

3.2.1.1.2.8 Bearing Load Assessment from 2D Analyses – Milestone 2.1.8

Design of the turbine and support system requires estimates of the loads produced during operation. ORPC has developed tools to estimate the loads for various turbine configurations based on results from 2D CFD simulations, and on results from streamtube and vortex model codes.

The radial and axial loads have been refined using the 3D CFD. ORPC has considerably greater confidence in these results than in previous estimates due to the 3D CFD's ability to model some of the complex axial flow components that are not considered in 2D CFD simulations or streamtube or vorticity models.

Table 15. TSR = 2

Maximum Load	**V = 2.5 *m/s***	**V = 3.5 *m/s***	**V = 4.5 *m/s***	
End Bearing Load	34,024	66,687	110,238	*kN*
Middle Bearing Load	68,048	133,375	220,477	*kN*
Axial Force on a Rotor	48,611	95,278	157,500	*kN*

Table 16. TSR = 2.5 – Operating Point of Turbine

Maximum Load	**V = 2.5 *m/s***	**V = 3.5 *m/s***	**V = 4.5 *m/s***	
End Bearing Load	39.419	77,261	127,718	*kN*
Middle Bearing Load	78,838	154,523	255,435	*kN*
Axial Force on a Rotor	55,442	108,667	179,633	*kN*

Table 17. TSR = 3.5 – Free Wheel Speed of Turbine

Maximum Load	**V = 2.5 *m/s***	**V = 3.5 *m/s***	**V = 4.5 *m/s***	
End Bearing Load	46,035	90,228	149,153	*kN*
Middle Bearing Load	92,070	180,457	298,306	*kN*
Axial Force on a Rotor	--	--	--	*kN*

The TSR = 3.5 is the design requirement for the bearings.

3.2.1.1.2.9 Bearing Specification – Milestone 2.1.9

In addition to the load requirements for a bearing, there are additional factors and specifications which must be outlined. The following details the requirements for a bearing solution for ORPC's TidGen®. Five bearings are required per unit unless the generator carries the load from one turbine end:

1. Operational loads: A 5 percent ripple at four or three per rev frequency depending on turbine foil count on center bearings and 30 percent ripple on thrust bearings.
2. Bearing shaft size is approximately 5 – 6 in. in diameter. (Note: The bearings will be installed on a stub shaft that is coupled to turbine driveshafts of 8 in. to 12 in. in diameter with 10.75 in. OD, 10 in. pipe, as the expected minimum shaft size for high flow sites).
3. Assembly Environment: Fully exposed open-air environment with temperature ranging from 0°F to 100°F (-20°C to 40°C) expected.
4. Operating Environment: Salt or fresh water: fully submerged at depths from 40 ft to 400 ft (12 m) to 120 m).
5. Pressure variation due to tidal height change of up to 15 psi (90kPa).
6. Corrosion resistant for design lifetime without damage to other longer life components that are not expected to be simultaneously serviced. Minimum design lifetime of 5 years without servicing.
7. Bearing needs to accommodate axial movement of +/- 0.25 in.
8. In addition to the axially accommodating bearings, one bidirectional (opposed) set of thrust bearings is required to locate the rotor per turbine system.
9. Bearing should be field-serviceable without turbine disassembly, preferably a spilt-bearing arrangement or a replaceable bearing module and/or section of shaft.
10. Operational time: roughly a 6-hour cycle of operation with speed ramping up to 82 RPM with roughly one hour of non-spinning time at slack tides. Peak speeds under failed generator and brake conditions may approach 110 RPM.
11. Self-aligning bearing assembly when integrated into the turbine system, tolerant of at least 1 degree of shaft misalignment and preferably 2 or more degrees.

12. Life: Ideally, the bearings will require no service for at least 5 years in service and we would look for more – the design objective is 20-year life wherever possible and 5-year service intervals for short lived components.

3.2.1.1.3 Problems Encountered and Departure from Planned Methodology

The results from 2D DES simulations were found to have no significant differences from the 2D RANS simulations. As a result, multiple runs with differing turbulence models with DES were not performed.

3.2.1.1.4 Assessment of Their Impact on the Project Results

The lack of additional turbulence results from DES CFD had no significant impact on the Project.

3.2.1.2 *Bearing Design*

Bearing design was performed under Subtask 2.2, Bearing Design and Preliminary Testing, and informed by laboratory testing at the University Alaska Anchorage (UAA) under Subtask 4.1, Flume Testing.

3.2.1.2.1 Original Hypothesis

3.2.1.2.1.1 Subtask 2.2 Bearing Design and Preliminary Testing

Under Subtask 2.2, ORPC would perform an assessment of suitability and longevity of the existing TidGen® bearing system with detailed load information generated from Subtask 2.1; compare the design information with experimental experience and data obtained from prior operation of the TidGen® TGU; and identify strengths and weaknesses of the existing bearing system. ORPC would then compare and document the characteristics, relative advantages and disadvantages of two new bearing types (PCD bearing and polymer roller element bearing). For each bearing design considered, ORPC was to specify a particular bearing to meet the design requirements in terms of life, friction, environmental suitability, capital cost and operations and maintenance (O&M) cost. ORPC was to select bearing type or types to design, fabricate, and test and will perform detail design of selected bearing(s) to match the selected demonstration system. ORPC would consult with bearing manufacturers to identify likely maintenance intervals suitable for the application.

Friction in the baseline TidGen® driveline design from the Vesconite sleeve bearings accounted for an estimated power reduction of 15 percent at full load, and bearings required complete replacement on a yearly basis. We were to reduce the frictional power losses in the driveline and to increase the maintenance interval by means of the improved bearing system.

Specific component metrics were to:

- Reduce the bearing friction losses to 5 percent of the rated power from 15 percent
- Increase the maintenance interval of the bearing system from 1 year to 5 years
- Increase the optimum TSR of the turbine from 1.6 to 1.9 by reduction of frictional losses

3.2.1.2.1.2 Subtask 4.1 Flume Testing

Under Subtask 4.1, ORPC would fabricate demonstration bearings replicating the final bearing selections, scaled down for testing in a bearing test facility utilizing a sediment flume test tank; testing was to include preliminary performance tests followed by extended testing of the bearings in a highly sediment-laden water flow. Test results were to include measurement and analysis of the bearings for frictional and wear parameters. ORPC were to generate design modifications to improve the bearing systems based upon information gathered from this flume testing and then repeat the detailed design

process for improvements to these bearings. ORPC were to perform life bearing tests in the test flume and finalize bearing specifications for application in the full-scale TidGen® Power System.

In conjunction with bearing testing ORPC would evaluate the performance of generator shaft seals as dependent upon final bearing selection. Shaft seals, recommended by the generator contractor, would be implemented on the flume bearing shafts where they would be exposed to the sediment-laden water. Similar loadings would be applied to the test seals as experienced by the generator seals.

Prior testing results for PCD bearing technology, as referenced in submitted reports to the DOE, indicated seals would not be required for either application in driveline or generator environments. ORPC would include seal requirements as well as any additional corrosion test data supporting final bearing technology selection.

At completion of flume testing:

- Bearing friction losses would demonstrate a reduction to 5 percent of the rated power from 15 percent
- Bearing wear would be demonstrated to be consistent with greater than 5-year maintenance interval
- Seal wear rate would be demonstrated to be consistent with greater than 3-year maintenance interval

3.2.1.2.2 Approaches Used

Marine hydrokinetic (MHK) devices require bearings with high load capacities, low friction, and long lifetimes, and must be suitable for use in low speed operations within a salt water environment. At the beginning of the Project there are no suitable maintenance-free bearings currently available with the capabilities and specifications to meet the Project milestones.

Previously, ORPC utilized a Vesconite (thermoplastic) journal sleeve-bearing as the main bearing in its advanced design cross-flow turbine. Vesconite is a polymer bearing material commonly used in the hydro power industry (Figure 44). Although these bearings were easy to implement and low cost, the bearings have shown to have high friction and wear rates and require replacement on a yearly basis. The cost of inspection and retrieval of the TGU is the largest operating expense for this technology and contributes significantly to a high levelized cost of electricity for power projects utilizing ORPC power systems. A suitable replacement for these bearings is necessary to improve system reliability and reduce operational costs.

Figure 44. New and used TidGen® Vesconite bearings. The used bearing (right) shows signs of heat damage and polymerization of the bearing material.

A review of alternative bearing technologies led ORPC to identify two suitable solutions to meet the stated milestone goals: a polymer roller element bearing and a PCD bearing (Figure 45). Both bearing solutions offer significant reductions in friction and have the potential of providing the necessary service life required.

Figure 45. Polymer roller element bearing concept (left) and Polycrystalline Diamond (PCD) conical bearing. The conical bearing shape for the PCD bearing is difficult to machine.

ORPC identified a plastic a polymer roller element bearing as a potential bearing solution. A properly designed plastic roller bearing would require no lubricants, would not corrode, and would have a lower coefficient of friction than a journal bearing. Selection of the proper strength and grade of material would be critical to the bearings life. After reviewing several potential bearing materials, Torlon was selected for its superior strength properties. Torlon comes in a variety of grades and strengths and would allow a bearing to be developed at an acceptable size. The roller element bearings were designed and built. Testing of the bearings was conducted in a flume at the University of Alaska Anchorage to determine the viability of this approach (Figure 46).

PCD bearings have been suggested for use as bearings in MHK devices. Each PCD bearing is comprised of numerous PCD discs individually bonded to a metal base (Figure 47). The diamond pucks are adhered to a metal substrate using braze. Due to the temperature sensitive nature of the diamond pucks, braze material options are limited to low temperature braze alloys, all containing various levels of zinc. Since zinc corrodes readily in marine environments, ORPC selected a braze material with the lowest possible zinc content for testing.

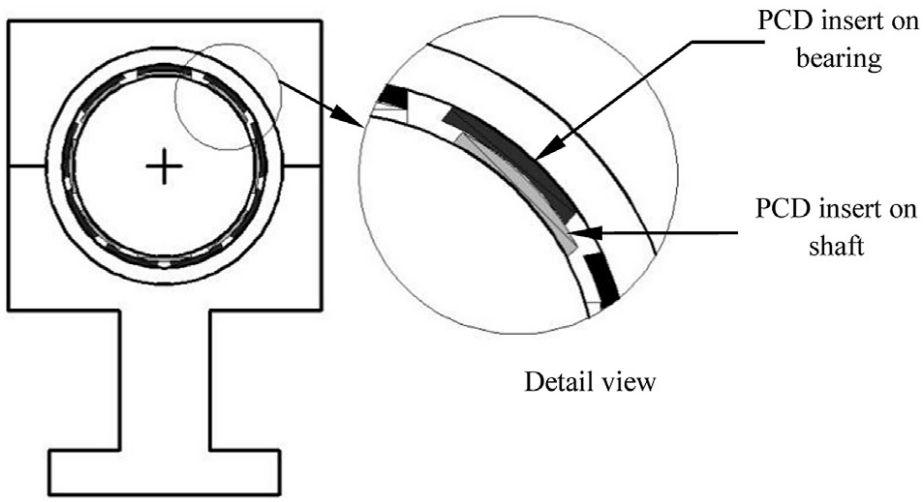

Figure 46. Typical PCD bearing 'puck' arrangement, showing contacting bearing elements

The base substrate material the pucks are adhered to, can be selected from a wide variety of materials, suitable for marine use. ORPC has had prior success with duplex steel. Accordingly, the substrate material was changed to a duplex steel for highest corrosion resistance of the base material. Previous test work in the UAA flume had measured PCD bearings performance. ORPC conducted various corrosion tests of the PCD bearings.

3.2.1.2.2.1 Flume Testing

Outstanding questions remained on technical aspects of both bearings, since the long-term use of either bearing in a subsea environment has not been demonstrated. ORPC initiated a series of engineering investigations into both bearing types to determine the suitability of each.

ORPC had previously completed a flume study with the University of Alaska Anchorage (UAA) to investigate friction and wear qualities of a PCD bearing in a simulated marine environment.[13] The flume test was designed to demonstrate the ability of a PCD bearing to operate in conditions that simulated an ORPC MHK device operating in a marine environment. The flume was also able to characterize the performance of bearings in environments with high concentrations of suspended sediments. The results of this initial test demonstrated the PCD bearings have an extremely low wear rate and low coefficient of friction. The wear in the load direction was unmeasurable and the coefficient of friction was significantly lower than a polymer sleeve bearing (0.02 for PCD versus 0.14 to 0.16 for sleeve bearing), (Figure 48 and Figure 49).

[13] Worthington, 2013.

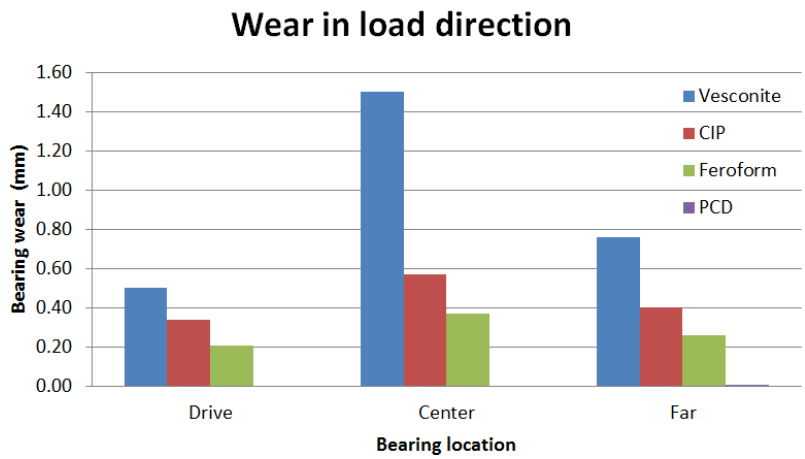

Figure 47. Wear of each bearing in the load-bearing direction for different types of bearing materials, with blue being the Vesconite used in TidGen®. The wear for the PCD bearing was so small as to be immeasurable.

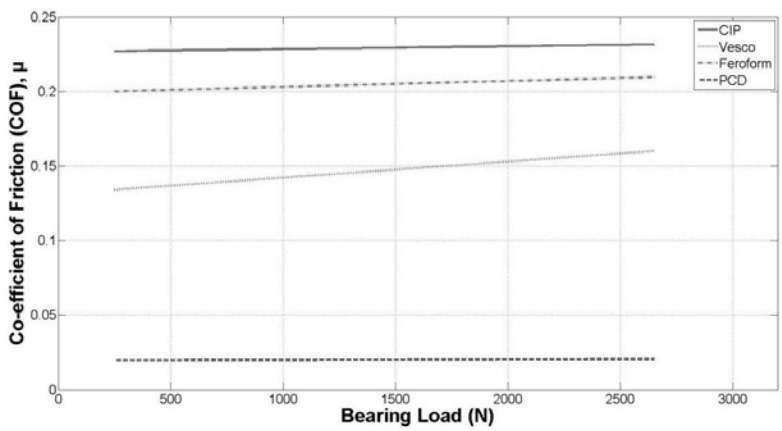

Figure 48. Co-efficient of friction versus load from flume testing. Of the polymer materials Vesconite had the lowest coefficient of friction, but the PCD friction factor was an order of magnitude lower than that of Vesconite.

ORPC designed a scaled version of a typical MHK polymer roller bearing for testing in the UAA flume. Materials were selected based on matrix of various Torlon grades, utilizing caged and non-caged bearing configurations. Torlon grades 7130 (30 percent carbon fiber reinforced), 4203 (electrical grade – extruded) and 4301 (bearing grade – extruded) were used.

The bearings were engineered, machined, and then assembled for testing at the UAA flume (Figure 50).

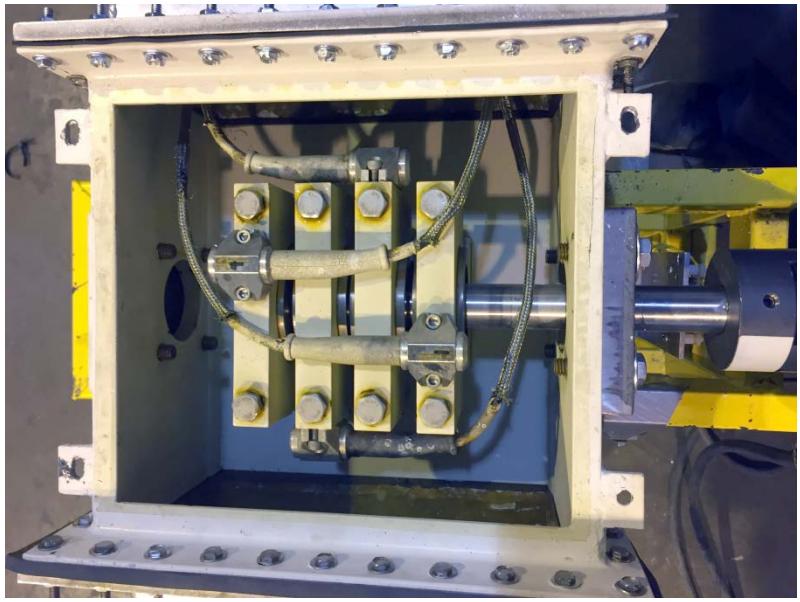

Figure 49. Bearings and accelerometers installed in UAA flume prior to testing. Four roller element bearing samples are loaded into the test rig.

A detailed test plan was developed, which included two separate flume test runs in two flume bays, a ramping of load over time, and measurement procedures. A total of 15 bearings were tested. The test was designed to determine which Torlon materials were most robust for an MHK bearing solution.

The first round of testing was ended after 24 hours due to particulate contamination in the flume. Debris in the flume contaminated the bearing races and caused premature failure in most bearing

materials. The first round demonstrated that one bearing material (Torlon 4203) was capable of operating and surviving in suspended sediment. The other bearing materials (4301 and 7103) both showed signs of premature failure (Figure 10).

In the second round of testing, the focus of the test was shifted to look more closely at performance at slightly lower loading of all polymers, without system contaminants. The results were similar to the first round of testing, with the 4203-material exhibiting superior wear characteristics and no failures. In fact, one 4203 bearing was reused from Phase I testing and did not fail.

Results from the UAA flume testing demonstrated excellent performance from the Torlon 4203 material for the rollers. Torlon 4203 withstood loads beyond that which would be expected based on a tensile-tensile fatigue test data by a factor of 4.4 times the number of expected cycles while the 7130 and 4301 materials failed at stress levels below the rated values. Thus, the test results not only demonstrated the viability of the 4203 material but demonstrated higher expected life for contact stress than the available tensile-tensile data, which is useful for confidence and reduction of size and cost of bearings utilizing the 4203 material.

Cooling proved to be an important consideration for plastic bearings. Open and unsealed bearing housings were engineered and produced for testing. Water levels were left unchecked (low) during a brief (6 hour) interval during testing. Rapid degradation occurred during this 6-hour window, which confirmed the need for adequate and continuous cooling during operation.

As part of the flume testing a preliminary evaluation of seal performance for a five-year service life was also conducted. The seals used in the flume test, to seal water in the flume where the drive shaft enters, were SKF radial shaft seal (designation 10178). The seals performed well over the life of the test. However, a major benefit of the PCD and polymer roller bearings is that both are designed to run in seawater. The seals only need to protect the bearing from intrusion of damaging materials and are not required to seal liquid or pressure differentials. Although sealing particulate matter is not a trivial task, especially over a long time in an environment that may include abrasive fine particulates, it is much less demanding than maintaining a liquid tight seal.

While testing indicated that only one variant of the plastic was suitable as a bearing material, but overall, a Torlon roller bearing was not considered to be a superior bearing solution than the PCD bearings. The flume testing steered the decision to focus on a PCD bearing solution for future work.

3.2.1.2.3 Problems Encountered and Departure from Planned Methodology

It was desirable to test mechanical seals, but budgetary constraints steered the Project to using less expensive, rubber lip-seals. This cost reduction allowed longer duration testing time periods which was deemed more critical than seal-testing, since seals would be unnecessary for Torlon roller bearings or PCD bearings.

Testing in sediment-laden water was part of the overall testing plan, to determine suitability of materials to deal with contaminates. Bearings were to be run in clean water, then sediment added at a later point, during testing. The flume proved to be filled with contaminants from prior testing, adding sediment was unnecessary. Several variants of the Torlon plastic rollers did not perform well with contamination and degraded rapidly, which provided an answer for the material durability under sediment water conditions.

3.2.1.2.4 Assessment of Their Impact on the Project Results

Both the polymer roller element bearing and the PCD bearing designs have been tested and proven to be offer unique advantages.

Milestone Goals:

- Reduce bearing friction losses to 5 percent of the rated power from 15 percent
- Increase reliability, consistent with five-year maintenance interval
- Increase optimal system TSR

Note that the milestone goals are stated in terms of operational parameters such as rated power, reliability, and operating TSR. These parameters are actually dependent on the details of the turbine system design, not just the bearings. Thus, a baseline system must be selected to evaluate the milestones. Additionally, available tools for turbine performance prediction, while useful for predicting trends, are often inadequate for accurate prediction of performance of a machine in a real environment. To provide a consistent metric, a turbine model that is quick, consistent and predictable, such as a stream tube model, is more useful than one which may be more accurate, but too time consuming to be useful, such as CFD. The performance metrics presented here are based on a streamtube model for the turbine performance, which is more than adequate for the purposes of demonstrating the gains from bearing enhancements.

The streamtube model is historically accurate in predicting optimum C_P and TSR. Figure 57 shows results from streamtube modeling of the TidGen®, fit to operational data at Cobscook Bay, Maine, in 2013. The highest curve represents an ideal condition that assumes no hydrodynamic or friction losses. The lowest curve represents the model fit to two operating points, at freewheeling and at the maximum operating condition. Note that the peak of a curve is the maximum C_P that could be achieved in perfectly steady state flow or with a control system that could perfectly maintain this optimum operating condition. In practice, operation at this peak C_P is difficult, requiring a highly effective control system as this represents a region where turbines typically begin to experience stall when flow speed suddenly drops. At aggressive control system gains optimum TSR approached the predicted 1.9, achieving 1.955 at higher control constants. For reference, the highest, most stable operating condition was further to the right of the peak, with a TSR of 2.14 with a corresponding power reduction of 17.8 percent due to the control system inefficiency.

For fitting the ideal curve to operational data points, the model drag parameter (μ) was increased to 0.53. Both fluid based losses (fluid drag) and mechanical friction drag compose this parameter. In the model, mechanical losses were assumed to be entirely due to bearing friction: other mechanical losses would be due to the couplings; however, these are negligible if the system is aligned properly. Additionally, the Project isolated contributions from bearing drag. The drag parameter was accordingly apportioned by applying the lower measured value of polymer sleeve bearing drag, 0.14. Choosing the lower parameter allowed for a conservative estimate of friction reduction. The solid red curve in the middle represented the modeled output assuming only the fluid drag with μ = 0.39. This curve represents an ideal turbine C_P isolated from mechanical driveline inefficiencies.

The first Project milestone was to reduce bearing friction losses to 5 percent of the rated power from 15 percent. Both bearings had similar coefficients of friction, with the PCD bearing material being the preferred option. The dotted blue curve in the middle represents fluid drag plus the much reduced PCD friction drag coefficient of 0.02 (Figure 57). This curve thus represents significant turbine performance increases above the measured performance represented by the lowest, solid blue curve.

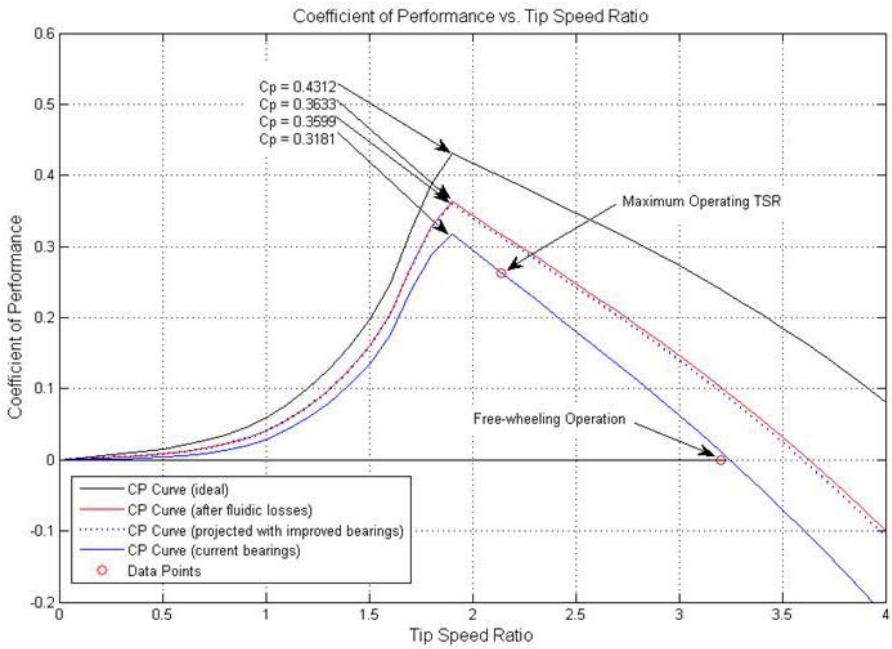

Figure 50. TidGen® coefficient of power versus TSR curve with different levels of mechanical loss model values applied.

Losses were calculated as ratios of estimated peak C_P for each curve, shown in Table 18. Fluidic losses were estimated by taking the ratio of the red curve peak C_P, 0.3181, to the ideal case of the topmost curve, 0.4312. Baseline mechanical losses were estimated by taking the ratio of the solid blue curve peak C_P, 0.3181, to the red curve peak, 0.3633. The improved mechanical loss was estimated by taking the dotted blue curve peak C_P, 0.3599, to the red curve peak, 0.3633. The baseline bearing losses were reduced from an estimated 12.4 percent to 0.9 percent, meeting the initial milestone goals of an approximate 10 percent reduction.

Table 18. Performance and loss estimates for bearings

	C_P, Turbine Efficiency	**Fluidic Losses**	**Bearing Losses**	**Total Losses**
No losses	0.4312	-	-	-
Ideal turbine C_P, fluid losses	0.3633	15.7%	-	-
Baseline	0.3181	15.7%	12.4%	26.2%
New Bearings	0.3599	15.7%	0.9%	16.5%

The second Project milestone was to increase reliability, consistent with a five-year maintenance interval. Both the PCD and polymer bearings have proven to be a long lasting (low wear) solution. No measurable wear was noted after flume testing for either bearing. Based on initial test data, both bearing solutions appeared capable of meeting the five-year maintenance goal, but the PCD bearing is believed to be more robust.

The third Project milestone was to increase optimal TSR. The bearing improvement program does not directly improve the optimal TSR, since the optimal TSR is dependent upon the foil design and not directly affected by the bearing friction. Indirectly, the demonstrated improvements in bearing friction will allow for more efficient operation at higher TSRs, consistent with the milestone goals.

ORPC feels both identified bearing solutions have successfully met the initial milestone design criteria. Testing results for both bearing types was informative and useful in developing this MHK solution. The results have identified two strong bearing solutions that can be implemented on future devices.

3.2.2 Driveline Build and Validation – Subtask 4.2, Driveline System Testing

3.2.2.1 *Original Hypotheses*

Upon completion of generator testing, ORPC would construct a section of a full TidGen® TGU PTO with new generator and bearings and would test it with applied lateral loads at the generator manufacturer dynamometer facility. Appropriate loads will be applied to the system to replicate those determined by analysis in Task 2 and as defined by the generator manufacturer in Task 3. A test plan would be created to replicate and test the expected operating conditions including turbulence at full load. The test plan would be reviewed and released by the Project team. Critical resonance frequencies of the driveline would be empirically determined during testing. Ramp-up and ramp-down of applied loads and torques would be implemented in the test regime. Power transmission performance of the driveline would be measured using suitable torque measuring instruments at various stages of the driveline. This test was not intended to be a life test, as a full water immersion would be required to properly estimate life of various components, but it would instead serve as a verification of the design work completed on the PTO. Generator wet bearing prototypes would be incorporated for initial analysis of performance and suitability under replicated generator load conditions.

Component metrics to be verified by driveline testing included reduction of friction losses, demonstration of rated power and efficiency, demonstration of design mass to support the Project target for increase in PWR, and demonstration of bearing wear under load to achieve targeted maintenance intervals of 5+ years.

At completion of driveline system testing:

- Driveline frictional losses would have been demonstrated to be less than 5 percent of rated power as compared to a baseline of 15 percent of rated power.
- Wear on all bearings would be substantiated by analytical model predicting 5+ years maintenance intervals.
- Complete PTO would demonstrate achievement of rated power.
- Complete PTO would demonstrate achievement of rated efficiency.
- Complete PTO would demonstrate achievement in target generator system mass to support Project PWR targets increase.

3.2.2.2 *Approaches Used*

Driveline system test required refined design of the driveline test components, design of the driveline test rig, testing and data post-processing.

3.2.2.2.1 Bearing and Driveline Test Components Design

The suitability of the PCD bearings in flume testing was proven but based on the assumption of good alignment and even loading on the puck surfaces. To ensure this performance was maintained in a full-scale driveline arrangement, careful design of the bearing housings was needed, along with refinement of the bearings suitable for driveline integration. Below is a description of component design for the driveline test rig.

3.2.2.2.1.1 Bearing Design Refinement

The PCD bearing requires a carefully designed driveline system to limit edge loading and obtain maximum life from the bearing. ORPC developed a specification document that detailed anticipated operational loading from the turbines. Operational loads were derived from CFD modeling and analysis of the turbine system. Anticipated turbine and driveline deflections were based on loads derived from earlier CFD modeling and analysis of the turbine system.

System loads drove the design of bearing, shafting and driveline components. The bearing diameters were designed around shafting and housing requirements necessary to withstand operational loads, resulting in a bearing diameter that had excess loading capacity. Shaft sizes were larger than the minimum bearing size and consequently, the bearing would withstand operational limits with some reserve capacity.

3.2.2.2.1.2 Driveline Configuration

Moving forward with PCD bearings lead us to select a driveline configuration that did not over constrain the driveline but also suited the PCD bearings attachment to shafting and housings. The design chosen used two sets of two turbines connected by a flexible coupling. At the center of each of these two turbine sets is a combined, axial and radial support and on the outside, two radial supports (Figure 59).

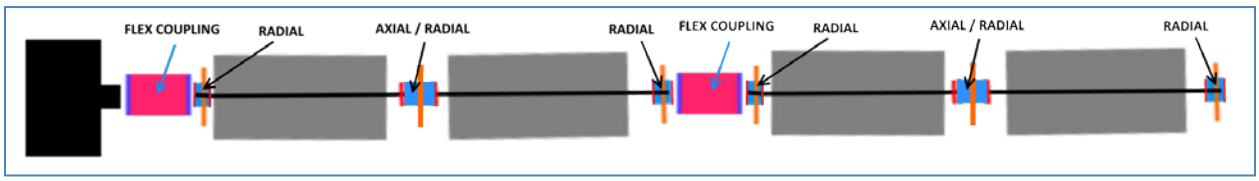

Figure 51. Four-turbine driveline configuration showing the arrangement of couplings and axial and radial bearings

3.2.2.2.1.3 Radial only / End Bearing supports

Combined / Mid Bearing Support

The combined radial/axial bearing support proved to be a more challenging design problem then the end supports. The selective weakening of the flexplates to accommodate angular deflection also eliminates the supports ability to take an axial load (Figure 63).

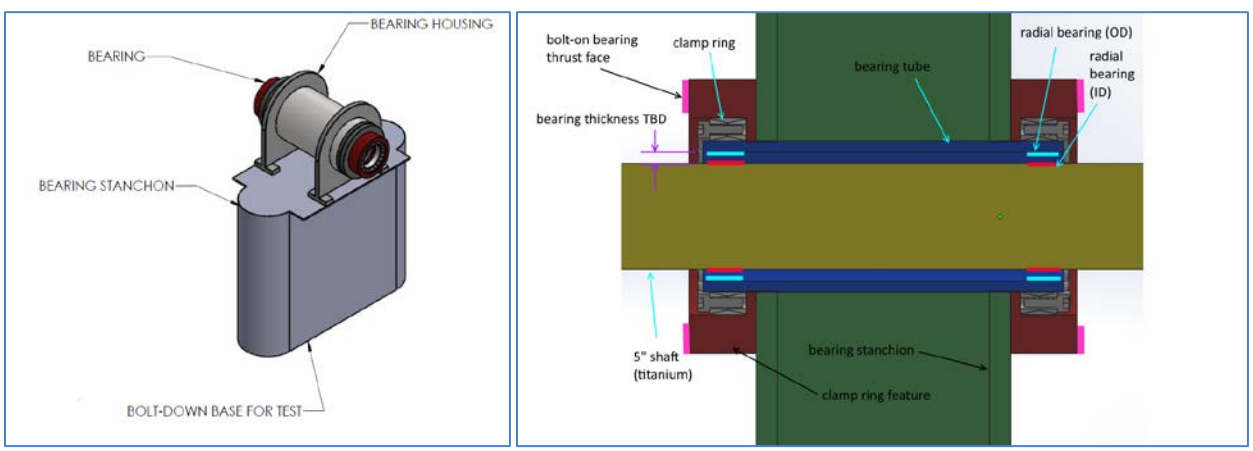

Figure 52. Early concept for a mid-bearing assembly

Initial concepts utilized a tube structure with a radial bearing and single direction thrust bearing at each end. Although this design accommodated all the necessary bearing components and supported turbine loads, it did not allow for shaft deflection and produced significant edge loading on the PCD bearing surfaces.

After some iteration and analysis, a 'cantilevered bearing block' design was chosen as the best path forward for the mid bearing support. The principle behind the design was to use a short beam element from the central housing support that transferred load into the chassis and support the radial and axial bearings at the end of those short sections. The stiffness of these beam sections could be tailored to match that of the bearing stub shaft and would allow the housing to support the shaft while matching the angular deflection of the shaft and keep good cylindrical contact in the bearings (Figure 64).

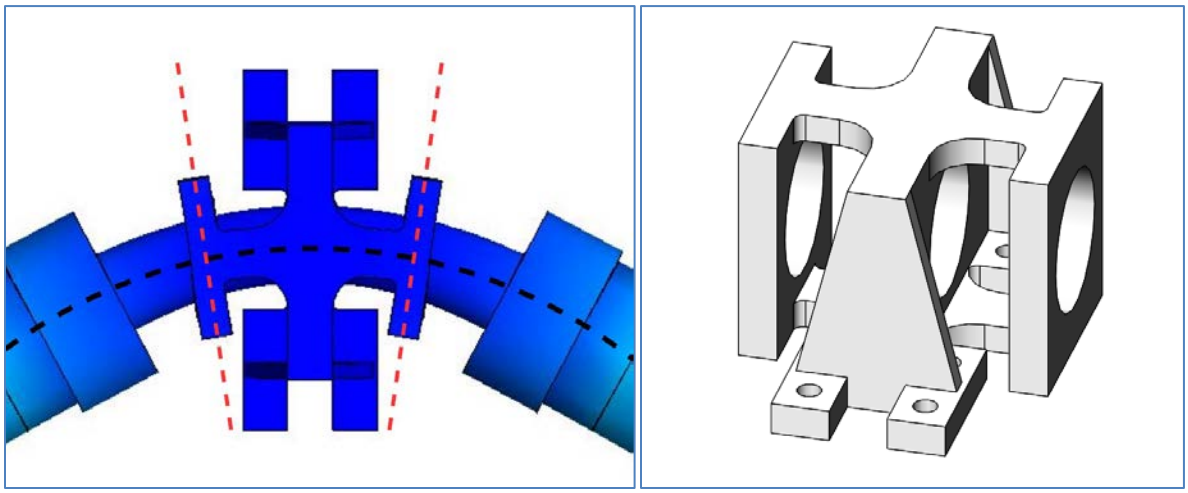

Figure 53. Mid bearing housing design utilizing cantilevered bearing blocks to maintain cylindrical contact on PCD bearings.

As with the end bearing, this housing was supported by a welded steel structure that transmitted loads into the test facilities reaction floor. This assembly was also fitted with seal and water cooling components to provide the water cooling and lubrication a submerged bearing would see.

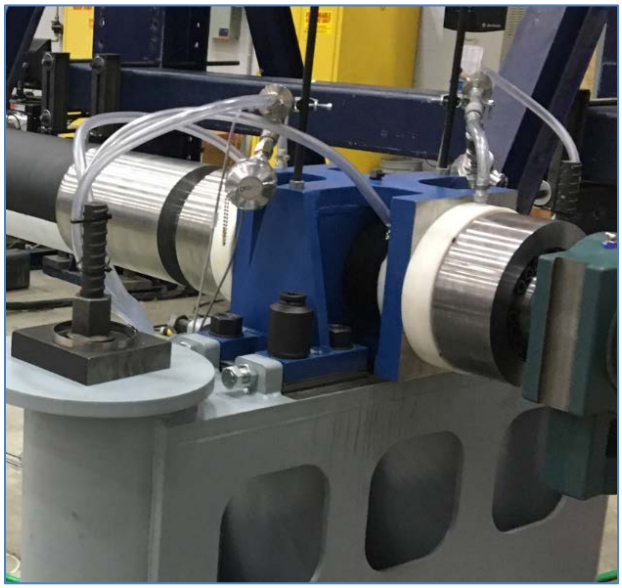

Figure 54. Final assembled mid bearing housing and assembly in the driveline test rig showing water cooling loops for bearing temperature control

3.2.2.2.2 Driveline Test

Due to delays in generator manufacturing and the high costs associated with testing a driveline section under full lateral and torsional loadings at the generator manufacturer, ORPC developed an alternate driveline test. A full-scale model of a driveline incorporating PCD bearings and engineered housings was designed and built for 5 months of testing at the University of Maine Advanced Structures and Composites Center (ASCC).

The purpose of this test was to characterize the frictional losses associated with the PCD bearings and test the suitability and functionality of some commercially available shaft couplings and expansion bushings in cross-flow turbine drivelines. To meet space limitations in the ASCC's lab, the span between the bearing housings was shortened so the bearing stanchions would match the spacing of anchor points on the floor at the ASCC.

Hydraulic actuators attached to conventional roller bearing housings were used to apply radial and axial loads to the driveline that simulated the hydrodynamic loads generated by crossflow turbines. A single torque sensor mounted near the dyno drive unit measured the total frictional torque generated by the driveline. In addition to this torque measurement, inlet and outlet temperatures with corresponding flow rates for water cooling of the PCD bearings were collected as another indication of the frictional losses in the bearings.

In addition to simulating and testing operational loads for our driveline, the test rig was designed to evaluate the influences of misalignment and uneven loading. During testing, the large roller bearing located in the middle of the drive shaft in Figure 65 was moved to both ends of the drive shaft to isolate loading applied to both the end and middle PCD bearing assemblies. After this loading isolation, the driveline was misaligned in both the radial and vertical directions, in different increments, to quantify the effects of static misalignment and measure any additional losses it creates.

After 5-6 months of testing and 200+ hours of run time, the test rig was disassembled and put in storage. The results showed that PCD bearings are a promising option for subsea turbines with no detectable wear and relatively low friction compared to other water lubricated bearings.

3.2.2.2.2.1 Test Setup

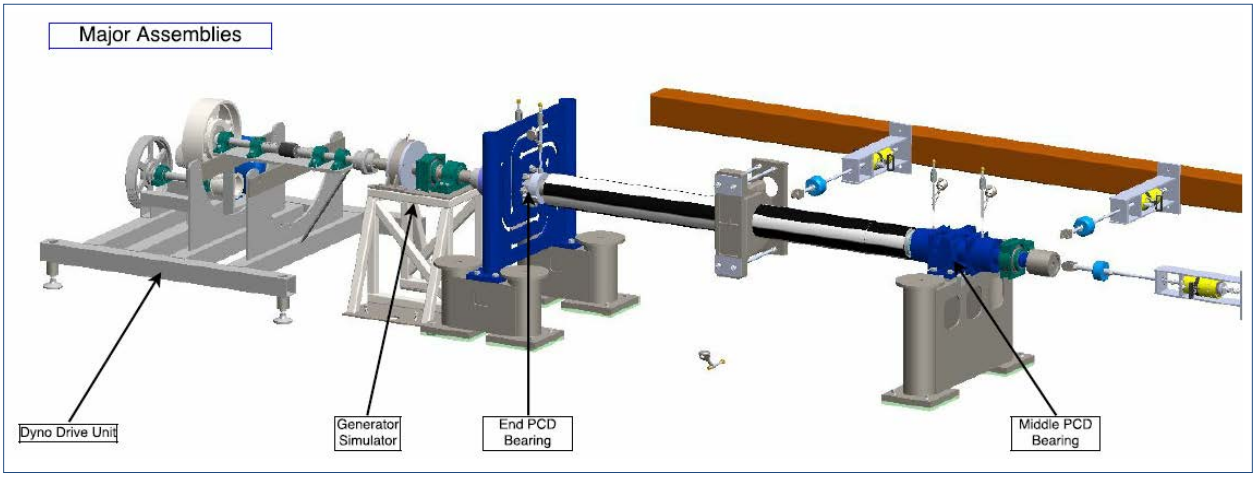

Figure 55. Major assemblies of the PTO driveline test rig

As Figure 66 shows, a full-scale test-system was designed to replicate an actual device with corresponding loading of the TidGen® system. The test-rig had to fit within the confines of the test facility, interface and attach to the test facility floor, and meet budgetary constraints to achieve success. The components were designed and tested at full scale, but overall length of driveshaft was shortened to fit inside the available space at the ASCC facility (Figure 67). This caused minor issues with evaluating issues related to shaft flexure, since the shaft was much stiffer than necessary and would flex in a different manner than the full-size system. The test rig could be purposefully misaligned to simulate shaft flexure.

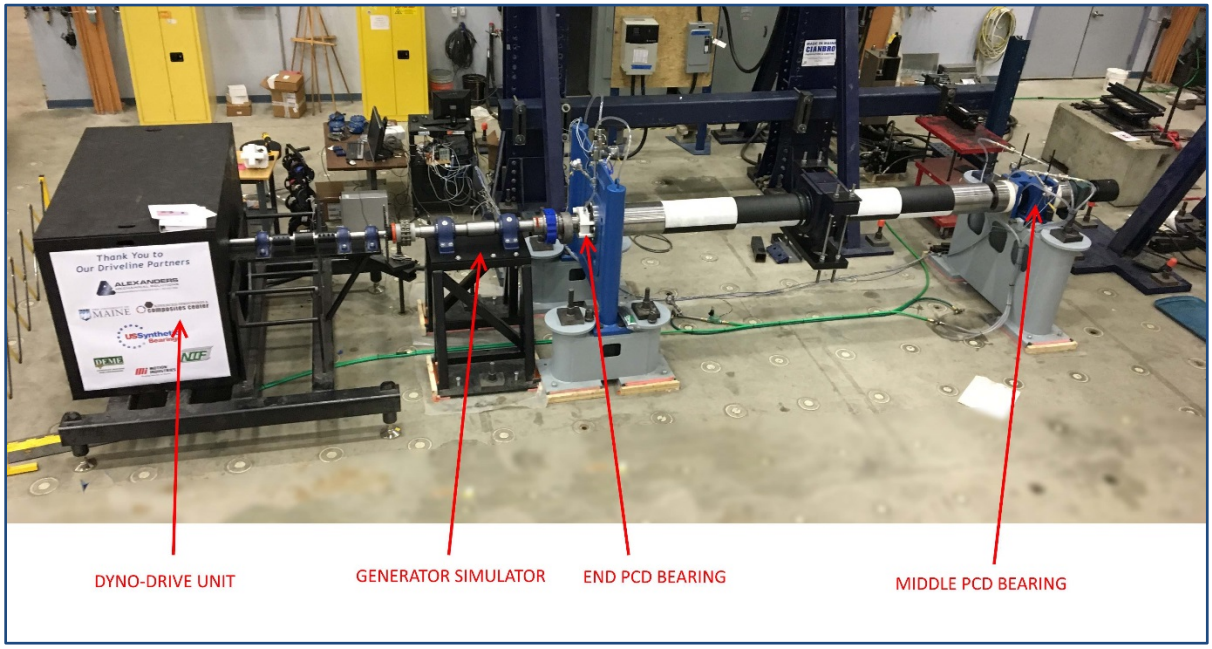

Figure 56. Fully assembled test rig at ASCC

Test Rig: Dyno Drive Unit

The "Dyno Drive Unit" provided the rotational shaft torque for the test rig. As repurposed equipment previously used to test the ORPC RivGen® generator and associated power electronics, it met the criteria for RPM and torque for a drive and was modified for this test. A suitable resolution torque-sensor was added to the system and minor adjustments made to the drive belt tensioning to make the unit operable for this test.

Test Rig: Generator Simulator

A part of the generator development effort included preliminary design, test and demonstration of a large PCD bearing suitable for incorporation into the generator. Such a bearing potentially allows for "wet gap" operation of the generator, where water fills the air gap between the rotor and stator. The test rig was developed with the intention of retrofitting a test generator bearing into the driveline. The bearing was held in a generator simulator that replicated the internal dimensions of the generator housing to test a PCD replacement bearing for our Rolls Royce Marine generator. The bearing was installed at the completion of the driveline testing effort, so the data could be isolated and evaluated separately from the remainder of the system. This separation also allowed us to reuse the sensors and hydraulic equipment from the driveline testing.

Test Rig: End PCD Bearing

The end PCD bearing and stanchion incorporated the flex plate and bearing housing. It was externally sealed and water-cooled to simulate the subsea environment. The water cooling apparatus had one inlet and two outlets to measure temperature rise and water flow through each bearing in the housing.

Test Rig: Middle PCD Bearing

The middle PCD bearing incorporated 2 pairs of thrust and radial bearings into a flexible housing. As with the other PCD bearing, it was externally cooled, and temperature rise and flow from each of the two bearing sets was measured.

Loading Bearings

Traditional rolling element bearings were attached to hydraulic rams to simulate the turbine loading on the PCD bearings. Two radial bearings applied a simulated radial force and one thrust bearing applied the axial forces. Friction for all three loading bearings is considered minimal compared the sliding friction in the PCD bearings, and a lump-sum of 5 percent of the total torque is considered attributable to these bearings.

Instrumentation

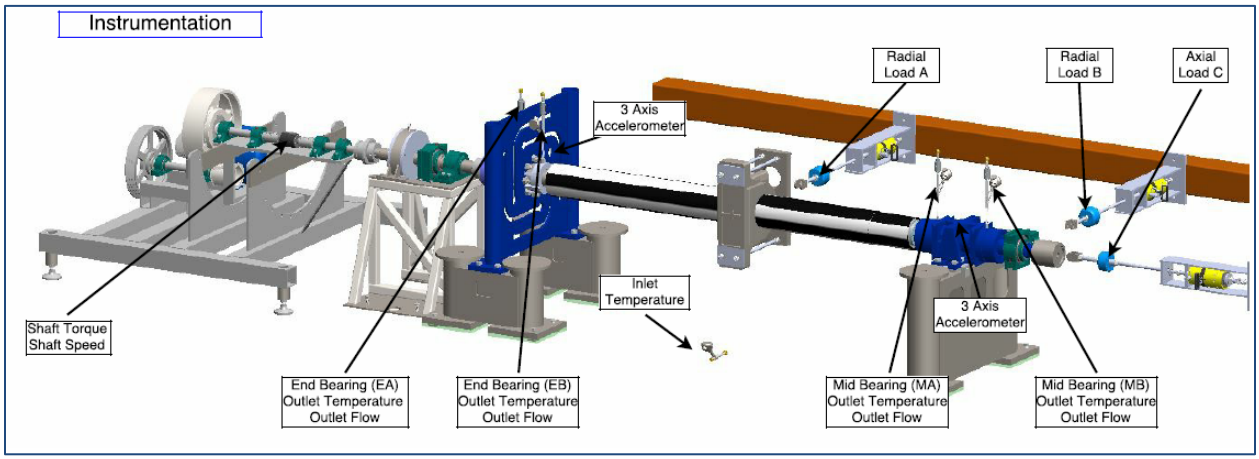

Figure 57. Map of instrumentation monitoring the driveline test rig with signal names and locations

The major instrumentation on this test rig revolved around measuring the power loss to friction in the PCD bearings. As Figure 6869 shows total applied loads (Load A, Load B, and Load C) as well as the torque created by the system provided a means to measure this power loss mechanically. Additionally, cooling water inlet and outlet temperature and outlet flowrates were used to measure the thermal power generated in the PCD bearings. These more localized measurements of individual bearings provided data on the relative performance of the different PCD bearing assemblies under different loading and alignment conditions. On top of the power loss measurements, 3 axis accelerometers were mounted on each PCD bearing assembly to monitor bearing and system vibrations.

Table 19. List of sensors in driveline test rig

Sensor	QTY	Link
Datum M425 Rotary Torque Sensor	1	https://datum-electronics.co.uk/product/rotary-torque-sensor-m425/
Interface Fatigue Rated Load Cells	3	http://www.interfaceforce.com/index.php?1000-Fatigue-Rated-LowProfile-Load-Cell&mod=product&show=1
ProSense Magnetic Flow Meters	4	https://cdn.automationdirect.com/static/specs/psfmm1001magmeter.pdf
ProSense TW04-01 RTD Thermowells	5	https://cdn.automationdirect.com/static/specs/psthermowellsl.pdf
PCB Triaxial Accelerometers	2	http://www.pcb.com/Products.aspx?m=356A15

Loading Configurations

As Figure 69 shows, the test rig was designed so that applied Load A could be relocated to preferentially load the two PCD bearing assemblies. These different configurations define some of the different stages of the driveline test.

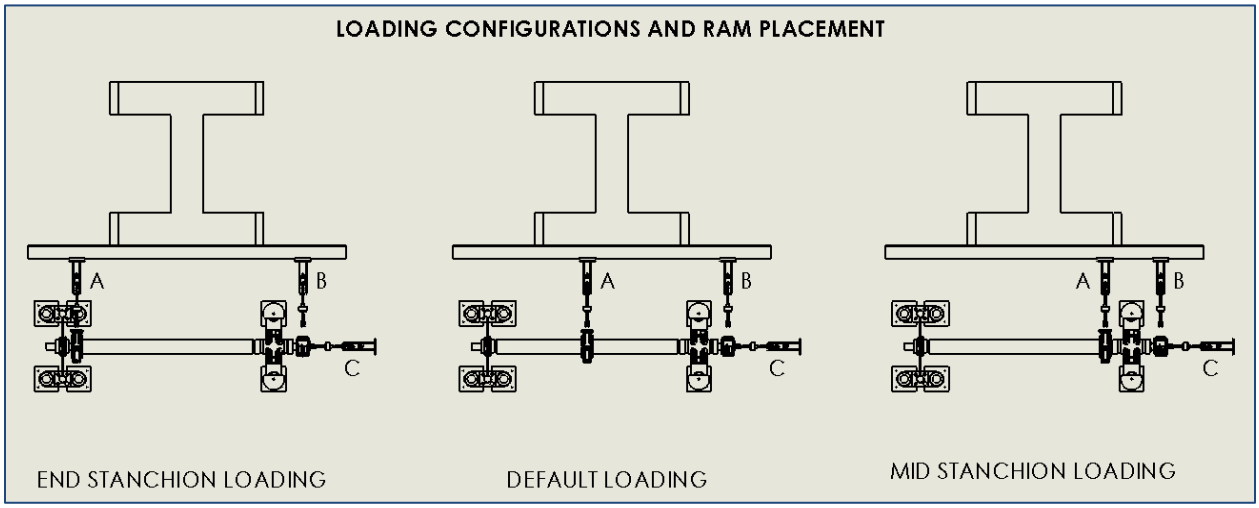

Figure 58. Schematic of the different loading locations for Load A cylinder. Default is with load at the center of the assembly. Alternative arrangements favor the individual PCD bearing assemblies.

Misalignment Testing

Another important aspect in characterizing the driveline design was its tolerance to misalignment. To capture this, the middle bearing assembly was moved radially and vertically in different magnitudes and combinations. The resulting driveline friction from misalignment was measured with and without applied loads. The directions of these misalignments are shown in in Figure 7070.

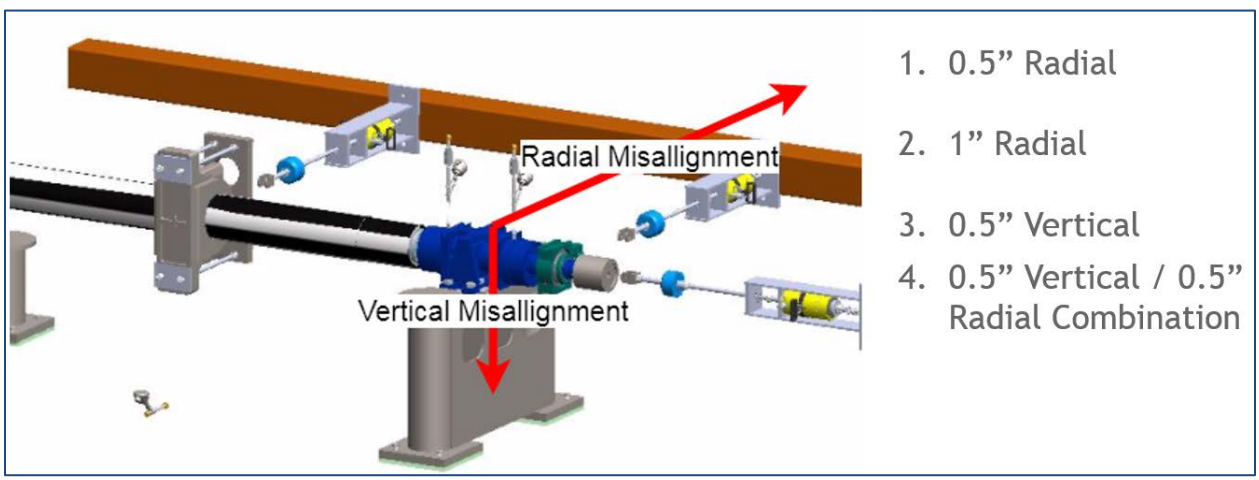

Figure 59. Illustration of the directions and magnitudes of the different driveline misalignment conditions tested.

Data Analysis

All data was captured and recorded at 1Hz by a LabView DAQ system designed by ASCC. These National Instrument formatted data files were written in 1 hour increments as the test ran and later post processed using some openly available numerical python libraries. This code loaded multiple data files,

converted units, plotted and combined signals into calculated values such as PCD CoF and thermal power generation (Figure 71).

$$\mu = \frac{Torque * \eta}{F_r * R_r + F_a * R_a}$$

$$\eta = \text{PCD Torque Fraction} = 95\%$$

$$F_r = \left|\left|\vec{F}_{LoadA} + \vec{F}_{LoadB} + \vec{F}_{gravity}\right|\right|$$

$$F_a = F_{LoadC}$$

$$R_i = \text{PCD Bearing Radii}$$

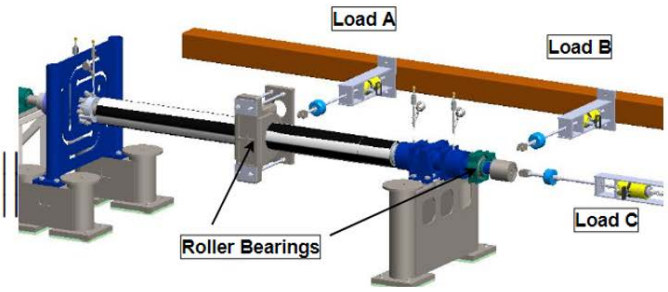

Figure 60. Lumped model of the mechanical measurement of PCD bearing coefficient of friction (CoF).

Test Operation and Discussion

Testing at ASCC was conducted over a three-month period. The testing can be broken down into multiple phases based on the hydraulic cylinder placement and the alignment condition of the driveline. Each of these operational phases is discussed in more detail below.

1. System setup / install / configuration
2. Break-in period
3. End PCD bearing isolation
4. Middle PCD bearing isolation
5. Misalignment operation / testing
6. Post-break-in period data collection
7. Generator bearing test

System Setup/Install/Configure

The system was assembled and instrumented over several weeks. Water cooling lines were run, sensors installed, and the DAQ and safety systems tested. Once all pieces were assembled, a system alignment was performed with a laser tracking system. This professional alignment assured that the driveline was aligned within 0.010 in.

Initial startup went relatively smoothly with some unforeseen delays and complications. The data acquisition formatting and post processing was finalized easily but it took some time to correctly set all safety trip limits so that the test could run unsupervised. Also, an international customs shipping delay in obtaining the torque transducer data-card was the last piece to be assembled before the system could collect meaningful data. Data was first collected on March 15, 2017 and testing continued through June 2, 2017.

System Startup/Break-In Period

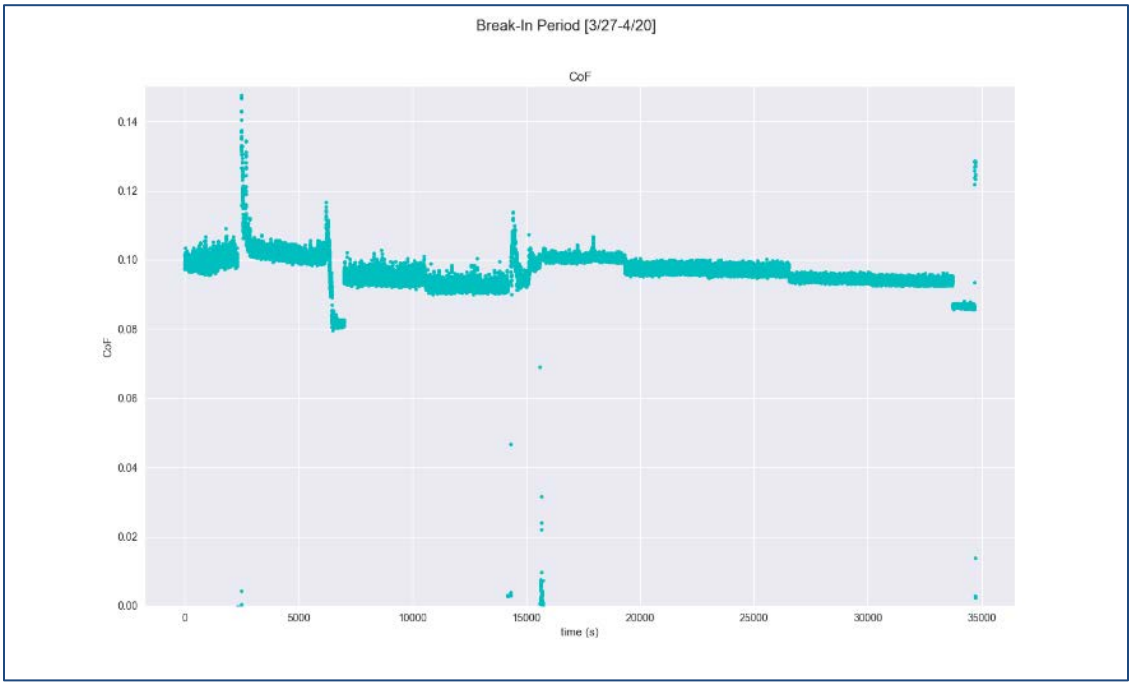

Figure 61. COF for break-in period showing a slight decline in CoF over a ten-hour period. Variations in CoF are related to changes in loads during this period

During the break-in period, the system was run, as aligned. Loads were varied, and the system had intermittent issues that were corrected. The DAQ system and control system were continuously improved and emergency shutdown safeguards were implemented to achieve autonomous operation. PCD bearings rely on having a smooth surface to achieve their lowest COF during operation. Newly manufactured PCD bearings have a relatively rough surface finish with a high COF (0.1-0.2). Without performing additional “polishing” after initial manufacture, the as-manufactured bearings have a “break-in” period to achieve minimum COF. The exact length of this break-in period varies but is directly related to overall loading, speed, and cooling. Since the material is very hard, it takes some time to polish the running surfaces to achieve a glassy, smooth, low COF operational characteristic.
As Figure 722 shows, the measured COF varied during break in and we did see a gradual decline during testing. Initial COF values ranged in the 0.1 range during this period and had slow and gradual decrease to 0.08 near the end of testing. Despite the incomplete break-in of the bearings, timing constraints pushed us to continue with other testing configurations.

End Bearing Isolation

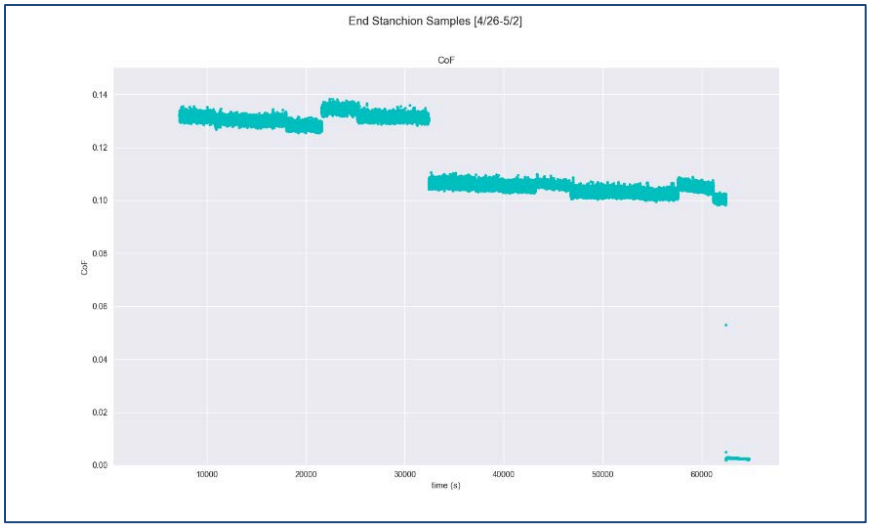

Figure 62. COF for period with loads focused near the end stanchion

The main hydraulic cylinder was moved to a position nearest the end stanchion to selectively load the bearings in the end-stanchion while imparting a minimal load on the opposite bearing (Figure 69). This was an attempt to "isolate" the end stanchion bearings and more precisely determine the COF for this bearing alone. Load Cylinder "A", now adjacent to the end bearing assembly, was heavily loaded while the remaining cylinders were left minimally loaded.

As was true for all test-configurations, the COF started at an initial, higher value and gradually decreased over the duration of the test. This is likely due to the "polishing" effect and introducing new sliding surfaces upon the system setup change. The resultant calculated COF for this bearing, at the end of this test, was a nominal 0.10. The bearings were not fully polished at this point which contributed to a slightly higher COF than was achieved at the end of the test.

Mid Stanchion Isolation

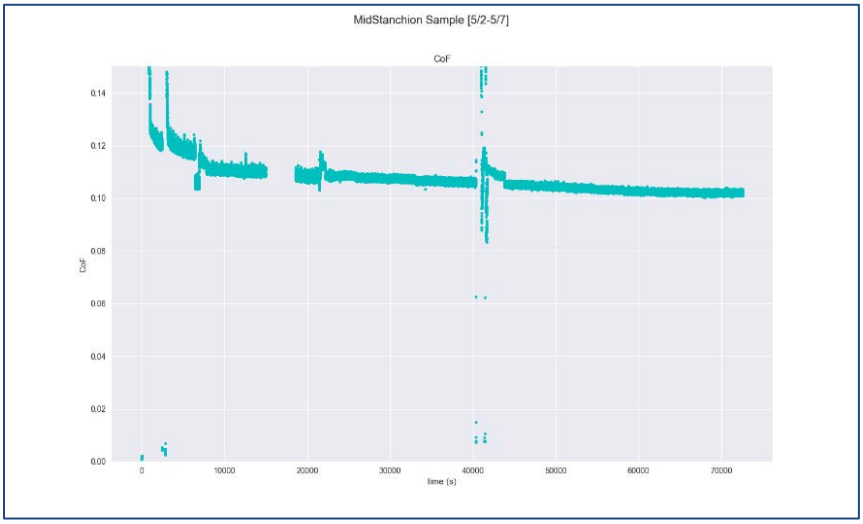

Figure 63. COF for mid stanchion isolation period

Load Cylinder "A" was then moved to a position nearest the middle bearing assembly (Figure 69). The calculated COF for this bearing, in this configuration, eventually reached a nominal 0.10. This is nearly identical to the previous test and confirms the overall performance of each bearing to be similar at this point in operation.

Deflected/Misaligned

The driveline design was engineered to accommodate misalignment and shaft deflection. Misalignment of bearings, relative to one another, can occur from system flexure, from operational loading, as well assembly alignment tolerances. This was a priority in the design since alignment and system flexure has been identified as a point of failure in previously deployed hydrokinetic-systems.

The middle bearing housing assembly had slotted mounting holes and removeable spacer plates to introduce known misalignments without moving the larger base it was attached to. Testing was performed at 0.5 in. and 1.0 in. of vertical and radial misalignments as well as a combination.

As the following sections show, radial or vertical misalignment limited to 0.5 in. led to a small increase in bearing friction. This ~10 percent increase was deemed an acceptable and practical bound on our assembly alignment tolerances. When we pushed the system into further misalignment, the friction increased dramatically. At more than double the aligned system friction, we could not fully load this test configuration do to exceeding operational limits of the torque-range on our torque sensor.

Misaligned Testing: 0.5 in. Radial

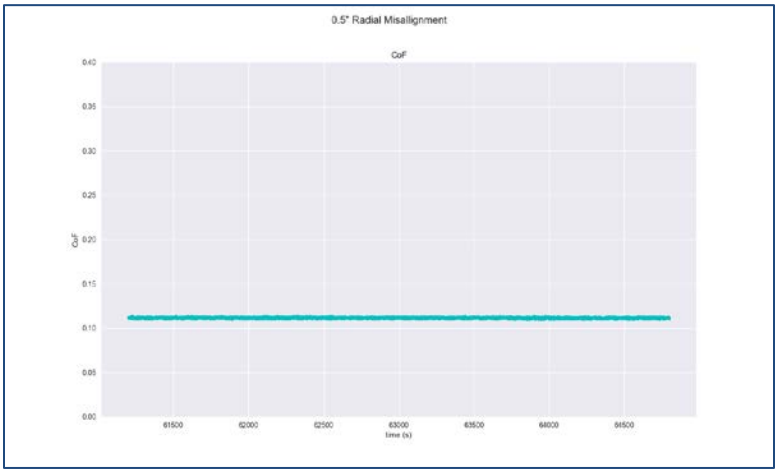

Figure 64. 0.5 in. Radial Misalignment CoF

Misaligned Testing: 1.0 in. Radial

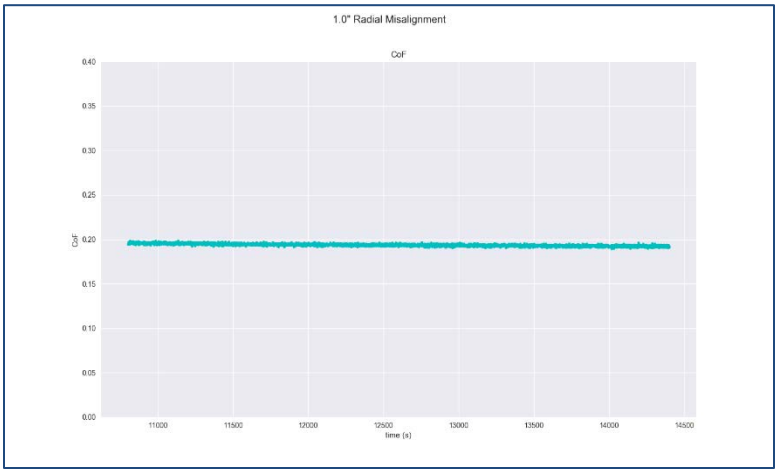

Figure 65. 1.0 in. Radial misalignment CoF

Misaligned Testing: 0.5 in. Vertical

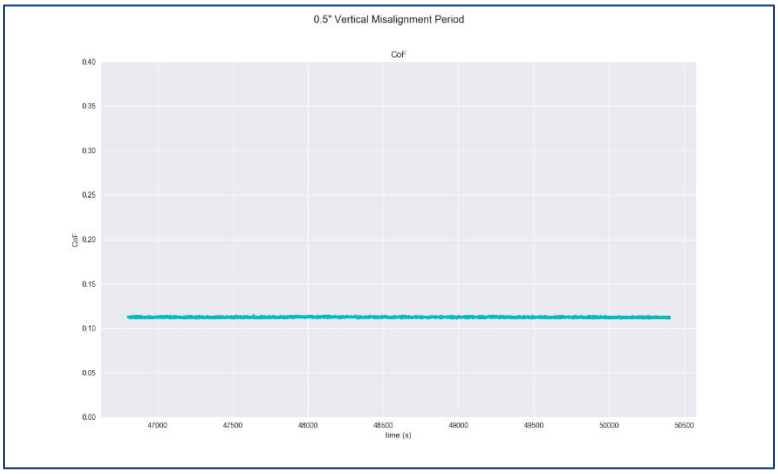

Figure 66. 0.5 in. Vertical misalignment CoF

Misaligned Testing: 0.5 in. Radial and Vertical

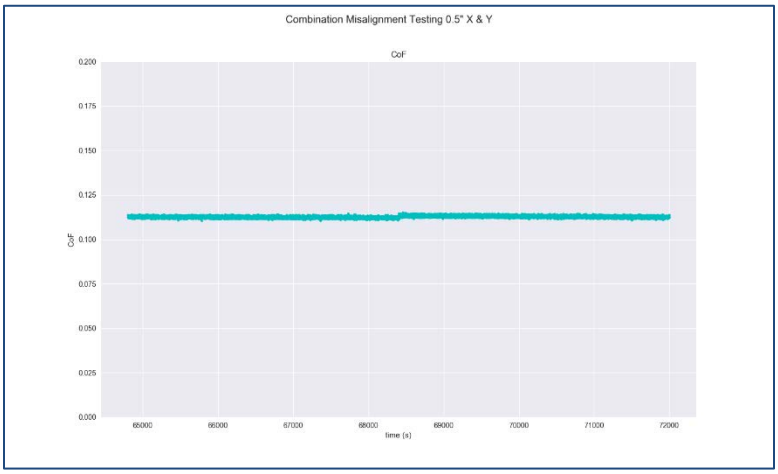

Figure 67. 0.5 in. Combination misalignment CoF

Final Aligned Data

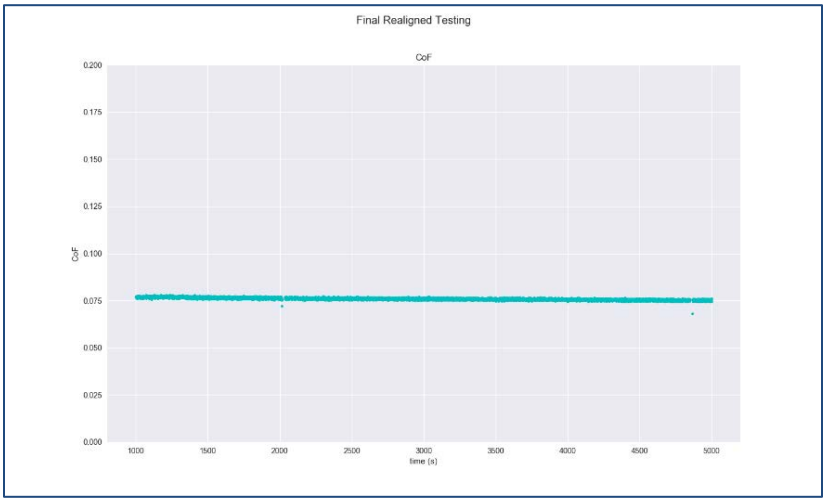

Figure 68. COF for final aligned test. There is still a slight decline in coefficient of friction over this test period of one hour

The last stage of testing returned the system back to the original alignment and standard, balanced loading. This was an important step to ensure repeatable results and to gather data at the last stage of the test, when the bearings were at their maximum break-in and polished state.

The end results aligned with expectations. The additional bearing loads from misalignment testing aided in polishing the surfaces, since the overall COF improved significantly. During this final stage of testing, we achieved a repeatable COF of 0.08, which is the best COF that had been measured during testing. Unfortunately, because of the high initial friction we were unable to run the rig at full load without overloading our torque transducer. US Synthetics has historical data on bearing performance that show an asymptotic break-in behavior; depending on housing design, bearing design and whether the bearing their experimental data has shown coefficients ranging from less than 0.01 to as high as 0.08 under similar conditions. Because of unexplained issues and evidence of incomplete break-in of the bearings, to be discussed below, the asymptotic behavior projects an eventual COF approaching a value ~0.04-0.05 where it will level off and remains. The subtle negative slope in the previous plots is consistent with that behavior except our loads and speeds did not bring us to the final possible COF. It is believed that continued operation and self-polishing would allow for even lower COF values – potentially achieving the 0.02 range that was initially expected.

In an actual deployed system, the turbines will provide more torque and load than we were able to budget into this test. That coupled with the many hours of operation a deployed system we are confident that we can achieve lower COF values than we were able to demonstrate in this test.

The PCD bearing surfaces begin with a relatively coarse surface condition from the manufacturing process. As the rotor and stator surfaces run against each other they gradually polish to a smooth glassy surface. The rate at which this polishing occurs is dependent on the contact pressure and surface speed of the bearing material. As the bearings begin to break-in and the surfaces start to match more and more the contact area of the bearing increases and the smoother surfaces have a reduced polishing effect. The result is an asymptotic reduction in the bearing friction with a majority of the improvement coming early on.

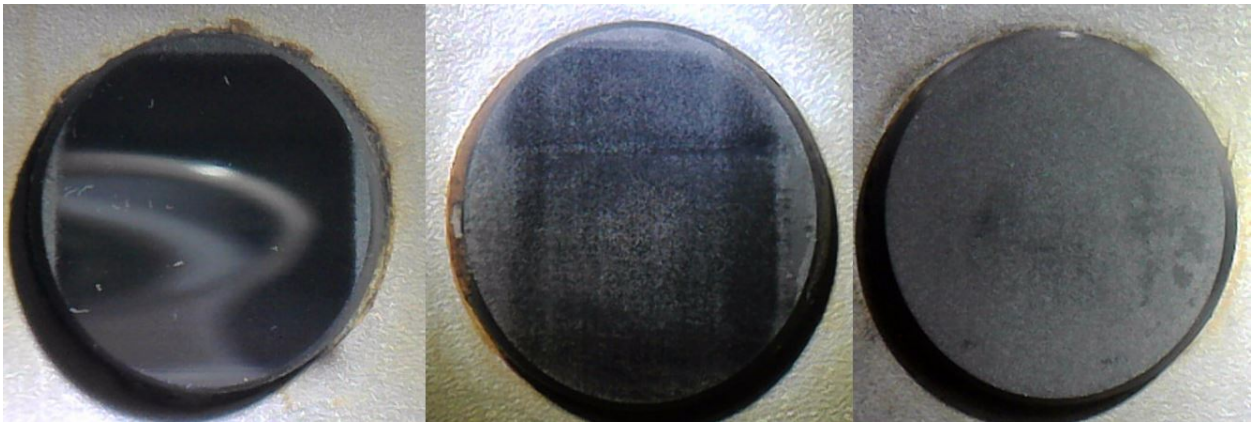

Figure 69. Spectrum of surface wear on PCD bearing inserts after driveline testing from fully polished to untouched

As Figure 8080 shows, examination of the bearings at the end of testing showed a wide range of surface finishes from completely glassy smooth to original fabricated surface condition. The diameters of the radial bearings were also measured to try and detect the wear, but the results were indistinguishable from measurements previous to testing. The polishing behavior appears to only effect the surface roughness and does not consume or remove the PCD bearing material. Although this was not a life test, these results align well with our expectations that these bearings will have a long service life.

3.2.2.2.2.2 Unexplained Behaviors

During testing, several unexpected phenomena occurred, that have not been entirely resolved or explained. Details are discussed below.

Vibration

Shortly after system startup, the drivetrain began to produce a ringing sound. It typically would occur when the axial load was applied to the mid-stanchion and frequency was independent of RPM or load applied. The measured frequency was dominant at 4,700 hz. Given the low operational RPM (60 rpm), this high frequency output was unexpected.

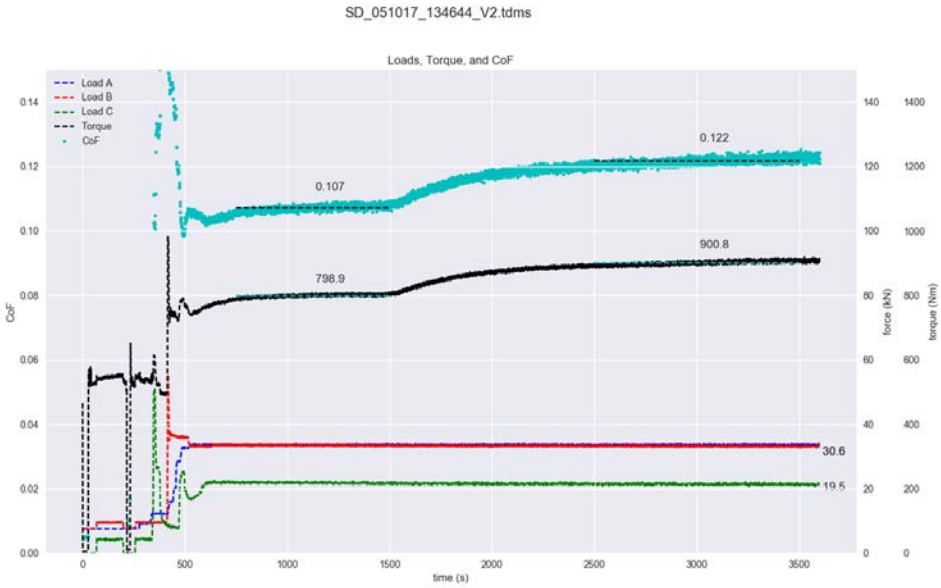

Figure 70. With no changes in applied load or cooling, the power loss increased by ~20 percent simply due to the return and steady increase of the unknown ringing vibration.

As Figure 8181 shows, the ringing increased the energy necessary to spin the shaft (artificially increasing COF). There were occasional periods after system start-up, when the system was not ringing, which then slowly ramped back into full ringing phenomena with no other load or RPM changes. The chart referenced above shows the COF increasing from 0.10 to 0.12 and provides us a good estimate of how much this issue affected the friction measurements throughout the testing.

All attempts to alter or remove this vibration failed. Adding mass to the outer shaft, adding mass to the bearing stanchion, and several other methods of damping were tried but neither the frequency or magnitude of the ringing was ever changed.

It is presumed that the ringing was torsional vibration along the shaft, emanating from the middle bearing stanchion. With no mass on the adjoining side of the bearing housing (only half of a driveline section was tested), torsional vibration was undamped and could freely ring. ORPC does not have vibration analysis software and it is not clear that this unexpected frequency would have been flagged as an issue prior to the build. Future design will require analysis to be performed and eliminate this from future design iterations.

Unexplained Phenomena: Temperature / Friction Swap Anomaly

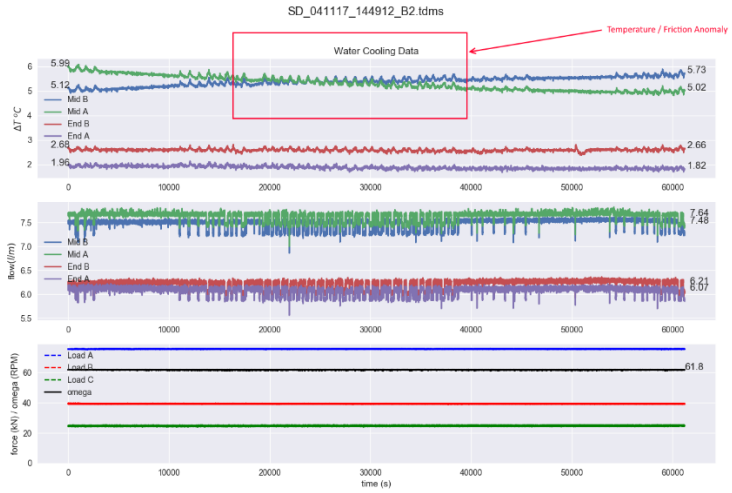

Figure 71. Temperature/friction anomaly

During the middle of testing, the measured temperature from the middle stanchion increased in an unexplained manner. One side of the bearing housing carried the thrust and radial loads, while the other side carried radial loads only. During most of the testing, the side that carried both thrust loads and radial loads had a higher temperature output, as was expected. As captured in the data, the friction/temperature increased in the side that was not loaded axially. This phenomenon persisted through much of the remainder of the test and mysteriously stopped near the end of testing.

The only related event that occurred during this time was loading bearing B shifted position down the shaft approximately 1 in. increasing the moment arm this load had on the shaft. How this is related to the permanent friction shift is still unknown, but notable.

3.2.2.2.2.3 Test Results Summary

To compare all the different loading cases and test configurations, the following tables show the steady state results from selected data files.

Table 20. Aligned testing steady state data summary

	Break-In	End Stanchion Isolation	Mid Stanchion Isolation	Final Testing
Load A (kN)	71.4	65.7	55	97.7
Load B (kN)	38.9	9.9	53.6	49.5
Load C (kN)	24.2	4.2	35.5	32.6
Torque (Nm)	1125	710	1234	1308
CoF (-)	0.095	0.106	0.102	0.086
Omega (RPM)	58.6	61.4	61.8	60.9
MB Heat Share (%)	33.8	20.1	56	20.4
MA Heat Share (%)	42.2	16.1	35.3	53
EB Heat Share (%)	14.4	35.4	5	16.2
EA Heat Share (%)	9.7	28.4	3.8	10.4
MB-ΔT (°C)	4.93	1.89	8.25	3.3
MA-ΔT (°C)	6	1.51	5.14	8.54
EB-ΔT (°C)	2.52	4.06	0.92	3.29
EA-ΔT (°C)	1.74	3.33	0.74	2.14
MB-Flow (l/min)	7.42	7.63	7.73	7.54
MA-Flow (l/min)	7.61	7.64	7.82	7.76
EB-Flow (l/min)	6.19	6.23	6.19	6.17
EA-Flow (l/min)	6.06	6.11	6.01	6.08

Table 20 shows selected data that characterized each of the aligned system configurations. The “Heat Share” percentage is calculated as the ratio of thermal power measured at each bearing cooling outlet over the total. This measure is the only data we have on individual bearing performance. In the end and mid bearing isolating cases you can see that a majority of the thermal power came from the bearing that was being loaded. Also, in the default loading cases the outlet on the middle bearing assembly that also contained a loaded thrust bearing, MA, showed a significantly higher thermal power output as expected.

Table 21. Direct comparison of radial misalignment conditions at unloaded and loaded cases

	Applied Loads [kN]			Measured	Calculated
	Load A	Load B	Load C	Torque [Nm]	CoF [-]
Aligned - "Unloaded"	9.8	10.3	4.3	439.6	0.215
Misaligned 0.5in - "Unloaded"	7.6	7.6	0	416.7	0.325
Misaligned 1in - "Unloaded"	7.7	7.6	0	844	0.654
Aligned - Loaded	32.5	32.1	21.2	867.8	0.121
Misaligned 0.5in - Loaded	34	33.7	22	932.3	0.124
Misaligned 1in - Loaded	33.4	32.2	20.6	1401	0.194
Aligned - Loaded	55	53.6	35.5	1234	0.102
Misaligned 0.5in - Loaded	54.4	54.4	35.8	1315	0.109
Misaligned 1in - Loaded	-	-	-	-	-

Table 21 shows the change in system performance as misalignment increases for 3 different loading cases. The first case is an unloaded condition which involved minimal pressure on the hydraulic system. The effects of system weight and friction from sources other than the PCD bearings is exaggerated in these cases but the trend shows a drastic increase in friction between 0.5 in. and 1.0 in. As the two levels of loaded data show, there was a small change between aligned and 0.5 in. misalignment, the increase after that though was so drastic that the final data point in this table could not be captured due to the torque limits of our sensor.

3.2.2.2.3 Generator Bearing Test

As part of the generator development, PCD bearings were adapted as potential bearings suitable for a “wet gap” generator, i.e., a generator that would operate with water in its “air gap” between the rotor and stator.

The driveline test rig accommodated a large PCD bearing in a simulator housing to replicate expected loading during operation. The design effort is described in the section below Sections 3.3.2.4 on Subtask 3.2 Generator design. The test effort is described in Section 3.3.4.3 below on Subtask 3.4 Test, Demonstration, and Final Report.

3.2.2.2.4 Component Metrics and Project Milestones

The driveline test allowed assessment of the PCD bearing technology for integration into the next generation TidGen® Power System. Specifically, the test set out to verify the effective coefficient of friction of the bearings within a viable driveline concept. As discussed above, a direct measurement of COF 0.08 was made with incomplete bearing break-in, and manufacturer data predicts an eventual lumped system COF of 0.05, but component testing indicates an ultimate limit of 0.02.

The test-system lumped coefficient of friction was slightly higher than the COF measured in previous laboratory testing, which was 0.02. Given manufacturer data on break-in behavior of the bearings, analysis of test data predicts a final COF of 0.05 once the bearings have been fully “polished” after sufficient time for break-in. Additionally, the mid-bearing stanchion had a slightly higher COF than the end bearing stanchion (based on temperature data) and performance could be improved to achieve a

lower, overall COF. Redesign of the mid-stanchion bearing assembly housing should be a goal of future designs. The methods used to measure driveline performance were successful but in further testing could be improved. The hydraulic loading system worked but introduced quite a bit of noise. The response time of the hydraulic rams was slow to compensate to the small displacements of the rotating driveline leading to transient loadings. When the data is examined over hours, as many of these plots show, the effect is not as noticeable. Future testing could benefit from a faster responding feedback-controlled loading system.

Another favorable outcome of this test was the success of the water cooling system and effectiveness of the calorimetry sensors in capturing the power loss in individual bearings. The net thermal power measured by these systems often lined up well with the more directly measured mechanical power output. The water cooling system relied on a single measurement of inlet temperature even though it was split into 4 inlet hoses and water was free to mix in between bearings in the housings. Future testing of PCD bearings would benefit from further isolation of individual bearings and more accurate measures of flow and temperature.

3.2.2.3 *Problems Encountered and Departure from Planned Methodology*

A significant departure from our planned methodology was the decision to test the driveline separately from the generator, due to cost, and scheduling concerns. Originally, we had intended the generator manufacturer construct and conduct the driveline testing, but the change in generator manufacturer and a consequent budgeting of the test work showed that it was more cost effective for ORPC to conduct the work directly.

Issues encountered during testing included a prolonged break-in and an unexplained vibration in the driveline. Initial system and component assembly went very smoothly. Configuring the test rig to successfully operate unmanned proved challenging. Establishing safeguards to catch any operational issues without unnecessarily tripping from conservative threshold limits had typical start-up issues.

The manufacturing process of the PCD inserts leaves them with a relatively rough surface finish and a corresponding initial higher COF. These bearings have an initial “break-in period” as the rotating and stationary halves of the bearings polish each other. The rate of the polishing process is a function of the pressure and surface speed the bearings are operating at. The high friction in the new bearings and the limited range of our torque sensor meant that we continued to see a decline in COF over the life of the test, but we could not speed it up by applying more load.

The high frequency ringing vibration that was generated by the system during operation was independent of the driveline RPM, was present with and without a load, and could not be changed or eliminated through any method of damping. The source of the noise emanated from the middle PCD bearing assembly but could not be isolated to a specific component. The vibration increased the friction generated in that assembly and was not removed from the published results.

3.2.2.4 *Assessment of Their Impact on the Project Results*

The decision to test the driveline independently from the generator only impacted load testing of the generator. This combined testing did not fit within budgetary constraints, since it would require submerging/cooling of the generator and required a high-torque drive-motor that was not readily available. Testing of PCD bearings did not require the shaft torque and did not affect bearing COF, the driveline testing replicated operational conditions without torque.

The prolonged break-in meant that we did not achieve the final low COF of 0.05 we were expecting but with the elimination of the vibration and the many hours of operation a deployed driveline would experience, our projections show that we expect to reach a COF that corresponds to a 2.3 percent power loss to friction, exceeding our goal of 5 percent.

3.3 Generator Development – Task 3.0 Generator Design, Build and Test

The Project envisioned the design, build and test of a generator which would ultimately be suitable for fully flooded seawater operation. This would require a generator design capable of operating in the presence of seawater without corrosion, and a bearing system capable of such operating conditions. The original generator concept design focused on a switched reluctance electromagnetic design for the generator with the understanding that the switched reluctance design would be more robust and tolerant of a seawater medium. A trade study was conducted to prove that hypothesis, but the results of the study indicated that there was little benefit to adopting a switched reluctance design over a more conventional synchronous permanent magnet design, and that the novelty of the switched reluctance design added more technical risk to the Project than was warranted. As a result of this analysis, ORPC determined that a permanent magnet (PM) design was a more appropriate design to achieve the Project goals.

3.3.1 Subtask 3.1 Initial Trade Studies, Simulations and Analysis

3.3.1.1 *Original Hypothesis*

ORPC would summarize the operating and design experience with subsea generators, controls, and electrical equipment and deliver to the electrical generator designer a generator design interface document to ensure compatibility with existing equipment. ORPC and the contractor would define, write and review requirements specification for hardware/software. The contractor would perform initial system design simulations/ calculations and design trade-offs. ORPC and the contractor would complete a draft test plan. The contractor would provide a plan for design simulation and evaluation of the generator. The contractor would provide input to and approve system design at System Requirements Review (SRR).

Specific objectives for this subtask were:

- 3.1.1 System Requirements Review
- 3.1.2 Trade off study
- 3.1.3 Draft Test Plan

3.3.1.2 *Approaches Used*

The original contractor for the generator design and delivery was RCT Systems, Linthicum, MD, who had significant experience in the design of switched reluctance electromagnetic machines. The switched reluctance machine (SRM) was believed to have advantages over a synchronous PM design typically used by ORPC. These advantages included a belief that the SRM design would be more tolerant of electrical damage caused by water intrusion into the generator, and that consequently it would be easier to build an SRM machine which could eventually be designed to operate with water in the air gap.

A kickoff meeting was held on March 27, 2014 at RCT Systems in Linthicum, MD. During this meeting initial system design simulations and calculations were performed, which focused the SRM design on an axial flux switched reluctance machine (AFSRM) as opposed to a radial flux arrangement.

A trade study was conducted to contrast and compare the axial flux switched reluctance machine (AFSRM) and permanent magnet synchronous machine (PMSM). The trade space criteria and weighting were defined with the intent to identify the preferred configuration for a subsea application. Basic specifications for each machine design required a 50kNm torque at 40 rpm and maximum rotational speed of 110 RPM. Based on the availability of already existing power electronics the drive module was selected for a 125kW power level, with higher power achieved by addition of more drive modules. A conceptual design of the AFSRM was developed to guide the trade study. Standard existing configurations of PM machine were used as a comparison

The scope of the tradeoff included the subsea electrical generator and generator drive converter and any required DC bus filtering. The drive module, common to both configurations, was not included in the trade study.

The tradeoff analysis work was completed, and the results documented and presented to ORPC on July 28, 2014.

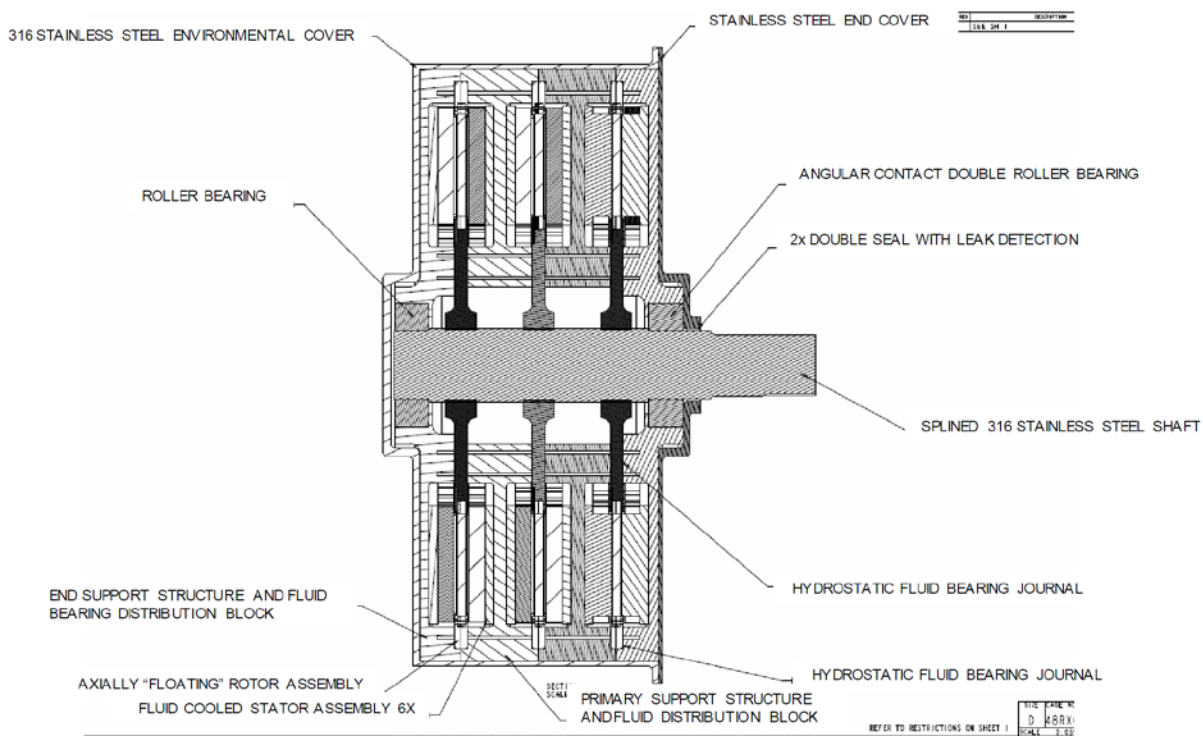

Figure 72. Subsea electrical generator and generator drive converter using an axial flux synchronous switched reluctance electromagnetic design

Results from the study indicated that both machines rated equivalent on performance at 40 rpm. The PMSM achieved better performance at extended speed range of 40-110 rpm. Both machines/systems could be extended to 500 kW output equally well.

Other conclusions from the trade study were as follows:

- Efficiency of the PMSM is better than the AFSRM.
- Both the dry weight and wet weight of the PMSM will be less than the AFSRM.

- Aspect ratio (diameter/length) of the AFSRM is slightly better than the PMSM.
- Volume of the electronics associated with the PMSM is lower than the AFSRM.
- Total material cost of the PMSM is lower than the AFSRM, primarily due to the high cost of copper in the AFSRM, and significant amount of iron.
- Angle/speed sensing required is easier with the PMSM.
- Both machines can be designed equally well against water intrusion, and both can be fluid filled.
- There is more design risk associated with the AFSRM due to increased complexity and fewer precedents.
- Manufacturing and assembly risk is higher with the AFSRM due to the complexity of the required bearing system and the machine in general.
- Handleability of the AFSRM is rated higher due to the fact that no voltage is present in a free-wheel condition, and there are no issues with end of life disassembly and disposal.
- Performing a braking or damping function is slightly easier with the PMSM.
- Acoustic noise performance will be better with the PMSM.
- Reliability of the PMSM will be higher, due to a less complex system.
- Maintenance and repair of the AFSRM will be slightly easier than the PMSM.

After all relative ratings and weighting, the relative “score” of the PMSM turned was 137 versus 118 for the AFSRM, indicating that the PMSM appears to be a better choice for this particular application. Consequently, and a PM machine was chosen as the type of machine to carry forward into the design phase. A draft test plan was created and presented to ORPC.

AFSRM Summary

SRM based PTO	Machine	Drive Electronics
Length /Dims	0.6m	1.397m x 0.508m x 0.381m
Diameter	2.07m	
Volume	2.0 m^3	
Weight in water	14780 kg	
Dry weight	16847 kg	386 kg
Material Cost	$124,131	$30,500
Efficiency	92%	95%

PMSM Summary

PMSM based PTO	Machine	Drive Electronics
Length /Dims	0.83m	0.635m x .381m x 0.254m
Diameter	1.8m	
Volume	2.1 m^3	
Weight in water	4369 kg	
Dry Weight	6497 kg	68 kg
Material Cost	$70,686	$22,500
Efficiency	95%	96%

Figure 73. AFSRM and PMSM summaries

Table 22. ORPC TidGen® PTO trade table comparing the SRM concept with the PMSM concept

	RCT Rating Relative(0-10)		RCT Weighting Impact (0.1 -1)	RCT Ranking		ORPC Weighting Impact(0.1-1)	Final Ranking	
Parameter of Interest	PMSM PTO	SRM PTO		PMSM PTO	SRM PTO		PMSM PTO	SRM PTO
Performance at Rated (40rpm, 125kW)	10	10	1	10	10	1	10	10
Performance at Extended (40-110rpm), 125kW Constant Power	10	5	0.75	7.5	3.75	0.9	6.75	3.375
Perf Extended , 500kW elex, coil change if required	10	10	1	10	10	0.7	7	7
Efficiency at Rated (shaft to DC Link)	9	6	0.9	8.1	5.4	1	8.1	5.4
Efficiency at Max (shaft to DC Link)	9	6	0.8	7.2	4.8	0.6	4.32	2.88
Efficiency at Extended (40-110rpm) 125kW Elex (shaft to DC Link)	9	6	0.5	4.5	3	0.9	4.05	2.7
Dry Weight -Machine	10	5	0.8	8	4	0.85	6.8	3.4
Wet Weight-Machine	10	4	0.5	5	2	0.1	0.5	0.2
Aspect (Diameter/ Length)	8	10	0.8	6.4	8	0.1	0.64	0.8
Volume- Electronics	10	5	0.5	5	2.5	0.4	2	1
Total Material Cost (indicative of future mfg cost ranking)	10	8	1	10	8	1	10	8
Resolver/Encoder	10	8	0.25	2.5	2	0.4	1	0.8
Water proofing	10	10	1	10	10	1	10	10
Withstand water intrusion	8	8	1	8	8	1	8	8
Fluid fill (volume of fluid and windage losses)	8	8	0.7	5.6	5.6	0.5	2.8	2.8
Design Risk (complexity)	10	5	1	10	5	0.25	2.5	1.25
Design Risk (precedent)	9	5	1	9	5	0.25	2.25	1.25
Mfg Assembly Risk	7	5	1	7	5	1	7	5
Safety (Loss of control, electric shock, EOL disposal)	6	10	1	6	10	1	6	10
Excitation (self, external)	10	8	0.5	5	4	0.5	2.5	2
Braking, Damping	8	6	0.5	4	3	0.9	3.6	2.7
Environmental (Acoustic)	9	6	0.8	7.2	4.8	0.9	6.48	4.32
Environmental (Fluid leaks, noxious materials)	9	9	0.9	8.1	8.1	1	8.1	8.1
Reliability/Robustness	9	8	1	9	8	1	9	8
Maintenance/Repair	8	9	1	8	9	1	8	9
			Total	181	149	Total	137	118

3.3.1.3 *Problems Encountered and Departure from Planned Methodology*

The trade study result was surprising in that the proposed SRM generator technology did not demonstrate being a better option as compared to permanent magnet generators. As a result, a change in project direction from developing an SRM design to developing a PM design was executed.

3.3.1.4 *Assessment of Their Impact on the Project Results*

ORPC's cost of energy analyses pointed to reliability as being the most critical factor for achieving Project SPA metrics. Consequently, the choice of a permanent magnet machine design over a potentially less reliable switched reluctance design was necessary to achieve the Project results. ORPC directed RCT Systems to continue with a detailed design of a permanent magnet generator, while in parallel ORPC worked with another, more proven generator manufacturer of subsea PM machines to mitigate technical and project risk. The manufacturer, SmartMotor AS, since acquired by Rolls-Royce Marine (RRM), performed a preliminary design to adapt their existing encapsulated permanent magnet systems

for ORPC's application. The two designs would be compared to each other as an additional trade study prior to procurement.

3.3.2 Subtask 3.2 Design Phase

3.3.2.1 *Original Hypothesis*

The contractor would perform a system preliminary electrical and mechanical design for the generator. Electrical simulation tools, such as PSIM, will be used for circuit analysis. An electromagnetic analysis to evaluate the magnetic circuit design would also be performed by the contractor. Team design reviews of modeling and simulation methods and results would be conducted. The Project team would evaluate design options and obtain preliminary hardware quotes for establishing a cost-effective design. The contractor would manage and coordinate results to ensure compatibility of data at the system level. ORPC and the Project team would approve the selected design configuration approach at the Preliminary Design Review (PDR). Approval for detail design and construction would be issued at the PDR stage and the contractor will order items identified as long lead.

The contractor would perform detail electrical and mechanical design using CAD tools. This design would include motor design and machine manufacturer interface for detail design of the generator, detailed design for the motor drive power and control electronics, considerations of packaging, thermal and EMI design and specifications for the control software. The Project team would prepare for a Critical Design Review (CDR) and approve detail design at CDR for transition to manufacturing.

3.3.2.2 *Approaches Used*

Preliminary electrical and mechanical design was performed by RCT Systems in preparation for a PDR. Electrical and magnetic circuits were modeled and analyzed. Cost estimates were developed for major components. Software requirements and design documents were worked, and software module design, coding and initial testing conducted. A PDR was held on the originally scheduled date of September 12, 2014, at which time the preliminary design was presented and continuation into detailed design was approved.

A software design review (SDR) was completed on November 20, 2014, where RCT Systems presented to ORPC their software, control interface, and control module designs. A crucial step to commercializing ORPC systems is the use of industry standard components and systems instead of custom built. This was done by the implementation of a standard communications protocol between the SCADA system and subsea electronics. RCT Systems incorporated this request into their software design by designing a generator drive converter which communicates via MODBUS to the SCADA computer.

Final designs for the generator were completed by RCT and presented to ORPC at a CDR on December 11, 2014. Areas of the design which were completed for this review included the following:

- Magnetic and mechanical
- Modal analysis
- Power electronics
- Control hardware
- Software
- Manufacturing plan
- Test plan

For the mechanical and magnetic design, some changes were made from the PDR to the CDR, including:

- Neodymium magnets on the rotor were specified instead of the originally planned samarium cobalt. This decision was made due to increased price of samarium-cobalt magnets. This will reduce the resistance to corrosion, which the samarium-cobalt material offered.
- Winding turns were increased from 1 to 2.
- Magnet geometry was changed to square. This change was implemented to lower cost and increase ease of manufacture. However, this change also reduced the magnetic flux density of the system.
- Rotor mounting ring changed from non-ferromagnetic (non-corrosive) material to stainless steel (ferromagnetic). This change counteracted the reduced magnetic flux density caused by the changing of the magnet geometry.

As a means of making the generator as impermeable to leaks as possible, an oil filled, pressure-compensated environmental housing was proposed to enclose the generator; this was included in the design. For leak prevention via the electrical connectors, a pressure-compensated, oil filled connector box was included in the design, which acts as a feed through for the electrical connectors. Although the electrical design of the AC/DC conversion system has been completed, this design did not include a mechanical, subsea worthy design for the housing for these electronics.

Key reliability features of the RCT design included a double boundary strategy with o-rings and oil reservoirs having separate leak detectors and oil moisture sensors. These features represented a significant improvement over the baseline generator; lower efficiencies were outweighed by a superior design in terms of leak prevention and tolerance. As a first design, maintenance intervals could only be assumed to be within 2 to 5 years, with the Project targeting 5 years for major service. Table 23 shows summary data for the RCT design.

The manufacturing plan revealed a large increase in projected cost of the final generator package. This increase in price was largely due to the proposed use of a 72-speed resolver required as a means of calculating rotor speed. This sensor accounted for 20 percent of the entire generator system cost.

Table 23. Summary Data for RCT Systems permanent magnet generator for ORPC's TidGen®.

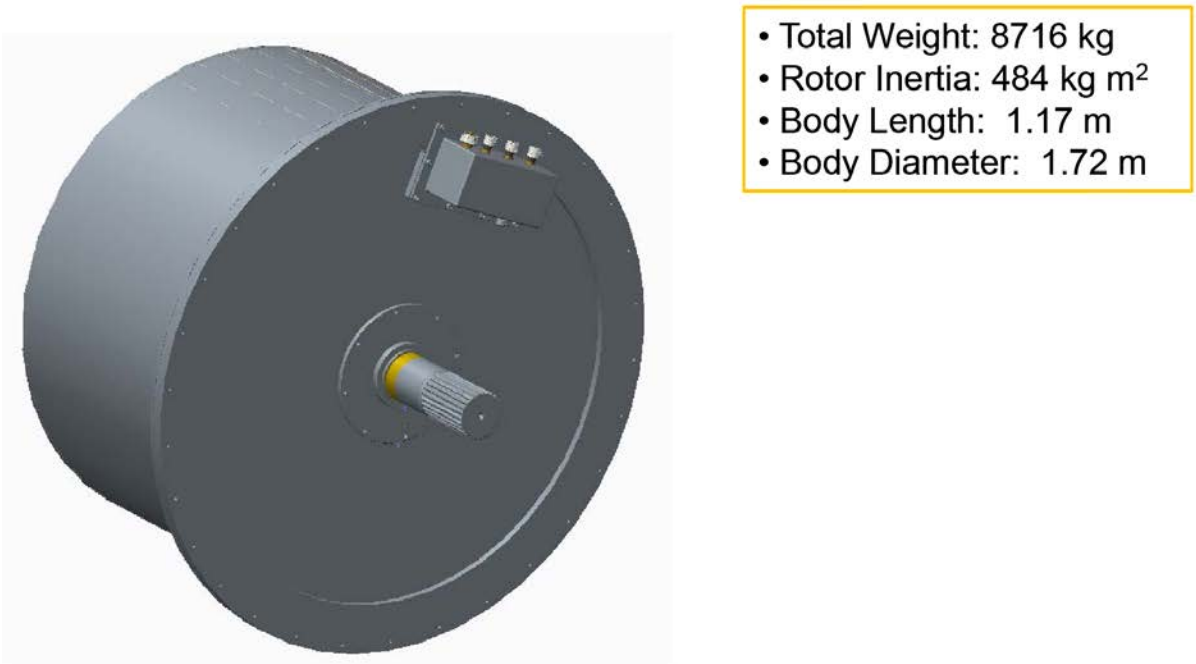

Figure 74. RCT Systems permanent magnet generator for ORPC's TidGen®

3.3.2.3 *Problems Encountered and Departure from Planned Methodology*

ORPC had performed an extensive survey of generator manufacturers for the Project, and originally selected RCT Systems on the basis of its existing switched reluctance machine (SRM) generator technology. SRM technology was a promising alternative to permanent magnet generators with respect to cost, weight and maintainability. The Project was structured with technology development gates, beginning with a trade study of alternate SRM designs in comparison to a baseline permanent magnet generator, then to be followed by preliminary and critical design phases. The surprising result of the trade study, that permanent magnet generators were superior in most categories including performance, led ORPC to pursue dual development paths – a newly developed permanent magnet design developed by RCT Systems and a permanent magnet generator utilizing the advanced encapsulation technology of RRM.

With nineteen years of experience with development, build and test of permanent magnet machines, RRM had a track record of multi-year, reliable subsea operation. RRM possessed a wealth of design and subsea operations experience in permanent magnet machines and power convertors. Their products were easily scalable to meet the RPM/torque specifications for ORPC's tidal applications. Advantages include proven, reliable field deployments such as subsea oil-filled machines that have been in operation for more than ten years and at service depths of 4500m, as well as commercialized encapsulation technology in tunnel thrusters developed by SmartMotor prior to being acquired by RRM in 2013. Their design for ORPC's application scaled an existing product already under qualification for RRM and was part of a detailed system validation program that leveraged a high-quality manufacturing facility as well as a new prototype and test center capable of testing frequency converters up to 1.7 MVA and generators up to 1 MVA in a back to back arrangement. With an extensive set of performance and reliability data and the provision of conditional monitoring capability, RRM provided a high confidence of being able to achieve the design goals for the Project.

A key feature of the generator for ORPC was the ability to transition easily from a hybrid oil-filled/encapsulated unit to a pure wet-gap encapsulated generator. The hybrid design provided technical risk mitigation and avoidance of catastrophic failure during performance validation by ORPC of the generator in actual field operation (beyond the scope of this Project). The advantage of the advanced encapsulation system provided an additional opportunity for eventual development of a wet gap system.

Table 24 compares the baseline generator for ORPC, produced by CPI, the RCT Systems detailed design and the RRM initial application design. RRM projected cost reductions included means to increase drive efficiencies and reduce costs, reduction of the air gap as manufacturing tolerances improved, and removal of the redundant oil-filled reservoir once the encapsulation is field validated.

Table 24. Generator Comparison for selection prior to procurement

	CPI	RCT	RRM
	Air gap, Radial PM	Double reservoir oil-filled, radial gap PM	Encapsulated, radial PM - initial systems oil-filled hybrid, subsequent systems without oil
Diameter of generator housing (m)	1.57 m	1.72 m	1.54 m
Length of generator housing (m)	1.11 m	1.17 m	1.3 m
Mass, no oil (kg)	9660 kg	-	10700 kg
Mass, oil filled (kg)	-	6925 kg	11060 kg
nominal operating speed (RPM)	32 RPM	40 RPM	40 RPM
Peak efficiency	0.923	0.889	0.917
Power rating (kW)	150 kW	125kW	150kW
Torque rating (Nm)	45,000 Nm	50,000 Nm	45,000 Nm
Power vs. Torque limiting	Power limited	Torque limited	Torque limited
Cogging Torque (impact acoustics) (Nm)	356 Nm	893 Nm	21 Nm

Table 25 compares the three generators for their impact on the Project SPA goals. The RRM generator outperformed the RCT Systems design in achievement of all SPA goals, for performance, availability and reduction in cost of energy. Given the parallel development by ORPC of wet bearings, the future generator would integrate the advanced encapsulation technology into a breakthrough wet gap system.

Table 25. Generator comparison for SPA goal impact for selection prior to procurement.

Values shown do not include new bearing impact – for direct generator comparison only	**CPI/Baseline**	**RCT**	**RRM (SmartMotor)**
	Air gap, Radial PM	Double reservoir oil-filled, radial gap PM	Encapsulated, radial PM - initial systems oil-filled hybrid, subsequent systems air gap
Seawater Intrusion, operate at 6 months full power, 3 months half power	Likely catastrophic failure or severe damage even with leak detection	Unknown, double-oil reservoir will provide limited window of operation with detection	Indefinite stator/rotor operation, target wet bearings as composite or diamond bearings to meet goal
TGU System Availability	79% assumes 2 spare generators, costly annual refurbishments	88% generator with 20+ year life, assume seal life > 1 year	90% generator with 22+ year life
PWR % over baseline, overall target 23%	-	28%*	27% with oil* 28% without oil
LCOE % improvement, overall target 25%	-	76.9%*	80.2%*

3.3.2.3.1.1 Detailed Application Design of the RRM Generator

ORPC contracted with RRM to complete the detailed application design, and to build and test a permanent magnet generator as well as a subsea-worthy converter electronics unit. RRM completed a design package for a CDR. The final generator design was adapted to ORPC's application, with mechanical interfaces, sensors, hybrid oil system requirements (compensators, seals) and electrical braking comprising design details finalized. The total system efficiency (shaft to DC converter output) was predicted at 90 percent at 32°C, and better at typical market, colder operating conditions. Seals were proposed to be a mechanical seal used with extensive field history on RRM thrusters. Although more expensive, the mechanical seal had been proven to meet five-year service intervals and was eventually selected as suitable for ORPC's operating conditions. Bearings would be field replaceable utilizing SKF standard tooling, with the end lids being separated into a bearing 'cartridge' that allowed the generator shaft to rest on internal geometry while minimizing risk of contamination during servicing. The end lid can be redesigned within limits to accommodate varying bearing types, including the PCD designs, so that the eventual conversion to a seawater filled system can be performed on the generator with modular replacement components.

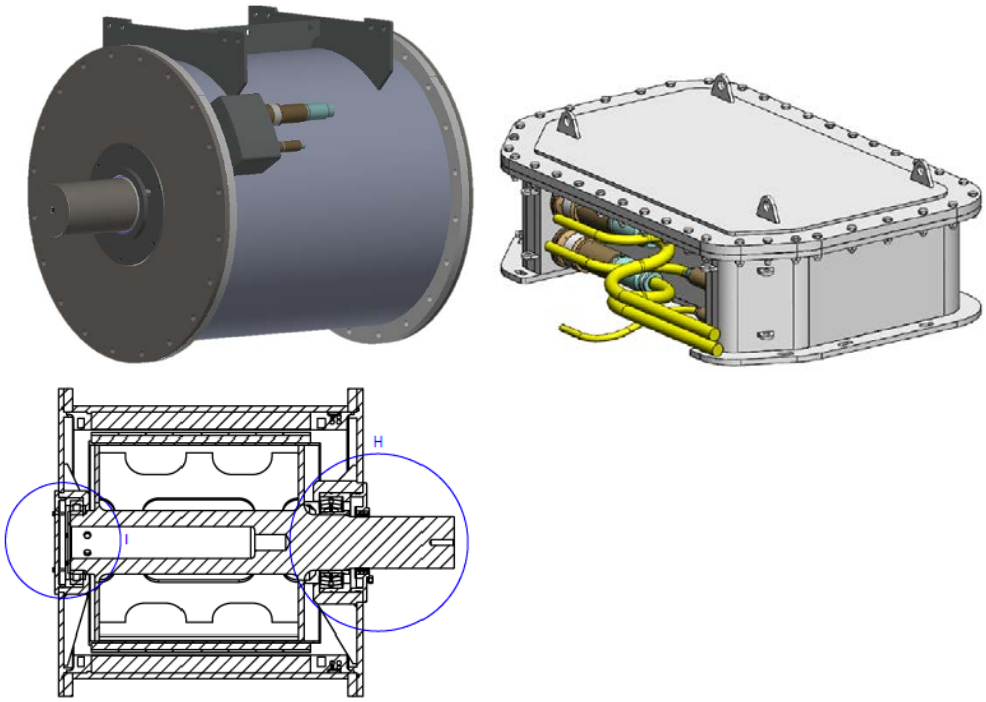

Figure 75. RRM AS avd. Trondheim. Generator and converter for ORPC application.

The converter was designed with thermal feasibility of a passive cooling system completed. The design incorporated commercial off-the-shelf components in a customized arrangement and enclosure. Dry-mate connectors were used as a cost-effective risk avoidance strategy related to delamination of wet-mate connector moldings employed in earlier TidGen® configurations. Overall generator system efficiencies for the CDR continued to meet or exceed preliminary design estimates (Figure 88).

Cathodic protection design was provided for the external shell of the generator and converter, which can be seen below in Figure 89.

The pressure compensation system used two horizontal pressure compensators centrally mounted on the non-drive end generator plate. The outputs of these connected to a common hose, which were an input to the generator to control the internal pressure of 500 liters of “Castrol Brayco Micronic SV/B”.

The brake design comprised a UPS powered latching switch that would be triggered by loss of shore power and a non-rotating generator rotor. This system will ensure that the stator windings will be shorted together at slack tide in the case of loss of power of shore.

ORPC and RRM worked with SKF to determine a suitable bearing monitoring system for the generator bearings. SKF would supply the sensors and monitoring module.

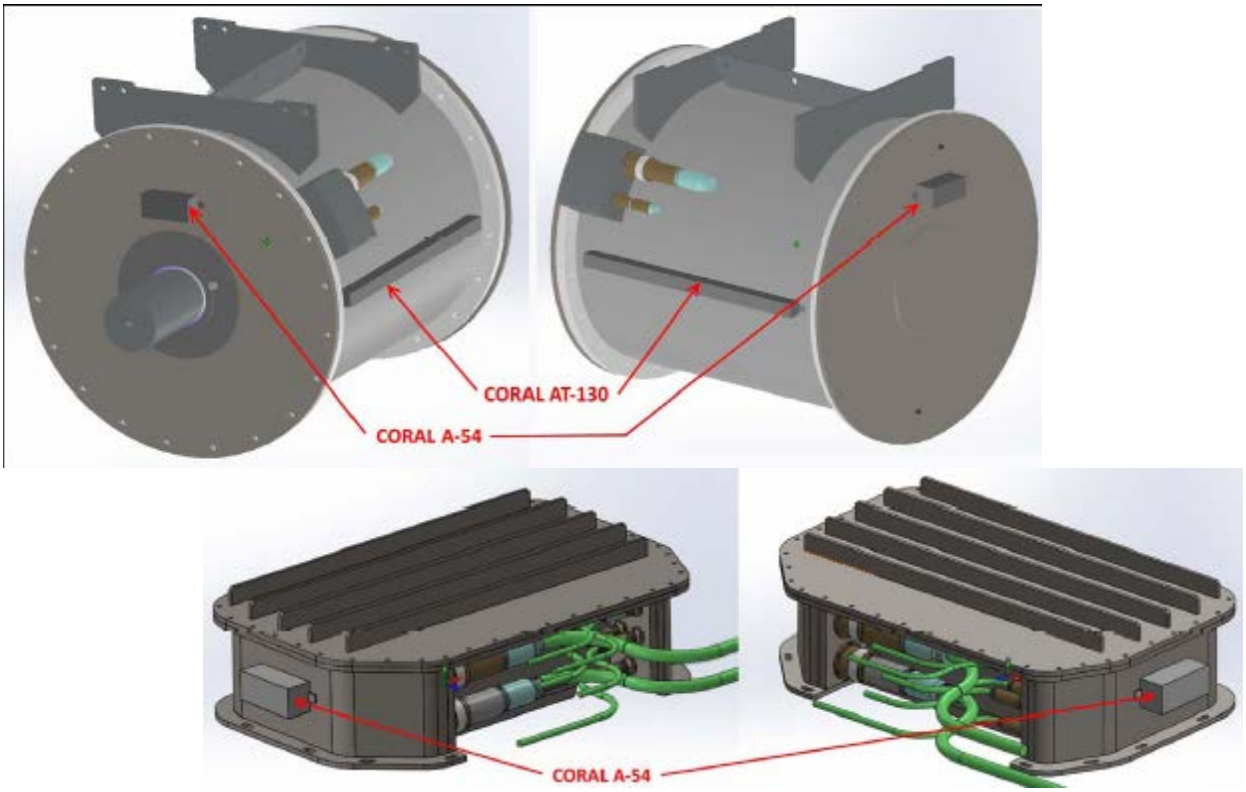

Figure 76. Final anode placement for converter and generator

Generator wet bearing design

ORPC worked with US Synthetic to develop a workable PCD wet-bearing concept to replace traditional grease roller-bearings in the wet-gap generator. ORPC planned on applying the PCD bearing technology being developed for the driveline system for generator bearings capable of operating in seawater. Load capacity of the diamond bearings, based on ORPC and US Synthetic analysis, would be more than sufficient for anticipated generator loading requirements.

A consideration for the generator bearings was a potential double seal design, one on either side of the generator bearings. For successfully validated diamond bearings, the seals would be low cost and only used as a barrier for particulate contamination.

ORPC conveyed initial bearing requirements to US Synthetic to develop alternatives for integration into the RRM generator (Figure 90).

Initial designs of USS diamond bearings for the RRM generator were within the capabilities of USS fabrication capabilities, although the diameter of this bearing nearly exceeded production equipment capability. The design concept utilized the same bearing removal and replacement procedure used for the SKF roller bearings. An interference fit “cartridge” mounted to the generators stator and a hydraulic sleeve secures the bearing to the shaft.

US Synthetic provided drawings and an updated quote for a radial bearing compatible with the non-drive end (NDE) of the generator (Figure 91). The large shaft diameter was problematic for bearing manufacture, due to limitations in available manufacturing equipment.

For the drive end bearing of the generator, ORPC worked with US Synthetic on appropriate concepts compatible with the design of the RRM generator. A solution for integrating the PCD bearing will likely involve a redesign of the cartridge system that RRM featured in the generator and which serves to facilitate field replacement.

3.3.2.4 *Assessment of Their Impact on the Project Results*

ORPC contracted with RRM to complete a detailed application design that adapted their tunnel thruster advanced encapsulation technology for ORPC's TidGen®. No significant problems were encountered during the detailed design phase of the RRM generator, with predictions exceeding those of the initial application design.

3.3.3 Subtask 3.3 Manufacture and Subassembly Test

3.3.3.1 *Original Hypothesis*

ORPC would submit a purchase order for RRM to complete application design, build and test a subsea generator based on design analyses performed in Budget Period 1. RRM would conduct a final design review with ORPC prior to fabrication. RRM would provide a report of all quality and acceptance data during manufacture and test and perform a factory acceptance test (FAT) of the generator to confirm no-load behavior.

RRM would produce and test a generator with conventional roller bearings. In parallel and as a separate effort, ORPC would develop bearings capable of performing in a wet gap version of the RRM generator. RRM would provide generator bearing requirements to ORPC, including load requirements and assembly interfaces so that the wet bearings can replace the conventional bearings as a modular assembly. ORPC would be responsible for technical design, development and specifications for the wet bearings. ORPC would produce the bearings for incorporation into driveline system testing in Task 4. Associated

milestones will include: a trade study to be performed by ORPC of bearing material and designs, utilizing much of the work already performed for driveline bearing design; final generator bearing design for inclusion in the driveline testing in Task 4; and a test plan for evaluating the wet bearings during the driveline testing in Task 4.

Specific objectives for manufacture and subassembly test:

- 3.3.1 Place orders for generator
- 3.3.2 Final Design Review
- 3.3.3 Quality and FAT Report
- 3.3.4 Generator Test Plan
- 3.3.5 Generator wet bearing trade study
- 3.3.6 Generator wet bearing design specification
- 3.3.7 Generator wet bearing test plan

3.3.3.2 *Approaches Used*

3.3.3.2.1 Generator Build

RRM successfully built the generator and converter electronics to meet design specifications. Production was completed for final acceptance testing (FAT) to occur beginning February 2017.

Figure 77. Converter Electronics Cabinet

Figure 78. Verification testing of generator and converter electronics

3.3.3.2.2 Wet bearing development

A wet generator bearing design was completed by ORPC in collaboration with US Synthetic (Figures 100-103). The PCD bearing would be compatible with the NDE side of the Generator. ORPC developed a test stand to be integrated with the driveline system test rig at ASCC. This testing would verify the bearing's

integrity and performance without risk to damaging the generator and allow for US Synthetic to develop their capabilities with larger bearings. The bearing would be loaded in representative operating conditions and assessed in stages to assess mechanical stability.

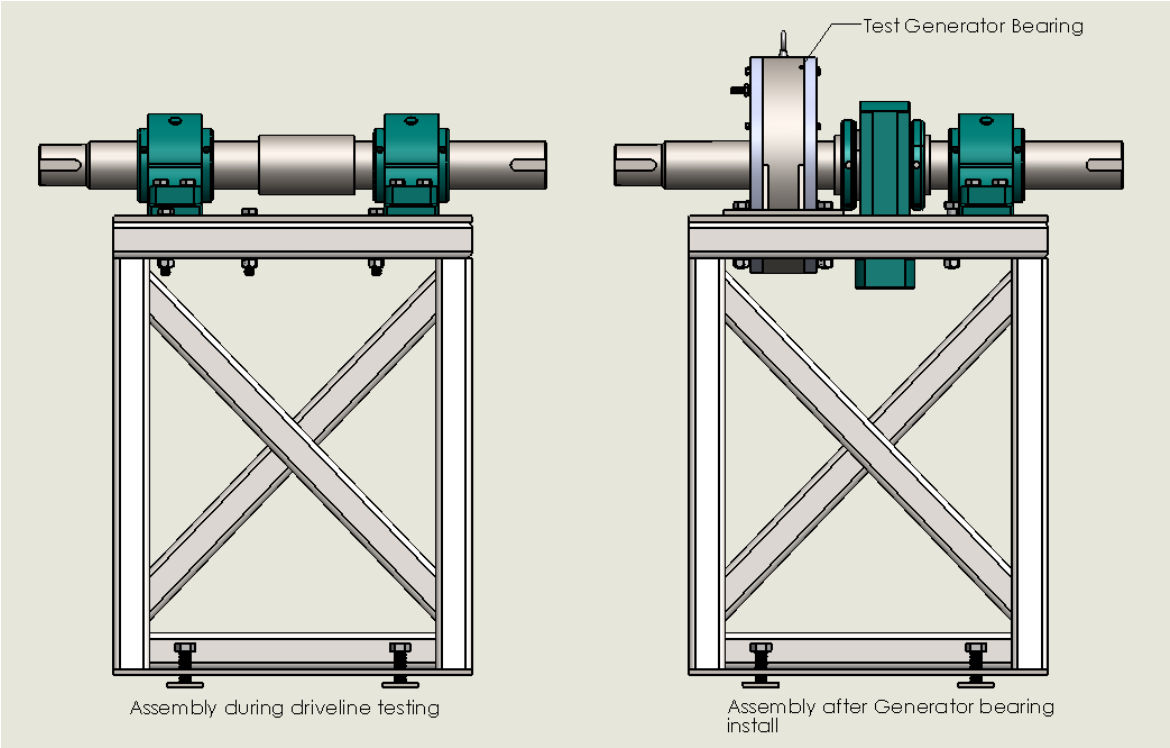

Figure 79. Driveline test stand for wet generator bearing

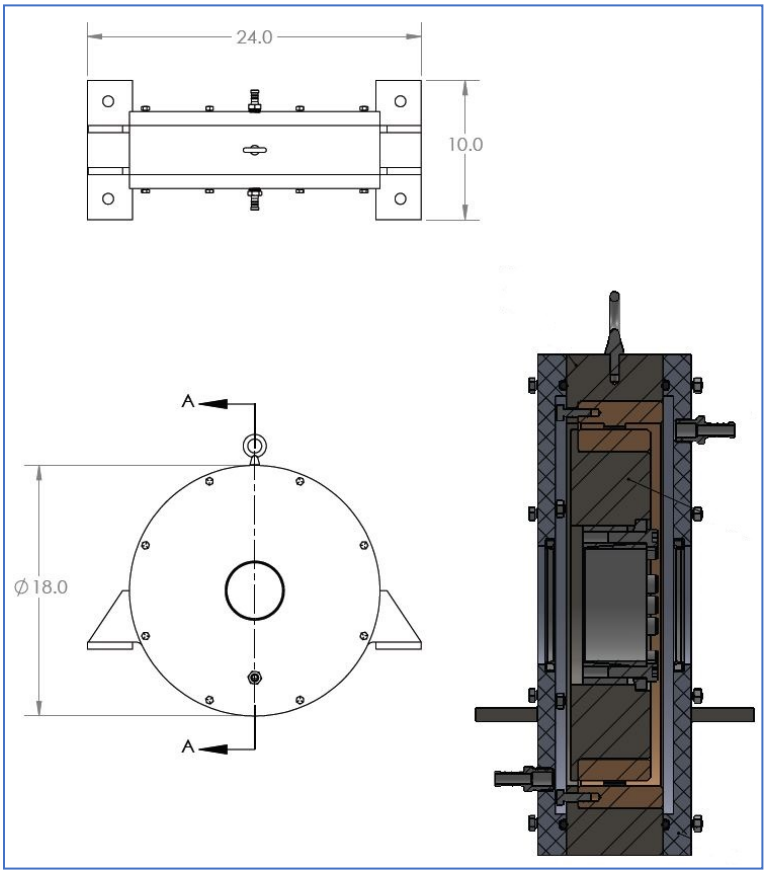

Figure 80. Bearing housing for test bearing

3.3.3.3 *Problems Encountered and Departure from Planned Methodology*

Due to the size of the system relative to RRM's tunnel thrusters, RRM was limited in its selection of supply chain partners for production of the stator and completion of the copper winding. As a result, RRM had to accept schedule delays as the supplier was in the middle of qualifying new facilities.

3.3.3.4 *Assessment of Their Impact on the Project Results*

Performance of generator testing had been delayed several months. Proposed design changes in future production would include utilization of a more common copper alloy for the windings, expanding RRM's supply chain flexibility to mitigate lead time risks.

3.3.4 Subtask 3.4 Test, Demonstration, and Final Report

3.3.4.1 *Original Hypothesis*

After completion of the FAT by the generator manufacturer, the system would be tested using the dynamometer facility to exercise the generator and electronics through the full range of specified operating conditions. To reduce Project costs, the generator test would utilize the same test setup for driveline testing as defined in Task 4.2. A full range of environmental conditions could not be examined as this testing would be performed in air. Testing would be performed according to the test plan developed and approved by the Project team. Preliminary test results would be reviewed by the Project team as they were developed. It was expected that adjustments to controls and driver electronics would be necessary at this stage in order to optimize performance the system. Performance analysis would be

conducted by the contractor and results will be reviewed by the Project team. A final test report on this portion of the effort summarizing testing protocols, procedures and results would be generated.

RRM would provide a report summarizing development testing of the encapsulation technology to provide a technical basis for subseaworthiness for generator operation in the event of seawater intrusion. The report will provide technical evidence of whether progress towards achieving the goal of being able to operate the generator at full power for up to 3 months in the event of a sea water intrusion or for up to 6 months at ½ power will be made.

Specific objectives for generator testing were the following:

3.4.1 Completion of generator testing
3.4.2 Generator test report
3.4.3 Generator test data
3.4.4 Achievement of rated power
3.4.5 Achievement of rated efficiency
3.4.6 Weight target to achieve target PWR increase
3.4.7 Report for immersion testing and subseaworthiness of encapsulation technology

3.3.4.2 *Approaches used*

3.3.4.2.1 Factory Acceptance Test Report

The factory acceptance test (FAT) of the generator from RRM took place on March 20-22, 2017. The intention of this test was to show functionality of the generator as per the documented design by IEC test standards which were outlined in the FAT report. All tests were successfully passed during the test period. The FAT included testing with reference to the DNV ship rules. For electrical equipment, the DNV ship rules refer to the following IEC tests which were performed during the FAT:

<u>Generator Tests (IEC 60034-1)</u>

1. Examination of technical documentation. Visual inspection. Verification of data on name plate.
2. Review test result from the withstand voltage test
3. Measurement of insulation resistance
4. Measurement of winding resistance
5. No load testing
6. Temperature rise test
7. Over-speed test

<u>Converter Tests (IEC 61800-5-1)</u>

1. Examination of technical documentation. Visual inspection. Verification of data on name plate.
2. Light load and function test
3. Insulation resistance tests
4. Rated current test
5. Temperature rise test
6. Control and monitoring system test

3.3.4.2.1.1 Measurement of Motor Parameters

Resistance and inductance measurements were taken between each of the phase output pins of the generator. These values are used to cross reference real and designed electromagnetic parameters and were used in FAT as an input to efficiency calculations.

	Phases U-V	Phases V-W	Phases W – U
Resistance (Ohms)	0.128	0.128	0.129
Inductance (mH)	11.0	11.8	12.1

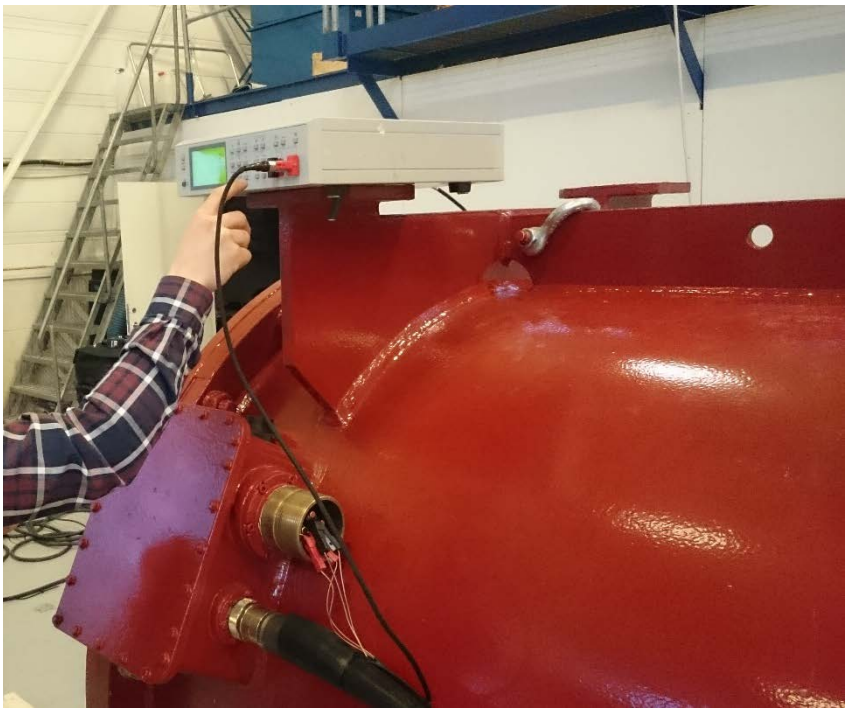

Figure 81. Measurement of resistance and inductance of stator windings

3.3.4.2.1.2 Open Circuit Voltage Test

This test was performed to monitor the output voltage of the generator when it was connected to no output load. This was accomplished motoring the generator to a speed of 55 RPM and then removing all current in the circuit and allowing the rotor to “coast” to a speed of 0 RPM. The waveform output of this test, captured by an oscilloscope logging at 100Hz, can be used as a footprint for the generator and confirms a uniform airgap and equally spaced rotor magnets.

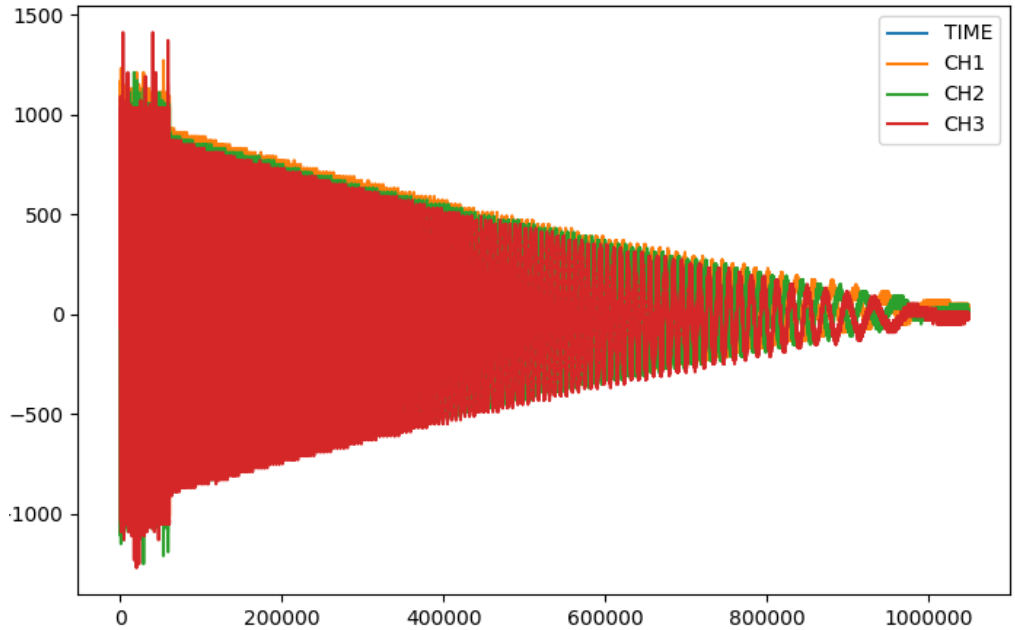

Figure 82. AC Voltage waveform from 3 phases during open circuit test

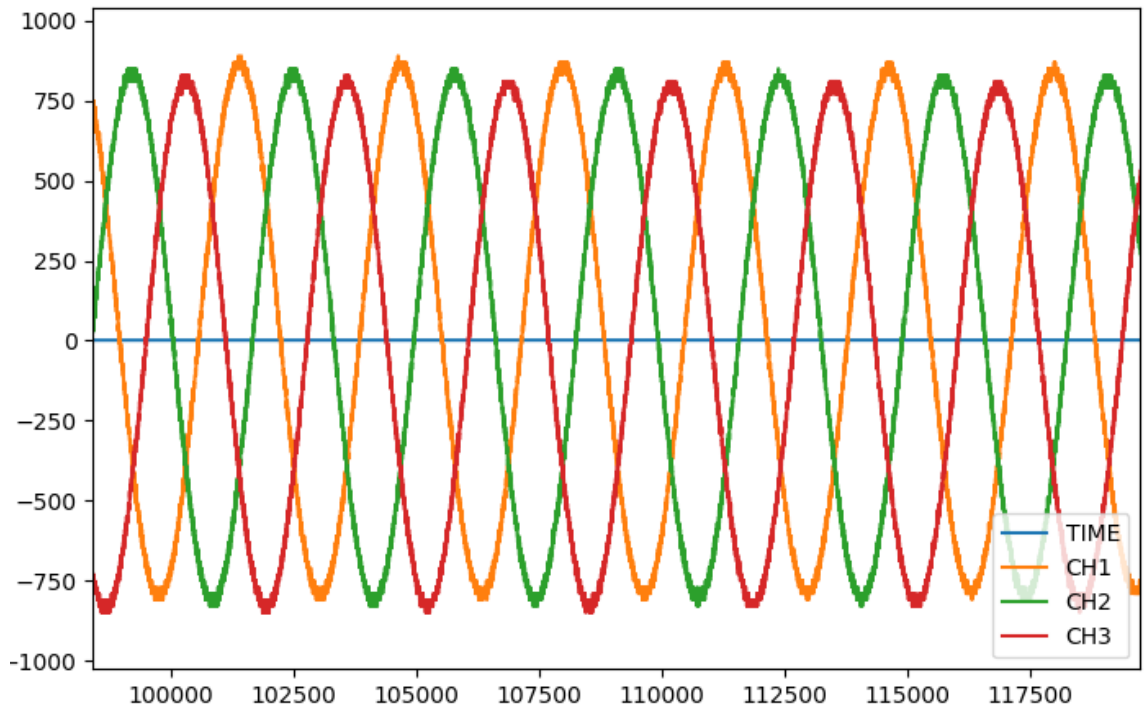

Figure 83. AC Voltage waveform from 3 phases during open circuit test, zoomed in at start of test

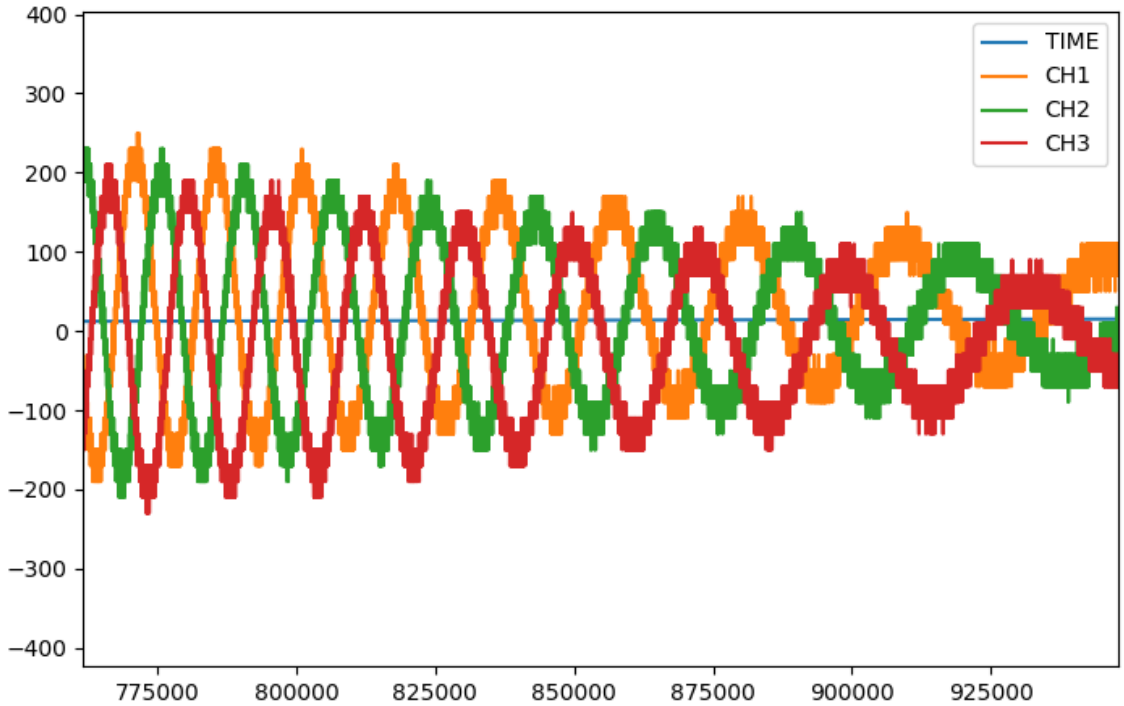

Figure 84. AC Voltage waveform from 3 phases during open circuit test, zoomed in at end of test. Note, symmetry, reduced frequency and amplitude with reduced speed.

3.3.4.2.1.3 Insulation Resistance Test

Insulation resistance (IR) tests were performed to evaluate the condition of the generator. This first measurement performed on a new machine gives a footprint of the insulation system for this machine and can to a degree tell if the machine has been properly manufactured. By comparing new measurements to older footprints, the condition and rate of degradation can be evaluated.

Tests were performed according to IEEE 43-2000 and the Megger MIT520/2 manual. All phases were tested simultaneously and only phase to ground test can be performed, as the phases cannot be separated due to a star connection. The following tests were performed and documented as part of the IR test and the generator performed to within the acceptable allowances.

- Step voltage ‘SV’ (1000V, 10 min)
- Dielectric discharge ‘DD’ (1000V,30 min)

Figure 85. Generator setup during IR test

3.3.4.2.1.4 Single Operating Points

For validation of the system at single operating points, the generator was operated at no load at various speeds which were each held for times of greater than 10 seconds. Included in the speeds tested was the maximum overspeed value of 132 RPM as specified in the design specification.

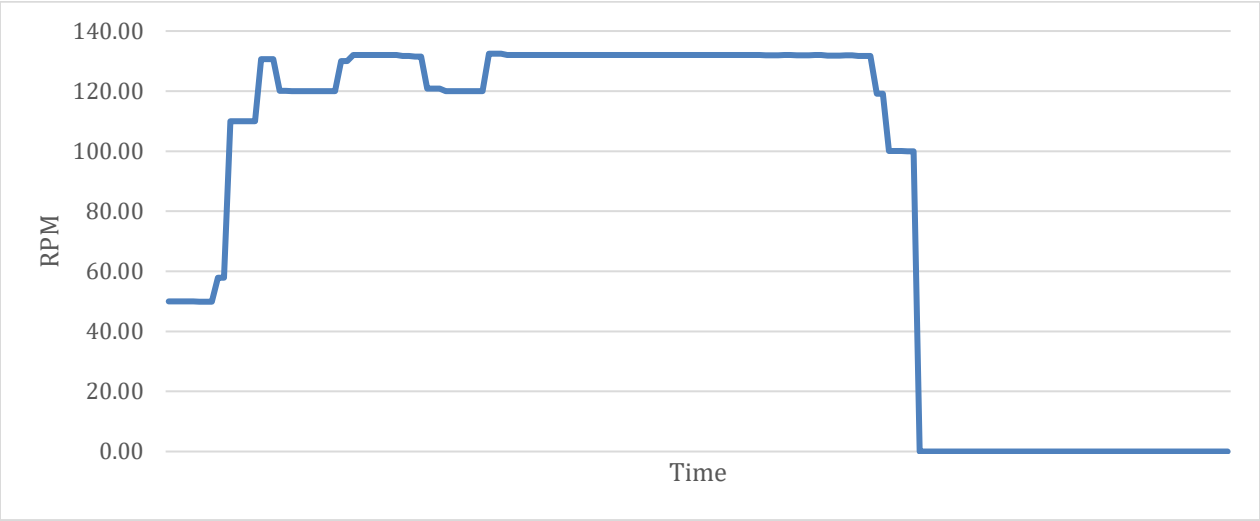

Figure 86. Generator speed data during overspeed test

Throughout the testing of the generator at single operating points, the converter control functionalities were tested as required in the design documents. Among the logical function of the controls that were tested were the following:

- Start/stop
- Operating in speed and torque modes
- Setting of reference values for speed and torque controls
- Alarm and trip settings
- Monitoring of operational values

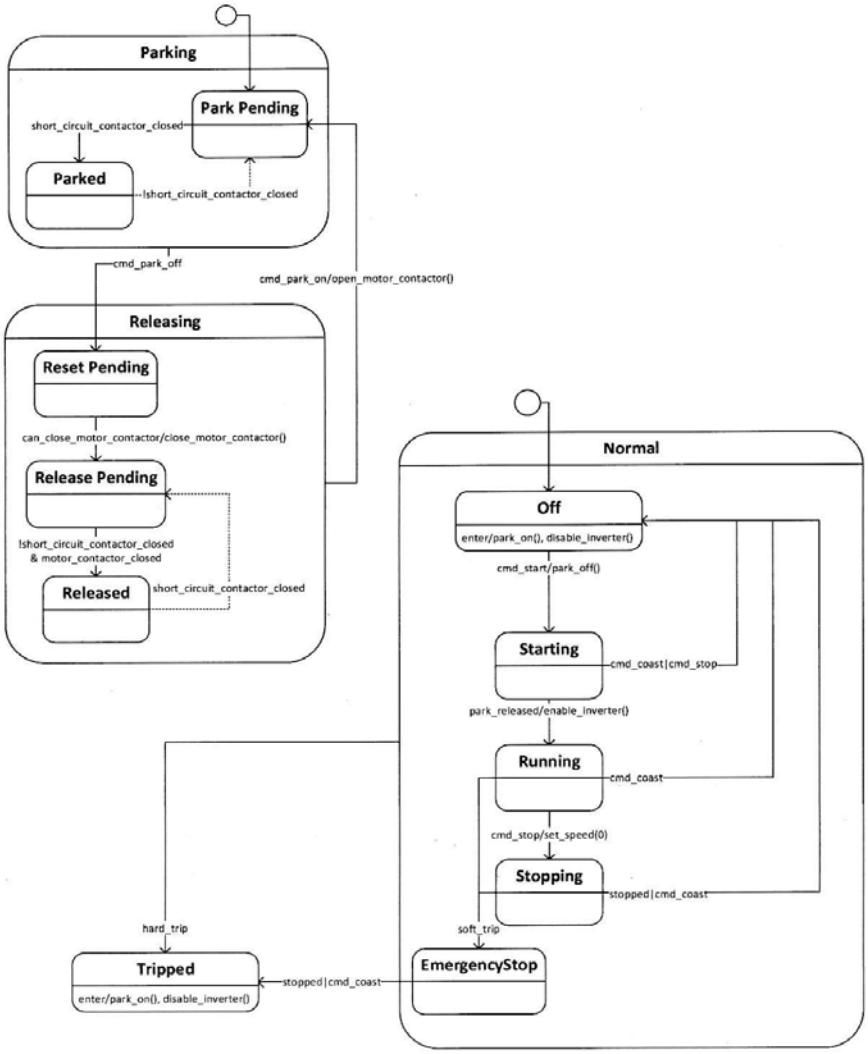

Figure 87. State diagram of drive

3.3.4.2.1.5 Efficiency Estimation

To estimate the efficiency of the generator the machine was run as a motor while submerged in water set to a controlled temperature. The generator was operated in speed control mode at speeds increasing in increments of 22 RPM up to the maximum operating speed of 110 RPM. This test was repeated at ambient water temperatures of 11°C, 16°C, and 27°C. The viscous torsional losses were estimated by subtracting non-speed related losses from the power required to rotate the rotor at each speed at each temperature. Results of this can be seen in Figure 111:

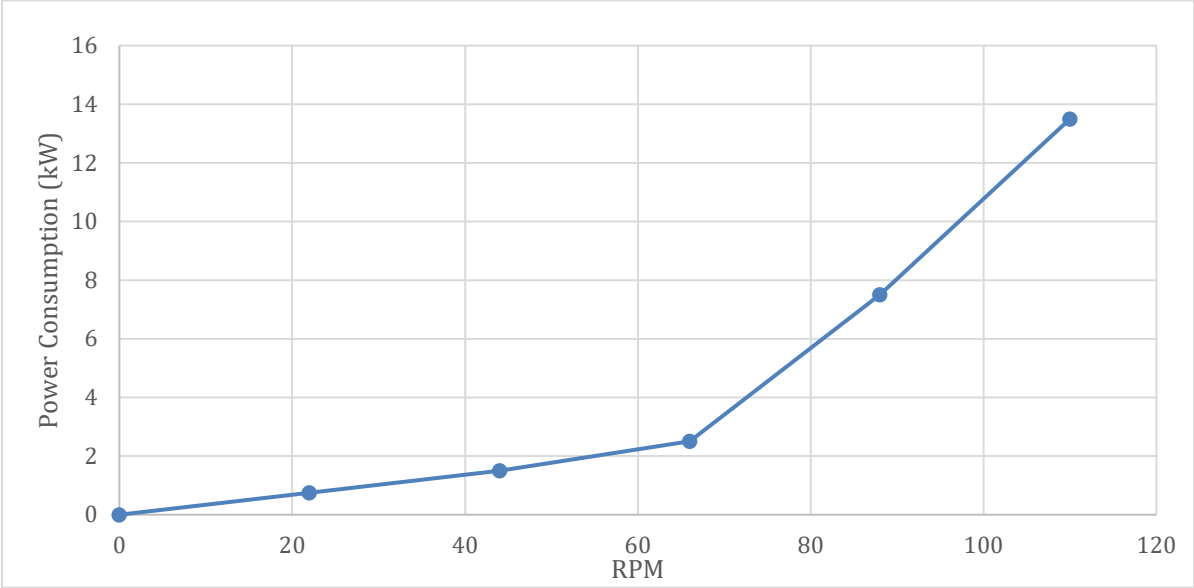

Figure 88. Generator no load power losses

Using power results from 2.8.1 generator power consumption can be measured. For the calculation the updated inductance, resistance, no-load loss and temperature rise was used. The efficiency is a calculated from the shaft power to the generator terminal power. This calculation includes the converter. The lower than anticipated temperature rise is what mostly influences the calculation and the increased performance in comparison to the design basis.

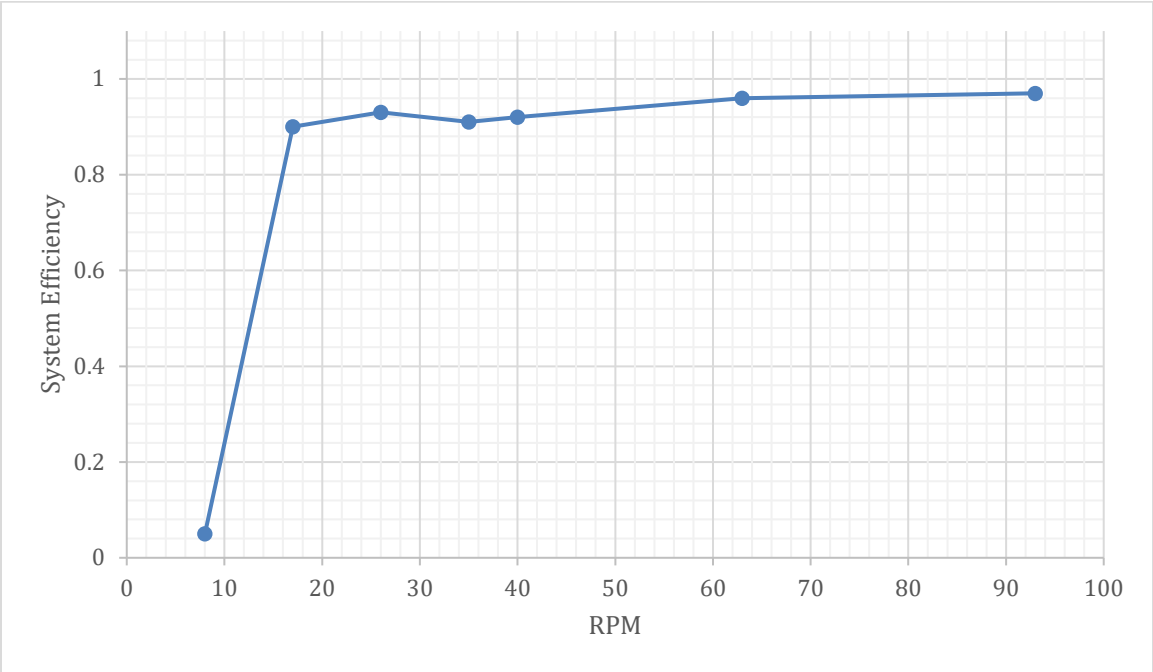

Figure 89. Generator and converter system efficiency

3.3.4.2.1.6 Temperature Rise Test

The temperature rise test is carried out to verify the guaranteed temperature rises for oil and windings. This test was used to clarify the insulation rating of the stator windings in particular. This test was run in a submerged test environment according to IEC 60034-1 temperature rise test requirements. This generator was designated as a Class H insulation system designed for operation at class F temperature. The temperature measurements were conducted using a 2-wire PT100 sensor setup, this measurement is not calibrated to account for the added resistance of the lead cables. The U-winding temperature sensor was measured through the supplied test signal harness (100 metres of 0.75 mm2).

Maximum winding temperature of 125 °C is set for the lifetime requirement. This means a maximum temperature rise of 93°C for an ambient water temperature of 32 °C. The maximum temperature rise measured in U-winding at 49°C.

Acceptance criteria for the converter is a temperature rise from 115°C at 32°C water temperature = 83°C. Maximum temperature rise of 52°C was monitored from ambient water temperature of 15.0°C to NTC temperature of IGBT 1 at 66.9°C.

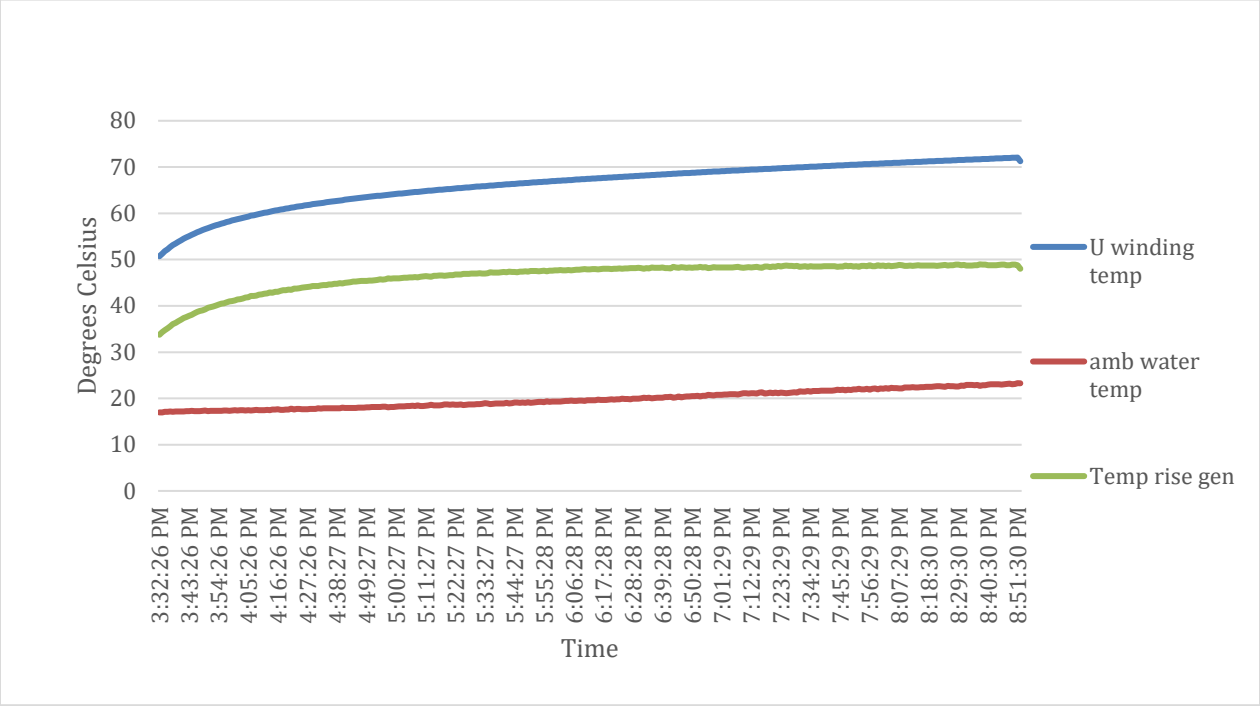

Figure 90. Temperature rise test data showing temperature rise of 49 degrees, showing cooling system outperforming predictions from design temperature rise of 93 degrees

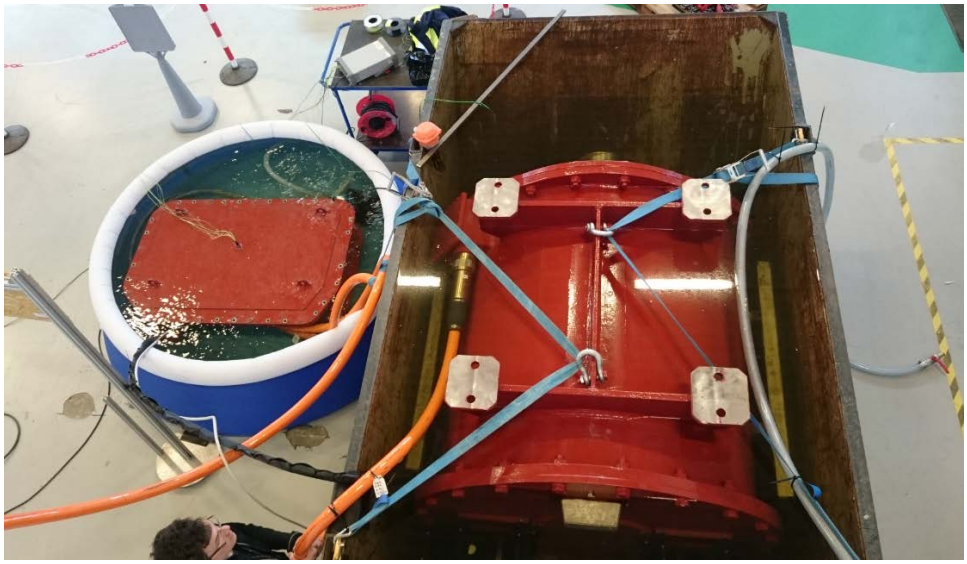

Figure 91. Temperature rise test setup

ORPC were provided final documentation for the generator including specification sheets, drawings, CAD files, and user manuals. The action items and documentation were reviewed in a final close-out meeting held between ORPC and RRM, and ORPC signed off on all deliverables from RRM.

The generator shipping cradle design was finalized and the generator and all ancillary items were loaded into a 20 foot container at RRM's facility in Trondheim Norway, the week of August 14, 2017 by Eimskip contractor JP Strom. The unit was delivered to the ORPC site in Eastport, Maine, on September 26, 2017. There were minor paint blemishes due to handling but otherwise no other physical damage was observed upon delivery. An on-board shock and temperature recording device was installed prior to the journey. No unusual shock or temperature events were recorded during the transportation. The generator is being stored in a heated storage area until it will be incorporated into the next generation TidGen® build and installation (beyond the scope of this Project).

3.3.4.2.2 Generator wet bearings

US Synthetics successfully manufactured the large, generator bearing. They achieved all critical tolerances in the fabrication of this bearing and did not encounter any major issues.

The fabricated bearing was installed in a "simulator" housing that replicated the generator internal dimensions. The remainder of the driveline test-rig was disconnected during this stage of testing to isolate the bearing and the toque loads. The bearing was loaded with a force equivalent to the loading it would see inside the generator.

This bearing performed similarly to the driveline bearings. It had an initial, higher COF during the "break-in" period and gradually declined. Near the end of the test, the torque and COF unexpectedly increased which is believed to be attributed to an external bearing holding the assembly that slipped, causing the PCD to shift and initiating a new "break-in period" for the running-surfaces on the PCD bearing. The bearing fault was not identified until the tear-down period and the apparatus ran uncorrected for the last three days of testing.

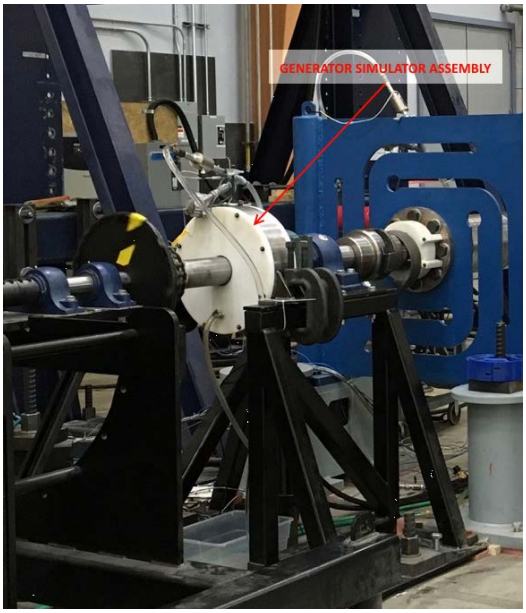

Figure 92. The generator simulator assembly installed in the PTO test rig. The PCD bearing is housed inside.

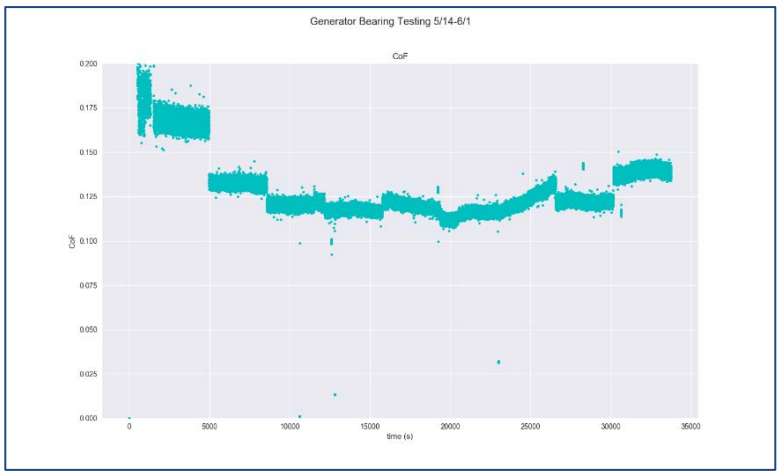

Figure 93. COF for generator bearing test

3.3.4.2.3 Encapsulation qualification

Figure 94. Stator housing

3.3.4.3 *Problems Encountered and Departure from Planned Methodology*

The generator testing was considered successful. Minor debugging of the control software was required, associated with appropriate versions of python versions of the underlying code. RRM has provided a full dump of the controls GUI, which is excellent and should greatly aid during commissioning. Other minor issues concerned getting accurate readings from the clamp-on AC current meters, which were resolved. Everything else ran smoothly. Of particular note is that it appears the cooling plate for the IGBT's work well. Predicted IGBT temperature at 225Arms was 115°C, and we measured temperatures ~60°C which plateaued after ~4 hours.

3.3.4.4 *Assessment of Their Impact on the Project Results*

Due to extended company vacation of RRM in mid-summer, the generator shipment was delayed and ORPC had requested a no-cost-time-extension through end of October, to cover shipping costs and logistics upon arrival in the US.

3.4 System Refinement and Integration – Task 5.0 System Integration Plan

3.4.1 Original Hypotheses

In parallel with component testing and dynamometer testing of the PTO system, ORPC was to commence design work to demonstrate how the advanced PTO system will be integrated with all ORPC TGUs. The work would focus primarily on the TidGen® TGU and assess how the advanced PTO would be integrated into TidGen® 001 or other units, then field-deployed and tested in an open water environment under operational conditions.

3.4.2 Approaches Used

ORPC incorporated the successful aspects of the PTO test and integrated them into the final design for the future TidGen® system design. Conceptual design of for the next generation system (Figure 121).

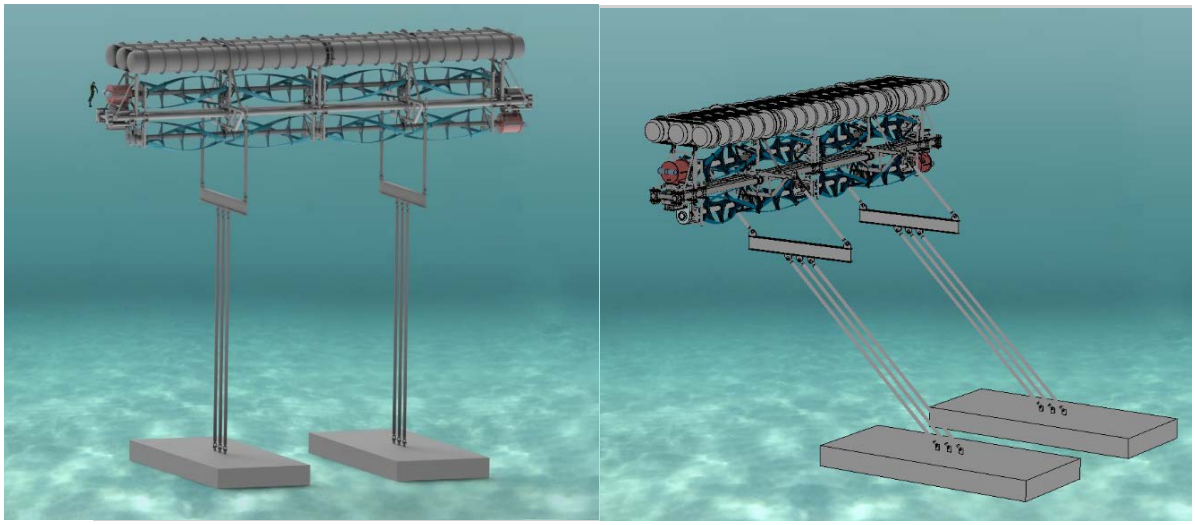

Figure 95. Conceptual next generation TidGen®. The system assumes integration of ORPC advanced technologies for controls, turbine and structural hydrodynamics, generator and power electronics, and mechanical drivetrain. The system would produce approximately 250 kW at a rated speed of 2.25 m/s, with dimensions 8.5 m X 34.6 m X 8.2 m.

The design mimics the PTO test with some modifications to improve the design. The integrated design still utilizes most of the PTO test component design: polycrystalline bearings, flex plates, and associated hardware used in the PTO test.

Some changes from the PTO test were necessary to allow the design concepts to work better within the constraints of chassis flexure and loadings. The basis for this integration plan are the loads and deflections exhibited by the system. The actual loads and system flexure have been better defined and incorporated into the design.

ORPC is now utilizing DNV-GL standards for design; the largest and most recognized offshore design standard organization in the world. The guidelines offer a reasonable, if conservative approach to overall design for off-shore and floating structures. We continue to refine our calculations and design, based on loadings and system flexure, and have utilized DNV-GL calculations to guide engineering decisions.

3.4.2.1 *Basic Loads – Forces Overview.*

The underlying driver behind all driveline design is a good understanding how the system is loaded during operation. The turbine loading is derived from CFD turbine modeling outputs. The turbine dimensions consist of a turbine with a diameter of 2.2 m and a length of 6.25 m. The position and the number of struts on the turbine were considered variables in the turbine design. Since the turbine induces loads on the driveline, it is crucial to consider the turbine configuration when designing the driveline. The location of struts changes how the loads are imparted on the driveline and certain configurations can have adverse effects on the driveline bending moment. For this reason, different turbine configurations were analyzed.

When considering load-cases, fatigue is the driving design factor. The high, reversing cycle count combined with the bending moments on rotating shafts drives component sizing. Of all the various operational loading cases, forces seen during torque limited operation have the highest cycle count and loading, making it the driving load-case for design.

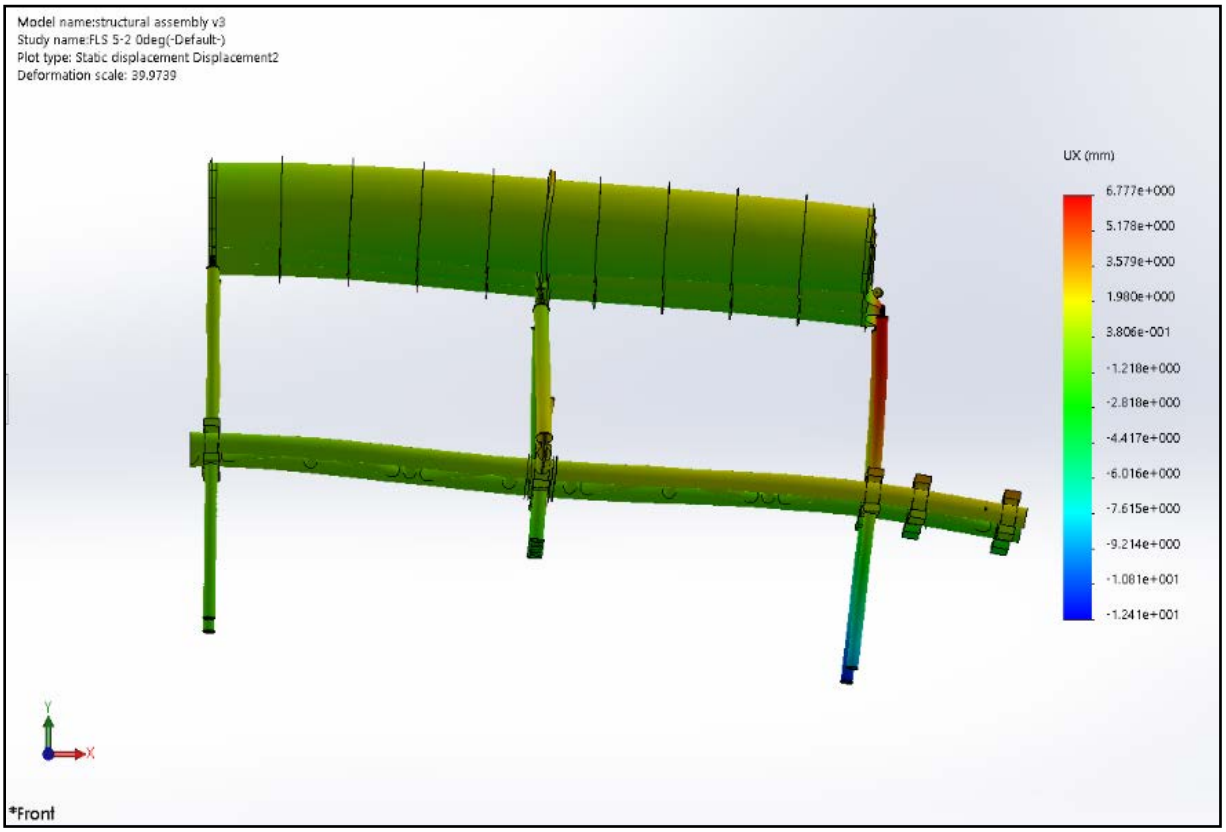

Figure 96. FEA analysis of system flexure

Additionally, the flexure of the total system plays a significant role in the alignment and forces acting on the bearings. Chassis displacement and flexure from operational forces (buoyancy, drag, etc.) is non-symmetrical, which requires a carefully designed and constrained system. Limiting flexure of the system within acceptable bounds is an important design parameter. The chassis design is outside the scope of the driveline design but is an input and interface requirement for chassis design.

3.4.2.2 *Turbine Configurations*

To analyze the turbine configurations ORPC utilized BluSource Energy Inc. to perform FEA analysis to evaluate the turbines structural performance.

Working with Blusource Energy, a novel turbine design concept was defined that allowed the mid stanchion bearing housing to keep the larger spacing between bearings while giving the foils the structural support required. This novel turbine design consists of three struts and two end supports as seen in Figure 1233. This arrangement of struts allows the mid stanchion bearing housing to overlap with the turbine keeping the reduced bending moments in the driveline.

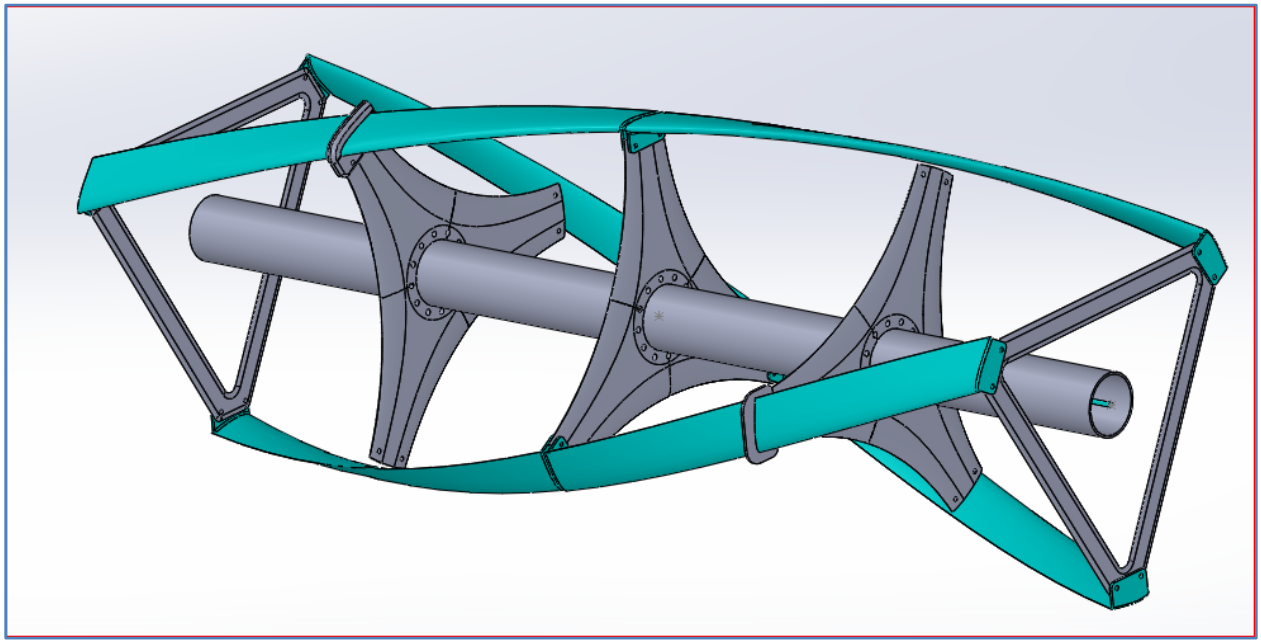

Figure 97. Five-strut configuration

3.4.2.3 *System Design Philosophy*

Overall system design follows typical best-design practices for most any bearing system. ORPC's tidal system will use multiple turbines to drive a common generator. The system must be able to withstand misalignment due to installation, manufacturing tolerances and also accommodate system flexure during operation. ORPC has developed several custom FEA tools to analyze turbine loadings during operation and has applied cyclical fatigue and loading factors to assure components are rugged enough to withstand long-term operational loading without suffering failures.
The two turbines are connected in the center at an axially fixed bearing assembly. This center bearing provides for radial and axial loading. On each end are radial bearing assemblies that allow the driveline system to move radially and allow for angular deflection without over-constraining the assembly.

The chosen system architecture minimizes the total number of mechanical elements required in the driveline assembly. Previous systems utilized a flexible coupling between each turbine, while the newer design simplifies this by only utilizing flexible couplings between turbine pairs. The driveline is separated into two-turbine unit sections that can be interconnected to create longer turbine assemblies, separated by flexible couplings. In comparison to previously engineered designs, total part count has been reduced, so overall manufacturing cost is lowered and the assembly is easy to maintain and assemble. There are tradeoffs between maintainability and overall cost that need to be balanced to obtain a system that is reasonably easy to assemble and maintain.

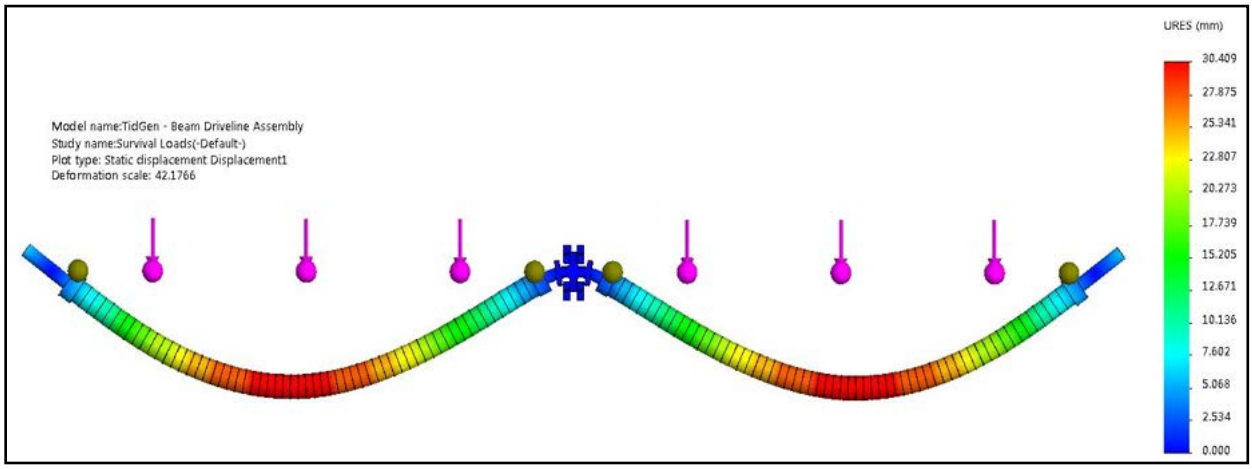

Figure 98. Driveline FEA simulation flexure in a typical ORPC turbine system

One aspect, inherent to cross-flow turbine design, is driveline flexure. The large radial loading and long turbine spans deflect driveline components and requires carefully engineered bearing solutions to accommodate. ORPC reviewed anticipated loading and developed a flexible bearing housing system to reduce bearing edge loading.

3.4.2.4 *Middle Bearing Housing: Combination Axial / Radial Bearing*

The mid-stanchion bearing assembly is the axially "fixed" bearing that handles axial loads for two turbines in addition to radial loading. The axial and radial bearings are separate assemblies that attach to the bearing housing. The housing and bearings are designed to work together and limit edge loading by matching anticipated flexing in the drivetrain to allow for driveline flexure while limiting bearing edge loading.

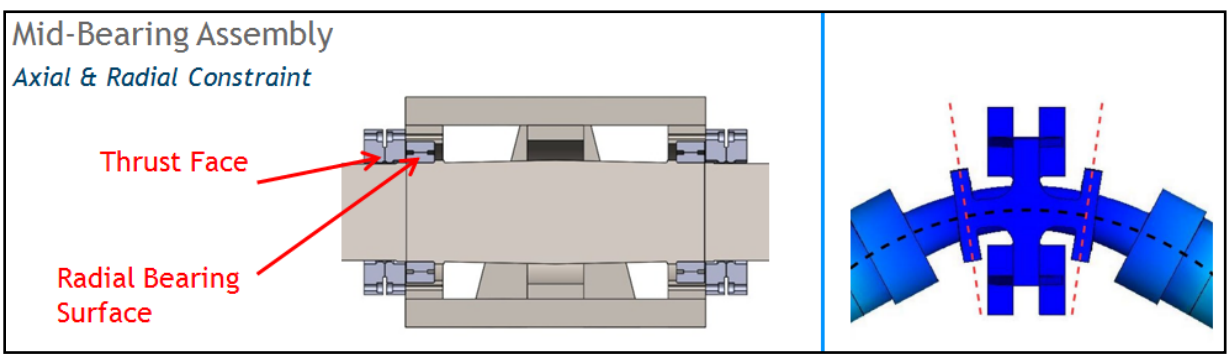

Figure 99. Middle bearing housing overview

The radial PCD bearings are nearly identical to the radial bearings on the end-stanchions but do not need to allow for axial movement so they have only one row of PCD inserts (end stanchion radial bearings have two rows).

3.4.2.5 *End Bearing Housing: Radial Bearing*

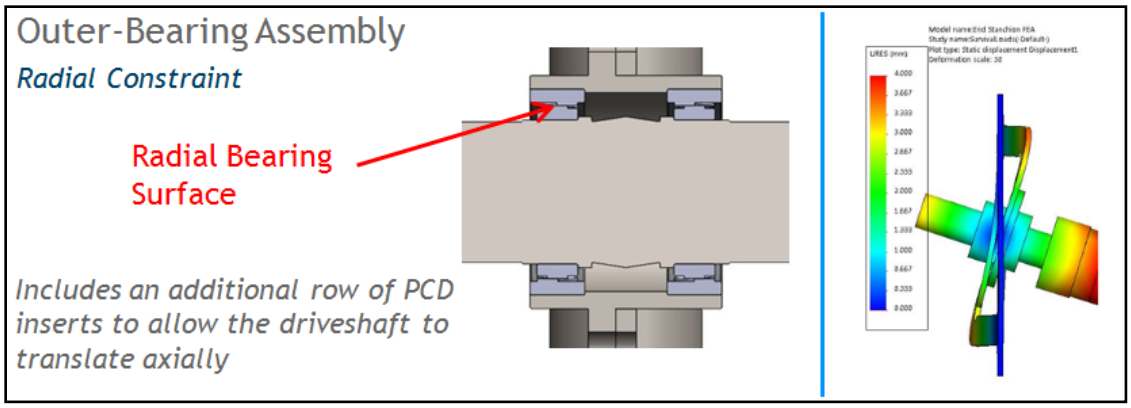

Figure 100. End bearing housing overview

The end-stanchion is a radial-only bearing. It houses a PCD radial bearing in a flex-plate that conforms to any bending in the shaft. The PCD bearings have two rows of inserts that accommodates axial movement.

3.4.2.6 *Generator Bearing Mechanical Design*

ORPC's newest generator is designed to be capable of operation in a fully water-flooded configuration. The interior is completely encapsulated to allow it to operate with seawater inside. While the generator is designed to handle this configuration, the roller bearings currently utilized are not capable of operating in this condition. The bearings utilized presently will require additional seals (or other methods) to protect against water intrusion into the roller elements and oil lubrication.

ORPC has developed a direct-replacement PCD bearing, capable of operation in the flooded condition. Due to budgetary considerations, only one bearing was manufactured and tested during this testing program. The operational loading is straightforward for this bearing and is within its operational capabilities, it only needs to handle the radial load of the rotor and a minimal amount of axial loading. The generator input shaft is isolated from the turbine drivetrain forces via a flexible coupling.

The current bearings in the generator are designed to be replaceable, and the radial PCD bearing tested could fit into the generator. Given the experimental nature of the bearing, the bearing was run only in the test-fixture to confirm the viability of the design concept.

3.4.3 Problems Encountered and Departure from Planned Methodology

3.4.3.1 *End Stanchion Bearing Design*

The end station design concept was successful at limiting bearing edge-loading and the PTO test-results indicated it performed well. The final design is utilizing essentially, the same design concept as tested in the PTO program. The only significant alteration has been to increase the size of shafting and corresponding bearing diameters for loading and high-cycle fatigue. The changes are not expected to alter performance in any appreciable manner. Incorporating minor changes to overall dimensions to optimize the strength and rigidity of the flex-plate may further improve the characteristic response for this application.

3.4.3.2 *Mid Stanchion Bearing Design*

The mid stanchion bearing performed reasonably well during testing but some limitations were revealed. Overall, the coefficient of friction for this bearing assembly was higher than expected. Special adaptations must be made to allow the flexure to work effectively on future devices with non-symmetrical deflection. The design to be implemented on the future TidGen® device will be improved in a few areas.

The most substantial design change was to widen the bearing housing. The housing has been extended into the turbine to reduce bending moments on the rotating shaft and reduce the chance of fatigue failure. Shown in Figure 132, is an FEA prediction of bending moments imparted to the shafting from turbine loading. Bending moments were reduced by greater the 50 percent by increasing the span between bearings. The reduces overall deflection, stress, and allows for reduced shaft sizing.

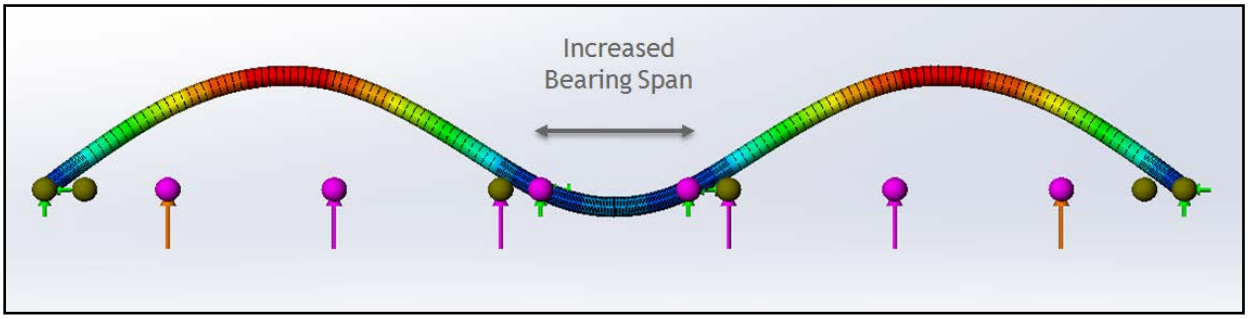

Figure 101. FEA Analysis of mid bearing flexure

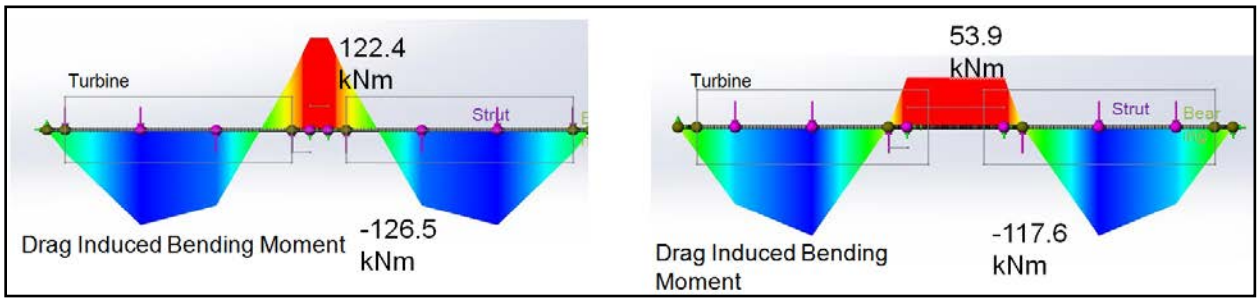

Figure 102. FEA bending moment predictions (left: 4 struts with narrow housing, right: 3 struts with wider housing)

The bearing housing was designed to deflect with the drivetrain to limit edge loading and maintain a parallel relationship between the inner and outer races of the PCD bearing. Matching the stiffness of the center shaft with the stiffness of the housing is possible, with careful design work. Unfortunately, this approach only works when the chassis deflection and loading are symmetrical about the middle of the bearing stanchion. Asymmetrical loading and chassis flexure will distort the housing in ways that cannot be stiffness-matched.

Further analysis of the future TidGen® chassis structure has revealed deflection and loading will not be symmetrical, which will be problematic for the alignment scheme of bearings and will require design changes from the original PTO design concept.

A design change to maintain even bearing contact between inner and outer races of the PCD bearing is necessary to provide the required life and performance of the middle PCD bearing. The end-stanchion worked well, due to the bearing assembly being "steered" by loads and conforming to any shaft deflection. The design of the middle bearing stanchion will have to mimic this self-alignment feature to assure the bearing aligns with deflection. Additionally, the thrust bearings must also align with loading to equally distribute loads over the entire surface of the bearing.

3.4.3.3 *Turbine Shaft Design*

The turbine shaft is a simple, metal tube for overall reliability and cost (as opposed to a composite). It will be reinforced at the ends and the strut-interface connection with the turbines needs to be finalized.

3.4.3.4 *Generator Bearing Design*

The generator bearing was designed, manufactured, and tested was successful. The bearing was the largest diameter bearing ever produced by US Synthetic. The loading forces were low in comparison to the size, leading to a very slow "break-in", self-polishing phenomenon. COF did steadily decline over the duration of the test and it is expected that COF would be further reduced with longer running times.

Issues related to direct replacement of a SKF roller bearing made the PCD bearing design difficult. The radial bearing manufactured could replace the SKF radial bearing currently installed in the generator. The corresponding opposite SKF bearing (radial / axial carb roller bearing) installed in the generator would be difficult to directly-replace without modification of the generator.

In review of optimal bearing designs for future generators, an externally mounted PCD bearing design was identified as being more appropriate for several reasons. Cooling is important to the PCD bearings and an external housing could accomplish this better than an internally mounted bearing. Inspection and maintenance of an externally mounted bearing would be easier too. Lastly, even though the generator is capable of wet-gap operation, it would likely still be "sealed" to prevent biologicals from growing inside the generator, causing undefined complications from marine growth. An externally mounted bearing would eliminate these issues.

3.4.3.5 *Driveline: Final Design*

Based on loading and information we have available today, a reliable drivetrain solution has been developed.

3.4.4 Assessment of Their Impact on the Project Results

The design issues encountered were considered as normal development issues and were informative in terms of bearing assembly design and corrosion protection for production bearing development.

3.5 Project Metrics

The Project metrics were established and reviewed in several tasks/subtasks:

- Subtask 2.3 System Performance Advancement (SPA) Goals
- Subtask 3.4 Generator Test, Demonstration and Final Report
- Subtask 4.2 Driveline System Test
- Task 6.0 Impact Analysis

3.5.1 Original Hypotheses

3.5.1.1 *Subtask 2.3 System Performance Advancement (SPA) Goals – Driveline and Generator Design Improvements*

Under Subtask 2.3, ORPC was to analytically determine the expected improvement in PWR and availability will be made for the advanced driveline and generator components as they apply to a complete TidGen® TGU. As part of this effort we were to define the specific SPA metrics and their respective Project targets.

Specific objectives were as follows:

- Definition of the SPA metrics
- Project SPA targets to include:
  - An increase of the Power to Weight Ratio for the TidGen® TGU by an estimated 23 percent to 4.9 kW/ton
  - An increase in the availability target to 98 percent
  - A reduction in LCOE of 25 percent

A baseline assessment of component performance metrics would be conducted using existing test and design data. We would ensure that consistent definitions of the component performance metrics would be utilized by all parties over the course of the Project.

Definitions and baseline values of the following component performance metrics would be created, documented and agreed upon by the Project Partners and delivered to DOE as an appendix in the Project Management Plan.

- Driveline friction definition, baseline value, and measurement procedure
- Basis for driveline maintenance interval
- PTO baseline weight (driveline and generator)
- PTO baseline power performance
- Failure metrics for generator components

3.5.1.2 *Subtask 3.4 Generator Test, Demonstration, and Final Report*

The relevant component and SPA metrics are as follows:

- Achievement of rated power
- Achievement of rated efficiency
- Weight target to achieve target PWR increase

3.5.1.3 *Subtask 4.2, Driveline System Testing*

The relevant component and SPA metrics are as follows:

- Driveline frictional losses will have been demonstrated to be less than 5 percent of rated power as compared to a baseline of 15 percent of rated power.
- Wear on all bearings will substantiate analytical model predicting 5+ years maintenance intervals
- Complete PTO will demonstrate achievement of rated power
- Complete PTO will demonstrate achievement of rated efficiency
- Complete PTO will demonstrate achievement in target generator system mass to support Project PWR targets increase.

3.5.1.4 *Task 6.0 Impact Analysis*

Under Task 6.0, Impact Analysis, ORPC would provide information and data to develop a model of the LCOE for an advanced TidGen® TGU utilizing the advanced PTO design enabled by this Project and following the DOE MHK LCOE reporting guidelines. Baseline assessment of the LCOE, PWR and availability would be performed at the commencement of the Project. Updates to the performance metrics would be made at the difference stages in the project, including at the completion of each of the design and test phases. The proposed improvements to the components were expected to improve the cost competitiveness of the ORPC MHK electrical power generating system. The final Impact Analysis will provide an economic analysis of impacts of SPAs proposed within this Project.

An increase in availability and reduction in driveline friction enabled by this Project would impact LCOE both by reducing maintenance costs and increasing energy output. ORPC would verify that the expected reduction in LCOE of 25 percent has been achieved.

3.5.2 Approaches Used

3.5.2.1 *Subtask 2.3 System Performance Advancement (SPA) Goals – Driveline and Generator Design Improvements*

At the end of the first design phase of the Project, ORPC had completed the definition, baselining and evaluation of component and SPA metrics.

For driveline friction and mechanical efficiency, flume testing in this and earlier projects established a coefficient of friction value of 0.14 for the baseline Vesconite sleeve bearings, and a predicted value for the PCD bearings' coefficient of friction as 0.02. Manufacturer data had provided historical estimates of 0.02 to 0.05. Translating driveline friction to mechanical efficiency was performed through analysis of field operational data of the baseline TidGen® deployed in Cobscook Bay, Maine, in 2012 and 2013. A baseline mechanical efficiency of 87.6 percent was estimated, with a coefficient of friction (CoF) value of 0.02 translating to losses of less than 1 percent. Final Project results were an estimated CoF of 0.05 translating to losses of only 2.3 percent, within the Project target of less than 5 percent.

For the maintenance interval, ORPC considered bearing wear and seal life. Wear during flume testing was not measurable in PCD bearings, and manufacturer history showed that the failure mode associated with the bearings was thermal fracture from lack of adequate water cooling or exceedance of load capacities rather than wear. Given the open environment and the exposure of driveline bearings, as well as a US Synthetic design with high safety margins, thermal fracture is a low risk of failure. PCD bearings also performed well in sedimented flow during flume testing, eliminating the need for seals, the most likely component to fail. As a result, the assumption for a 5-year maintenance interval is achievable for the bearings.

The generator provided by RRM indicated achievement of required weight and efficiency to achieve the Project targets for power to weight (PWR) and reliability. The assessment of PWR achievement of the technology improvements are discussed in the following sections on generator testing and final SPA predictions.

The component metric for increasing TSR, as proposed in Task 2.0 Driveline Design, was determined to be not applicable for final project metrics. Streamtube analysis of baseline operational data showed that

the target TSR of 1.9 as already achieved. Figure 135, an initial streamtube analysis, describes the impact of mechanical losses on performance and TSR.

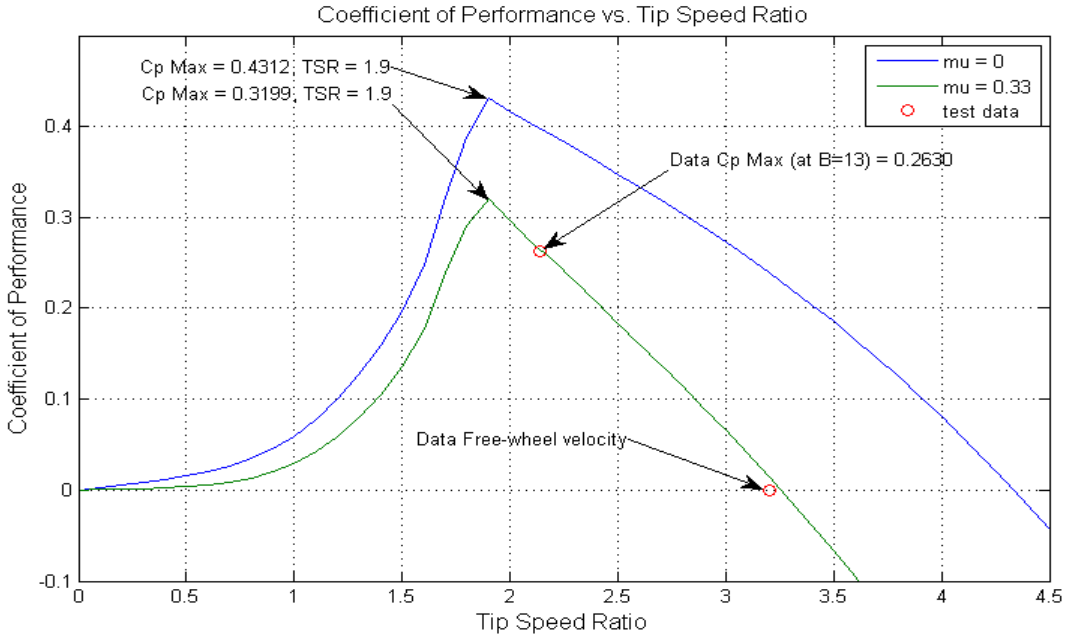

Figure 103. TidGen®-001 C_P vs. TSR per streamtube modeling fitted with actual operation data in Cobscook Bay. Note that the operating points, indicated in red circles, were stable operating conditions used to fit the model, shown in green, with the ideal, lossless performance shown in blue.

As seen in the Figure 135, the effect of introducing frictional losses, through increasing the parameter mu lowered Cp without impacting TSR. As a result, the metric was deemed already achieved and not applicable to Project success.

Given the component metrics above, an estimate of AEP was developed in collaboration with NREL as a required metric for calculating the LCOE. This methodology is described in the section below for Impact Analysis, which derives LCOE predictions based on Project performance and the reference array and site data provided by the DOE.

3.5.2.2 *Subtask 3.4 Generator Test, Demonstration and Final Report – Component Metrics*

RRM generator testing, as reported in D17-0006, Generator Test Report for Power Take-Off, dated July 24, 2017, and was submitted to the DOE in the course of the Project effort.

Table 26. Assessment of component milestones for the RRM generator.

Milestone	Goal	Actual
3.4.1, 3.4.2 & 3.4.3: Completion of generator testing and provision of test report and test data	ORPC completes FAT successfully, and provides test report and data to DOE	*Meets requirement.* Satisfied by this document and provision the generator test report by RRM.
3.4.4 Achievement of Rated Power	150kW, DC output at converter terminals, at 40RPM	*Exceeds requirement.* Rated power required torque of 38kNm at 40RPM. Measured torque was 39.3kNm, for rated power = 164.6kW.
3.4.5 Achievement of rated efficiency	90% total system efficiency at 32 degrees C (corresponds to 92% efficiency at minimum ambient temperature -4 degrees C)	*Exceeds requirement.* Rated efficiency = 92% for DOE reference site; meets requirements at maximum operating environment temperature.
3.4.6 Weight target to achieve target PWR increase	11,060kg, as presented at Go/No-Go Decision Review, February 2015 (weight includes generator + drive electronics and oil-filled)	*Meets requirement.* Final as-built design weight: 10,920kg

3.5.2.3 *Subtask 4.2 Driveline System Test – Component Metrics*

The driveline system testing was performed to assess the next generation driveline system concept that incorporated PCD bearings designed by US Synthetic Bearings for ORPC's TidGen® application. The testing was conducted as part of Subtask 4.2, with the processed results to be used for evaluation of achievement of overall Project goals.

The milestones 4.2.3 through 4.2.7, were defined in the Statement of Project Objectives (SOPO), covering PTO Friction Reduction, Rated Power, Rated Efficiency, Mass Reduction, and Bearing Wear. Milestones cover both the measured driveline friction and performance data of the advanced encapsulated generator, produced by Rolls-Royce Marine as Subtask 3.4 of the Project, and referred to in the previous section.

Table 27 outlines Project milestones achieved through completion of the PTO driveline system testing as reported in document, D-xPTO-10042, DOE PTO Driveline Test Report. Supporting data and/or analyses are included in the following section.

Table 27. Milestone summary for Task 4.2, PTO Driveline System Testing.

Milestone	**Goal**	**Actual**
4.2.3 PTO Friction Reduction	Driveline frictional losses will have been demonstrated to be less than 5% of rated power as compared to a baseline of 15% of rated power.	*Exceeds requirement.*
4.2.4 PTO Rated Power	Complete PTO will demonstrate achievement of rated power.	*Exceeds requirement.* Generator acceptance testing in Task 3.4 (reference milestone 3.4.4) measured a rated power of 164.4kW, exceeding requirements of 150kW.
4.2.5 PTO Rated Efficiency	Complete PTO will demonstrate achievement of rated efficiency.	*Exceeds requirement.* Generator acceptance testing in Task 3.4 (reference milestone 3.4.5) measured a rated efficiency of 92%, exceeding the requirement of 90%. Driveline testing verified generator integration with the PCD bearing driveline design.
4.2.6 PTO Mass Reduction	Complete PTO will demonstrate achievement in mass per unit power of 20% as compared to baseline.	*Meets requirement.* Available power calculations with the RRM generator and PCD bearings show a mass per unit reduction from baseline of 22.1%.
4.2.7 PTO Bearing Wear	Complete PTO will demonstrate achievement of 5+ year maintenance intervals for all bearings through measured bearing wear and supporting engineering analyses.	*Meets requirement.* PCD bearings had no measured wear after driveline testing, or from testing of scale model bearings by the supplier. Failure mode is thermal fracture rather than wear; with a driveline design that avoids edge loading of PCD bearings and promotes water flow through bearings during operation, PCD bearings show potential to last for entire system service life of 20 years. Validation in open water is required for predictions greater than 5-year component life.

3.5.2.3.1 Supporting Analyses

3.5.2.3.1.1 Friction Reduction

Driveline testing in Task 4.2, documented in D-xPTO-10042 PTO Driveline Test Report, measured coefficient of friction (COF) of the driveline test rig as 0.08 with an expected COF 0.05 with full break-in polishing of the bearings.

At the Go-No-Go meeting in February 2015, ORPC presented its estimate of baseline TidGen® mechanical losses of 12.4 percent by utilizing streamtube model theory to analyze historical operational data. The streamtube models are proven to be accurate for estimates of TSR and C_P for cross-flow turbines at peak performance, and ORPC's fitted models correlated well with actual operating data of the TidGen® in Cobscook Bay in 2013. Through comparison of streamtube model peak efficiencies for different values of friction losses, estimates of parasitic power losses can be made.

Figure 134 shows several TSR-CP curves for the TidGen®'s baseline four-foil turbine. The black curve, with a peak C_P of 0.4312 at TSR 1.9, represents an idealized, lossless turbine. The lowest curve, shown in blue with peak C_P of 0.3181, was fit to stable operational data, shown by the red circles. Fitting of the curve was done by adjusting the model's parameter for friction losses, mu. This value was 0.53 and represented the baseline TidGen®'s lumped driveline system friction. The parameter, mu, was assumed as a sum of turbine fluidic losses and driveline mechanical losses. As the driveline bearing friction is the dominant component of mechanical losses, ORPC estimated the mechanical losses as 0.14, corresponding to the measured COF of the baseline Vesconite sleeve bearings. The corresponding COF component for fluidic losses was thus assumed as 0.39.

An idealized curve with no mechanical losses is shown in red, with peak C_P of 0.3633. This value is the idealized turbine C_P for the baseline TidGen®. The ratio of 0.3181 to 0.3633 gives an estimate of efficiency as 87.6 percent, or a mechanical loss of 12.4 percent.

The performance improvement for the PCD bearings is shown by the dotted blue line. The streamtube model used a bearing COF of 0.05 for a combined mu of 0.44. The peak C_P for the improved driveline system is estimated as 0.3548. The ratio of 0.3548 to 0.3633 gives an estimate of mechanical efficiency as 97.7 percent, or a mechanical loss of 2.3 percent. The final projected improvements for friction reduction are from 12.4 percent to 2.3 percent losses, meeting the target of < 5 percent mechanical power losses.

3.5.2.3.1.2 Rated Power and Rated Efficiency

The generator FAT produced by RRM measured a rated power of 164.4 kW, exceeding the required 150 kW. Rated efficiency was measured as 92 percent at 40 RPM. The requirement was for 90 percent at 32 degrees C. Driveline testing indicated that integration of the generator to the driveline was viable, as demonstrated by the simulated loading on the PCD test bearing for the generator. The wet-bearing design performed as the driveline bearings with no issues found during testing. The FAT test results were provided to the DOE for Task 3.4, in D17-006, Generator Test Report.

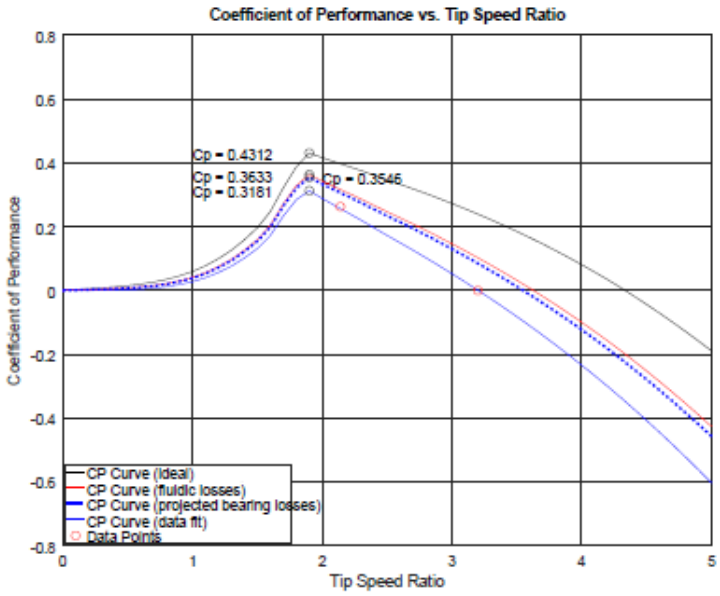

Figure 104. Streamtube models used to estimate mechanical losses of the baseline TidGen® Power System and predicted improvements with polycrystalline diamond bearings.

It is worth noting that generator efficiency improves at lower temperatures, however, where the TidGen®'s primary markets are. Water temperatures in coastal Maine and coastal Washington (Admiralty Inlet) do exceed 15 degrees C. RRM has estimated improvements of 1 or more percentage points of efficiency at this temperature. Fitted data from the FAT projects an efficiency of 93 percent at 40RPM and up to 96 percent at higher speeds. This is shown below in Figure 137.

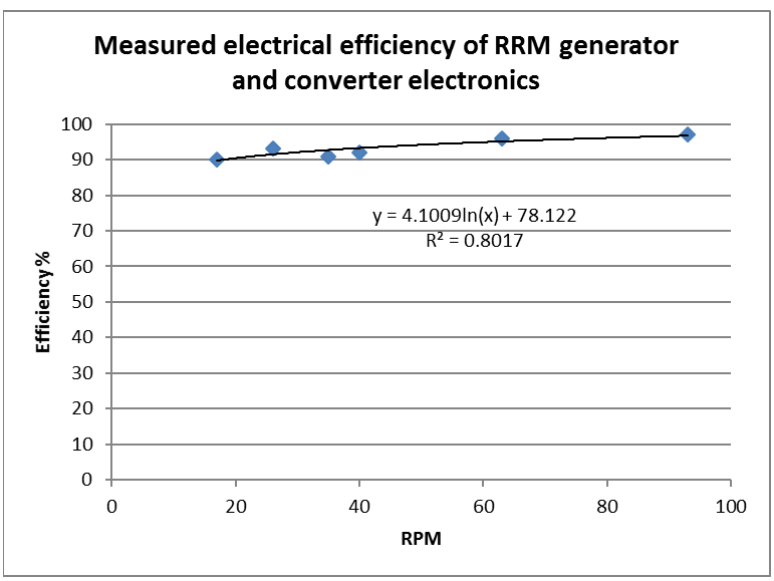

Figure 105. Factory Acceptance Test results provided by RRM performed in February 2015 for electrical efficiency at 32 degrees C.

Overall system power and efficiency, as measured onboard at the generator terminals, is represented by the system power curve shown in Figure 136138. System parameters are given in Table 228. Efficiency improvements were realized in generator and PCD bearings. Major gains were realized in overall cost

reductions due to the improved reliability of both technologies. This is discussed in the section below for Project SPA goals. The RRM generator operates in torque limited mode once the maximum torque is reached. Power increases linearly in this operating region. For power output greater than 150kW, an additional converter electronics unit is required.

3.5.2.3.1.3 Mass Reduction

The mass differential for the Project from baseline is dominated by the generator. Final generator weight was measured as 10,960kg (refer to Appendix A and document D17-0006 Generator Test

Report). The generator was designed for future operation as a wet-gap system, where the redundant oil-filled reservoir could be modularly removed. An approximate weight of such a system is 10,000kg, depending on integration design of the PCD bearing technology.

Mass per unit power is the inverse of the Power to Weight Ratio (PWR), discussed below in the section for Project SPA Goals. The RRM generator mass is greater than the baseline TidGen® generator (produced by CPI, now defunct), which was 9660kg. However, given the greater reliability, the available power has increased considerably. The available power is derived by multiplying the system power curve by the annual site velocity distribution, and then applying the system availability. The discussion for PWR shows the derivation of available power at the DOE reference site data for Admiralty Inlet. Calculations show a reduction in mass per unit power of 22.1 percent, meeting the target of 20 percent.

3.5.2.3.1.4 Bearing Wear

To determine longevity of the PCD bearings, ORPC measured bearing wear from the driveline system testing of Task 4.2. Additionally, because performing life testing was beyond the scope of this Project, ORPC had the supplier, US Synthetic Bearing, perform scale model bearing testing to failure. The synthetic polycrystalline diamonds historically had shown no wear for bearing applications. Neither driveline testing or model-scale testing results indicated any measurable wear of the bearings, consistent with the supplier's experience.

The critical failure mode driving component life of the PCD bearings is from thermal fracture rather than wear. The bearings require modest flow through the bearings for heat dissipation as well as precision in alignment to prevent edge loading. The model-scale bearings were tested to failure and met design conditions with a safety factor of 1.5.

With the above results, ORPC believes that predictions for 5-year service life has been verified, with potential to achieve 20+ year component life, which would eliminate the need for costly replacements.

3.5.2.4 *Task 6.0 Impact Analysis*

The Project's SPA goals included improvements in Availability, Power-to-Weight Ratio (PWR), and reduction in LCOE. The section above, Section 3.5.2.1 for Subtask 2.3, outlined methodologies for estimating AEP and LCOE, based on the Project results. Table 29 provides a summary of the final project achievement of SPA goals.

Table 29. Summary of project achievement of SPA goals.

SPA Metric	Goal	Actual
System Availability	Increase in the system availability from 79% to 94%	*Meets requirement.* Improvements in generator and bearing reliability result in conservative estimates of 93.7%.
PWR	Increase in PWR of 23%	*Exceeds requirement.* The PWR was assessed as system available power at Admiralty Inlet (kW/metric ton). The PWR for the improved system is 0.65 kW/ton, an improvement of 28% over the baseline value of 0.50.
LCOE	Reduction in LCOE of 25%	*Exceeds requirement.* Final projections are $2.49/kWh, an improvement of 81.7% over the baseline $13.58/kWh (calculated for the DOE reference site of Admiralty-Inlet Lower). AEP for a single system increased from 136.6MWh to 182.3MWh, for an improvement of 32.7%. The number of systems required in an array producing 136,000MWh annually decreased from 998 to 746.

Availability

Availability improvements was based on significant reliability gains for the RRM generator and PCD bearings. Baseline availability (annualized) included 2 weeks of planned downtime and 8 weeks of unplanned downtime primarily due to the poor component life of the CPI generators. A conservative estimate of grid outages was 7 days. Refer to Section 3.5.2.1 for Subtask 2.3, above, for baseline assumptions and methodologies.

Assumptions for the improved system were a reduction to 1 week of annual planned downtime for service inspections plus an additional 2 weeks every 5 years for major service. Planned downtime was estimated as 9.8 days. Unplanned downtime as assumed to be 2 weeks per event, occurring twice every 5 years. Over time, this is expected to be greatly reduced; a conservative estimate was assumed for early operation predictions. Unplanned downtime was reduced to 5.6 days.

Final projections are an increase in system availability to 93.7 percent (94 percent). Through reducing unplanned events to once every 5 years and, with conditional monitoring, zero times, the availability would increase to 94.5 percent and 95.3 percent, respectively.

PWR

The PWR was estimated by calculating system available power at Admiralty Inlet (kW/metric ton) and then dividing by the overall power system weight. Multiplying the system power curves by the annualized site velocity distribution gives a weighted average of power. Applying the system availability results in an estimated available power for the TidGen® at Admiralty Inlet.

The PWR for the improved system is 0.65 kW/ton, an improvement of 28 percent over the baseline value of 0.50. Table 31 overviews the baseline and improved calculations for PWR calculations.

LCOE

The LCOE was based on improvements in AEP and changes in CAPEX and OPEX. The following formula from the DOE was used for calculations:

$$LCOE = \frac{ICC * FCR + O\&M}{AEP}$$

Where:

- **ICC**, installed capital costs, represents all capital expenditures associated with the planning, design, manufacturing, deployment, and project management of a wet capex (WEC) array.
- **FCR**, fixed charge rate, is the annual return, represented as a fraction of installed capital costs, needed to meet investor revenue requirements.
- **O&M**, operations and maintenance costs, includes all routine maintenance, operations, and monitoring activity (i.e. non-depreciable).
- **AEP**, annual energy production, describes the average annual energy generated (after accounting for device or array availability) and delivered to the point of AC grid interconnection (i.e., the measurable basis for power purchase contracts).

AEP is a sum calculation of efficiencies as illustrated Figure 137139.

Improvements in AEP were primarily a result of better mechanical driveline efficiencies, high generator electrical efficiency, and greatly increased system availability.

Table 32 shows system specifications used to derive AEP. Appendix C provides additional details used for calculations.

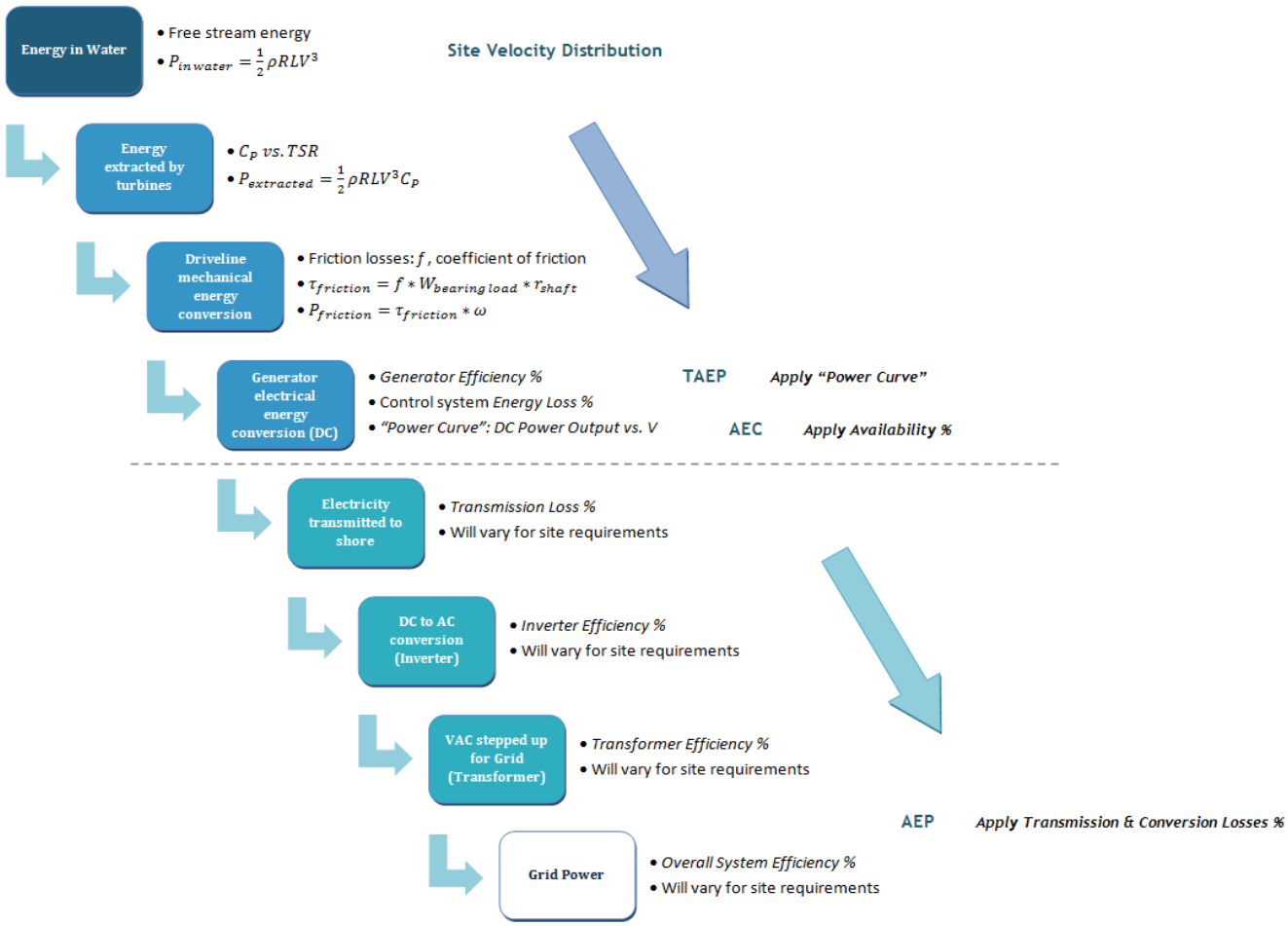

Figure 106. AEP is calculated based on itemized water-to-wire efficiencies.

3.5.2.5 *LCOE Calculation for the System Integration Design*

The calculation of AEP and LCOE for the system integration as described in Section 3.4 follows the same methodology.

ORPC has made significant gains in recent and parallel development efforts to address hydrodynamic performance, power take-off efficiencies and reliability, overall system availability, and installation and mooring methods that achieved breakthrough reductions in cost and deployment times. The objective of the systems integration analysis was to define an achievable, near term system architecture that would fully utilize the capabilities of the advanced power take-off system developed within this Project while integrating the parallel technologies that have been either been demonstrated in the field or are predicted by design tools that have been validated by actual deployments.

By utilizing the cost and performance models developed in collaboration with NREL for the baseline and earlier impact projections, ORPC identified specific cost and performance changes based on the following technology improvements:

- The high reliability PCD bearing and generator technologies developed in this Project, incorporating the next generation driveline design and advanced encapsulation permanent magnet generator produced by Rolls-Royce Marine, predicting an increase in mechanical efficiencies from 88.2 percent to 97.7 percent, an increase in system availability from 79 percent to 94 percent, and increasing service intervals from occurring annually to every 5 years.
- The control system and associated power electronics developed in the DOE funded Project, Advanced Energy Harvesting Control Schemes for Marine Renewable Devices (DE-EE0006397), which in demonstrated effectiveness on a non-linear adaptive control system and cost-effective and more efficient COTS power electronics. The control system eliminated all losses associated with instabilities at peak in turbulence, resulting in a control system efficiency of 100 percent.
- As part of the DOE-funded Project, OCGen® Module Mooring Project (DE-EE0002650): buoyant tensioned mooring system that replaces a piled foundation with a buoyancy pod suspending a turbine and floating at an optimal water column depth above clump-weight anchors and reducing installation times from several weeks to one-day events while eliminating the need for cranes and expensive deployment rigs.
- Integrated fairing based on the prototype deployed on the RivGen® in 2015 that demonstrated an increase in overall system efficiencies over an un-faired deployment in 2014, from 27 percent to 35 percent.
- Optimized turbine and fairing that anticipates a relative hydrodynamic efficiency of 15 percent. Together with the effect of the fairings, increase from an estimated 0.36 turbine CP, prior to mechanical drivetrain losses, to 0.52, based on 2D and 3D CFD models validated from TidGen® and RivGen® deployments.

3.5.2.5.1 Availability

System availability for the conceptual system integration design makes the nearly the same assumptions for the system that incorporates only the PCD bearings and RRM generator. The one exception is reducing the number of unplanned events from a two-week event occurring twice every 5 years (the major service intervals) to only once. Table 34. below summarizes assumptions.

The reasoning is that ORPC will be designing many lessons-learned from the baseline 2012 Cobscook Bay installation, many focused on manufacturing quality and durability. Current design work is being performed with consultation from DNV GL, as an additional third party resource for designing reliable power systems.

3.5.2.5.2 LCOE

LCOE reduction is based on improvements in AEP and changes in CAPEX and OPEX. The following formula from the DOE was used for calculations:

Table 35 shows system specifications used to derive AEP. Figure x shows the power curve comparisons of the baseline system, the isolated impact of the PCD bearings and RRM generator technologies, and their integration into the next generation system as defined in Section 3.4 on the System Integration Plan.

System costs are summarized in Table 35. Costs are given in terms of costs in dollars per rated power, as has been presented by NREL for LCOE Impact Analyses throughout the Project. Two scenarios are presented for the new architecture, with 5 year and 20+ year bearing life.

As discussed above for the LCOE analyses on only the PTO improvements due to PCD bearings and the RRM generator, changes related to PTO improvements are minimal in terms of single system costs, with a modestly more expensive driveline system and negligible differences in generator costs. However, higher power production requires an additional $100,000 for converter electronics. CAPEX reductions from implementation of the advanced controls power electronics are on the order of ~$125,000 for reduced instrumentation requirements, more cost effective and efficient inverters and commercial SCADA system. CAPEX costs related to installation are substantially lower, as a retriever and crane are not required for the OCGen® deployment system. The largest source of cost reductions is a result of the reduced number of systems for equivalent array energy production.

OPEX costs are similarly affected by the reduced number of TGUs. Additionally, fewer deployment and retrievals are required due to the improved reliability of the power take-off system. Deployment and retrieval costs are much less, and modular strategies will reduce annual maintenance to 1-day.

Final estimates for LCOE are $1.26/kWh for assuming 5-year bearing component life, an improvement of 90.7 percent from the baseline costs. As shown in the PTO Driveline System Test Report (D-xPTO-10042), the PCD bearings have negligible wear in ORPC's operating conditions, and it is reasonable to assume design refinements to allow for a 20+ year component life, which would require no replacements. With potential 20+ year component life, the bearings will not require replacement, consequently reducing estimated LCOE to $1.06, for an improvement of 92.2 percent.

The above estimates are based on near-term integration of demonstrated technologies. Future design efforts would likely incorporate current technology development efforts, such as improved hydrodynamics from turbine-turbine and turbine-structure interactions. The value, however, of the improved reliability of the PTO technologies developed in this Project are critical steps in achieving competitive LCOE for marine renewable energy systems.

3.5.3 Problems Encountered and Departure from Planned Methodology

No problems were encountered in generation of the impact analyses.

3.5.4 Assessment of Their Impact on the Project Results

All Project SPA targets were achieved.

4 PRODUCTS

4.1 Publications

The following publications were prepared under this award:

Muljadi, E., Gevorgian, V., Wright, A., Donegan, J., Marnagh, C., & McEntee, J. (2016). Electrical Power Conversion of River and Tidal Power Generator. https://doi.org/10.1109/NAPS.2016.7747916

Muljadi, E., Gevorgian, V., Wright, A., Donegan, J., Marnagh, C., & McEntee, J. (2016). Electrical Power Conversion of a River and Tidal Power Generator: Preprint. https://www.nrel.gov/docs/fy16osti/66866.pdf

Muljadi, E., Wright, A., Gevorgian, V., Donegan, J., Marnagh, C., & McEntee, J. (2016). Dynamic Braking System of a Tidal Generator: Preprint. https://www.nrel.gov/docs/fy16osti/66396.pdf

Muljadi, E., Wright, A., Gevorgian, V., Donegan, J., Marnagh, C., & McEntee, J. (2016). Power Generation for River and Tidal Generators, https://www.nrel.gov/docs/fy16osti/66097.pdf

Muljadi, E., Wright, A., Gevorgian, V., Donegan, J., Marnagh, C., & McEntee, J., (2016). Turbine Control of a Tidal and River Power Generator. https://doi.org/10.1109/NAPS.2016.7747912

Muljadi, E., Gevorgian, V., Wright, A., Donegan, J., Marnagh, C., & McEntee, J. (2016). Turbine Control of a Tidal and River Power Generator: Preprint. https://www.nrel.gov/docs/fy16osti/66867.pdf

4.2 Inventions/Patent Applications, licensing agreements

There were no inventions or patent applications filed under this award.

5 REFERENCES

Bachant, P., Wosnik, M., Gunawan, B., Neary,V.S , *Experimental Study of a Reference Model Vertical-Axis Cross-Flow Turbine,* Submitted for publication, Under Review

Brabandere, K, De., (2004). *A voltage and frequency droop control method for parallel inverters*, IEEE Annual Power Electronics Specialist Conference, 4:2501 - 2507 VOL 4.

Buhl, M.L., (2005*). A New Empirical Relationship Between Thrust Coefficient and Induction Factor for the Turbulent Windmill State*, National Renewable Energy Laboratory, Technical Report NREL/TP-500-36834.

Chapman, J.C., Masters, I., Togneri, M. & Orme, J.A.C., (2013). *The Buhl High-Induction Correction for Blade Element Momentum Theory Applied to Tidal Stream Turbines*, Renewable Energy, Volume 60, December 2013, pp. 472–480

Cooley, C.H., Khonsari, M.M. & Lingwall, B. (2012). *The Development of Open Water-Lubricated Polycrystalline Diamond (PCD) Thrust Bearings for Use in Marine Hydrokinetic (MHK) Energy Machines*, https://www.osti.gov/servlets/purl/1056274/

Glauert, H., (1999). *The Elements of Aerofoil and Airscrew Theory*, Cambridge Science Classics.

McEntee, J. (2013). *TidGen® Power System Commercialization Project, Final Technical Report*, US Department of Energy, DE-EE0003647

Murray, J.C. & Barrone, M. (2011). *The Development of CACTUS, a Wind and Marine Turbine Performance Simulation Code*, 49th AIAA Aerospace Sciences Meeting including the New Horizons Forum and Aerospace Exposition 4 - 7 January 2011, Orlando, Florida

Paraschivou, I. (2002). *Wind Turbine Design with emphasis on Darrieus Concept*, Polytechnic International Press

Strickland, J.H., (1975). *The Darrieus Turbine: A Performance Prediction Model Using Multiple streamtubes*, SAND75-0431, Sandia Labs, Energy Report.

Worthington, M., Ravens, T., & Ali, M. (2013). *Abrasion Testing of Critical Components of Hydrokinetic Devices*, Final Technical Report, US Department of Energy, DE-EE0003631